The Echo Cliff Structure:
Identification and Analysis of a Possible Kansan Impact Structure

by

Adam Eldon Lane

B.S., Northwest Missouri State University, 2016

A THESIS

submitted in partial fulfillment of the requirements for the degree

MASTER OF SCIENCE

Department of Geology
College of Arts and Sciences

KANSAS STATE UNIVERSITY
Manhattan, Kansas

2018

Approved by:

Co-Major Professor
Dr. Matthew Totten

Approved by:

Co-Major Professor
Dr. Abdelmoneam Raef

Copyright

Abstract

This study examines an ovoid drainage feature southwest of Topeka, Kansas, whose discovery sparked a flurry of activity. Geomicrobial and surface gamma ray surveys indicated possible vertical migration of hydrocarbons, and a ground magnetic survey produced anomalies that resemble the profile of a crater. The area was dubbed the Echo Cliff structure and considered analogous to the Ames structure in Oklahoma, an Ordovician impact structure remarkable for significant hydrocarbon recovery. However, four wells drilled in the area were dry and abandoned. The Echo Cliff structure did yield further indications of its origins by the discovery of possible shocked quartz in drill cuttings from the Ordovician Simpson Group. Our study integrated well log analysis, geophysical modeling, and petrographic analysis to verify or refute the proposed identity of the Echo Cliff structure. Well logs from the area were used to create a structural and stratigraphic cross-section in Petrel® 2016. A gravity survey was conducted in the study area and combined with an aeromagnetic survey, donated by Applied Geophyics, Inc., to use as the basis for geophysical modeling within GM-SYS®. Finally, drill cuttings from the Simpson Group of two wells in the study area were mounted for thin sectioning. These thin sections were examined for planar deformation features, which are indicative of an impact event. The structural and stratigraphic cross sections indicated minimal variation in the subsurface, which is uncharacteristic of an impact event. The GM-SYS® geophysical models seem to indicate that variations in the topography of the Precambrian basement and faulting from the Bolivar-Mansfield Tectonic Zone are responsible for the geophysical anomalies and possibly the current drainage pattern of the study area. Finally, no planar deformation features were observed in any of the examined thin sections. Therefore, there is currently no evidence in support of the claim that the Echo Cliff structure is an impact structure.

Table of Contents

List of Figures

Acknowledgments

I would first like to thank Ken Walker of Stroke of Luck Energy & Exploration, LLC for partnering with the Department of Geology for this study. Thank you to George Petersen and Verne Dow for the previous work on the study area. Thank you also to S. Parker Gay Jr. of Applied Geophysics, Inc. for donating the aeromagnetic survey. I am also grateful to the AAPG Foundation and John W. Robinson whose grant partially funded this study. I am also indebted to my advisors Dr. Matthew Totten and Dr. Abdelmoneam Raef for providing advice and guidance during this endeavor. Finally, I would like to thank my fiancée, Alexandria Richard, for her love, support, and manual labor without which this study would not have been possible.

Chapter 1 - Introduction

Compared to our moon, Earth appears to have suffered few impact events. However, Earth's natural processes are excellent at erasing history. Only 190 impact structures have been confirmed to date (Spray, 2018), which may leave an untold number left to discover.

Impact Structures and the Petroleum Industry

Impact events may cause local changes in the subsurface that may be favorable for the entrapment of economic deposits of minerals and hydrocarbons (Grieve, 1997). Hydrocarbons are epigenetic deposits, which means they are created and trapped after impact (Grieve, 1997). Hydrocarbon reservoirs may form in the central uplift, crater rim, ring grabens, ejecta, and potentially the fractured rock beneath the impact structure (Donofrio, 1997). In North America, seventeen confirmed impact structures occur in petroliferous areas, of which nine produce hydrocarbons (Donofrio, 1997).

Impact structures may also form anoxic lacustrine or marine depressions that are favorable for deposition of organic-rich rocks that can serve as both a hydrocarbon source rock and stratigraphic trap (Castaño et al., 1997). In effect, besides forming potential reservoir rocks, impact structures can form localized but complete petroleum systems (Castaño et al., 1997). The Ames structure in Oklahoma, Bosumtwi crater in Ghana, Newporte structure in North Dakota, Ries crater in Germany, Flynn Creek structure in Tennessee, and Siljan structure in Sweden all have formed local petroleum systems after impact (Castaño et al., 1997).

The Proposed Echo Cliff Structure

Interest in the study area (Figure 1) began with the recognition by a consultant for a local independent oil and gas company of an ovoid drainage feature in the southwestern portion of the Forest City basin. Geomicrobial and surface gamma ray surveys of the area indicated possible

vertical migration of hydrocarbons. Results from these surveys and surface expression of the area appeared similar to hydrocarbon producing impact structures (George Petersen, personal communication). With interest growing, a surface magnetic survey was conducted along two roads in the study area, creating two perpendicular transects (Daniel Merriam, personal communication). The Ames structure in northern Oklahoma, an Ordovician impact structure remarkable for significant hydrocarbon recovery (Carpenter and Carlson, 1997), was selected as an analog due to the similarity of the profiles (Figure 2). A remote sensing specialist with experience in analyzing the Ames structure (Koger and Wiley, 1997), was requested to perform a similar analysis. The remote sensing interpretation (Figure 3) revealed concentric ellipsoid features, lineaments, and areas where possible vertical movement of hydrocarbons have inhibited vegetation growth (David Koger, unpublished data). Based on these surface similarities to the Ames structure, the ovoid drainage feature was dubbed the Echo Cliff Structure, borrowing its name from the nearby Echo Cliff park near Dover, Kansas. Between 2008 and 2011, four exploratory wells (Andrew Wendland 1, Andrew Wendland 2, Phillip Wendland 1, and Dorothy Wendland 1) were drilled into the proposed structure. Unfortunately, the wells were dry and subsequently abandoned. An impact origin for the Echo Cliff structure was further supported by the discovery of possible shocked quartz sand in drill cuttings from the Ordovician-aged Simpson Group (George Petersen, personal communication). Interest in further development of the Echo Cliff Structure waned until the involvement of Stroke of Luck Energy and Exploration, LLC.

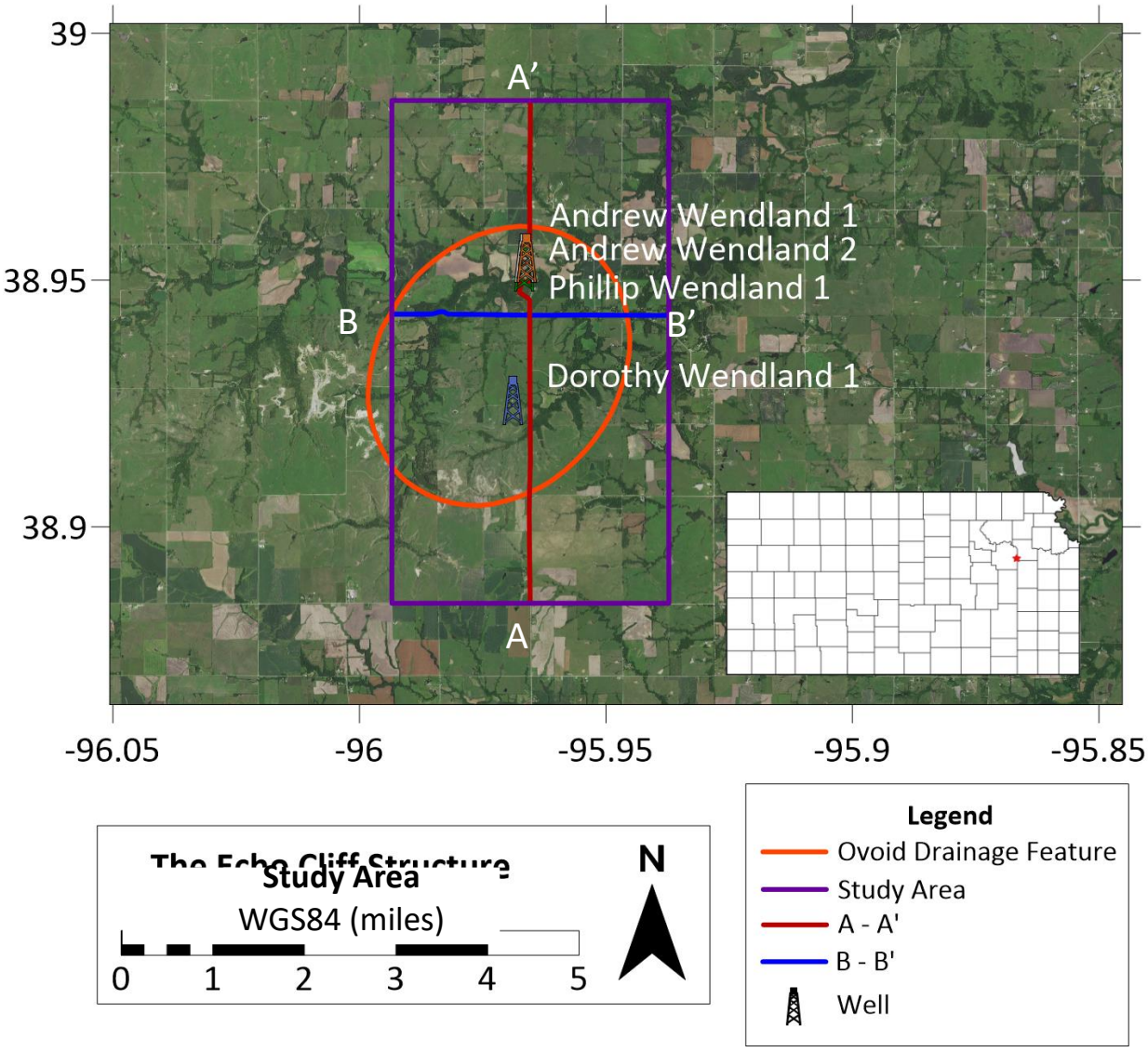

Figure 1: The study area with wells and ground magnetic survey transects overlain. Andrew Wendland 1, Andrew Wendland 2, and Phillip Wendland 1 are in such proximity that they appear as one icon. The surface magnetic survey transects are designated as A - A' and B - B'. On the inset map, the study area is designated by a red star.

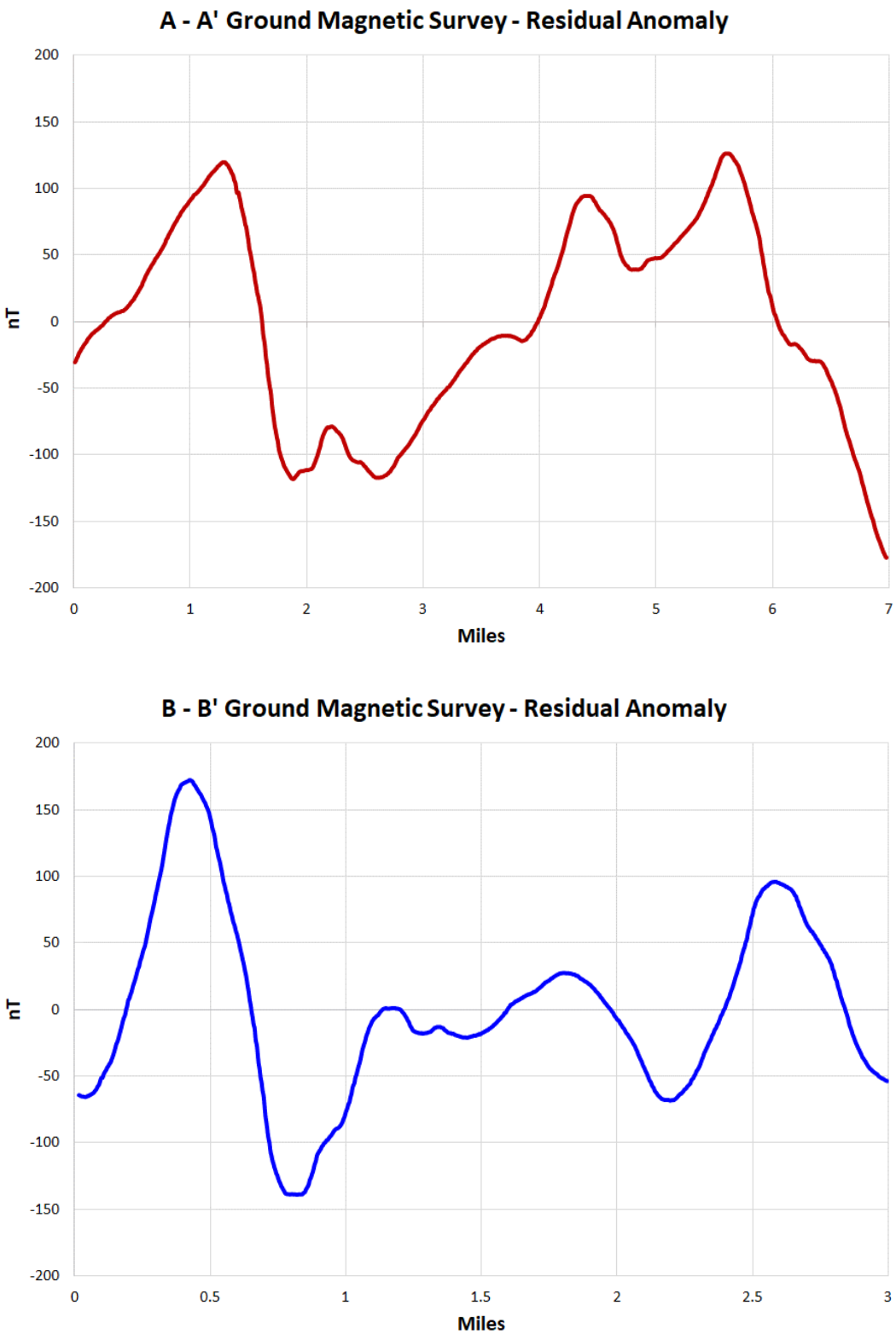

Figure 2: Residual anomaly A - A' and B - B' transects of the surface magnetic survey in the study area. The A - A' and B - B' transects intersect at ~ 4 miles and ~ 1.5 miles respectively. Based on Daniel Merriam (unpublished data). See Appendix B for data.

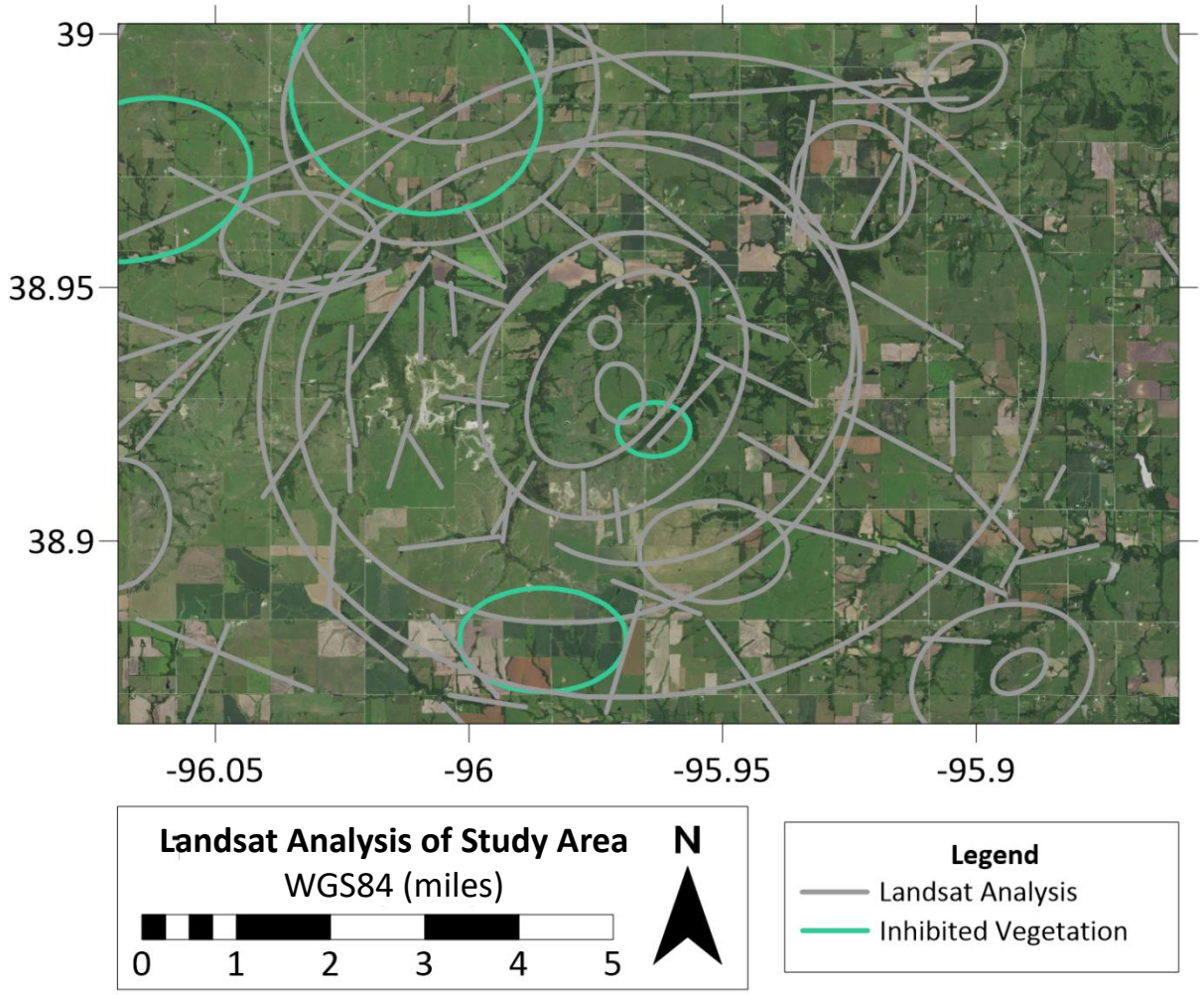

Figure 3: Landsat analysis of the study area. Ellipses and lineaments indicate possible subsurface structures. The aquamarine ellipses represent potential hydrocarbon inhibited vegetation. Based on David Koger (unpublished data).

Objective

The Echo Cliff structure has been proposed to be an Ordovician impact structure due to possible surface expression, magnetic anomalies resembling the profile of a crater, and the recovery of potentially shocked quartz sand grains from drill cuttings using a stereo microscope (George Petersen, personal communication) (Daniel Merriam, unpublished data). Verification of this interpretation requires confirmation of shock metamorphism using thin sections of rocks from the area (French, 1998). Surface expression and magnetic anomalies are non-unique and

can only indicate a possible impact structure that then needs to be correctly verified (French, 1998).

The objective of this research is to further test the hypothesis of the Echo Cliff structure being an Ordovician impact structure. To test this hypothesis, a comprehensive investigation that integrates subsurface correlation of well data, geophysical modeling, and petrographic analysis of drill cuttings was initiated. Specific questions that guided the investigation include the following:

1. Does the subsurface structure of the study area reflect anomalies consistent with an impact structure?
2. Are the geophysical models of the study area consistent with an impact structure?
3. Do recovered quartz sand grains exhibit shock metamorphism?
4. Is there enough evidence to verify the proposed identity of the Echo Cliff structure as an Ordovician impact structure?

Importance of Study

If verified, the Echo Cliff structure would be the only confirmed hypervelocity impact structure in Kansas (Suchy, 2007). Also, the location of the Echo Cliff structure within the Forest City basin may enable significant hydrocarbon recovery in a typically low production basin (Anderson and Wells, 1968).

Chapter 2 - Geologic Background

Forest City Basin

The study area is in the southwestern portion of the Forest City basin (Figure 4), which has a long but unremarkable history of hydrocarbon production. The first exploration well west of the Mississippi River was drilled into the basin in 1860, but even with that early start, production has been lower than surrounding basins (Anderson and Wells, 1968). Anderson and Wells (1968) suggests that the Forest City basin was too shallow and subjected to extensive erosion, which did not hinder hydrocarbon migration but inhibited trap development.

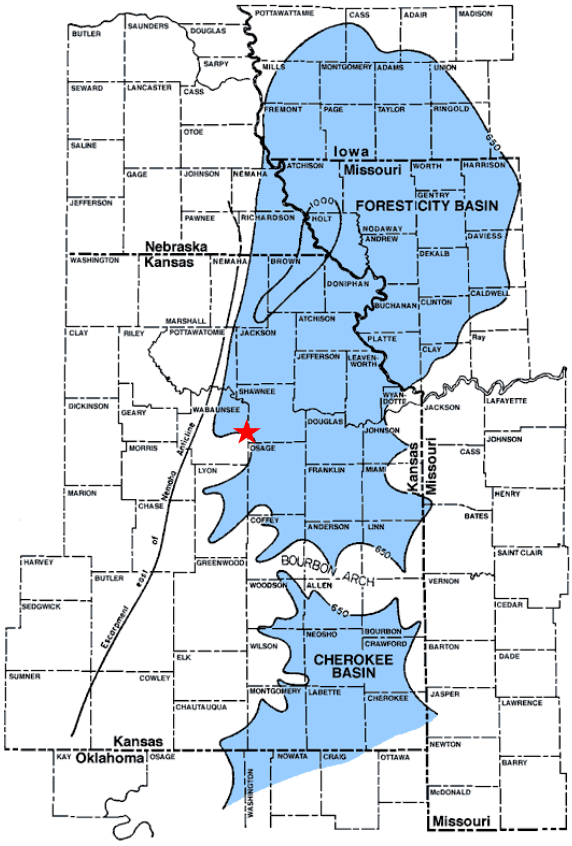

Figure 4: Map of the Forest City basin in relation to the northern Cherokee basin, Nemaha anticline, and Bourbon arch. The 1000 foot contour outlines the deepest part of the Forest City basin. The study area is indicated by the red star. Modified from Lee (1943).

Two production trends dominate the Forest City basin in Kansas. One is lenticular Pennsylvanian sandstones near the Kansas City area, and the other is a series of anticlines in lower Paleozoic reservoirs that trends along the Nemaha uplift (Hatch and Newell, 1999). One of these anticlines houses the oil pool below the prolific Davis Ranch field ~ 16 miles west of the study area (Smith and Anders, 1951). Recently, the Forest City basin in Kansas has been the target of coalbed methane exploration (Newell et al., 2001) forming the Forest City Coal Gas Area. The nearest exploration well outside of the study area, Thompson 1-33, ~ 0.25 miles south, is a plugged and abandoned Anadarko Petroleum Corporation well that was drilled to produce natural gas from coals in the Cherokee Group. Coalbed methane production, however, has not been as successful as in the Cherokee basin to the south (Newell et al., 2001). Estimated undiscovered conventional reserves for the Forest City basin are 20 million barrels of crude oil, 70 billion cubic feet of gas, and < 10 million barrels of natural gas liquids (USGS, 1995).

Postulated Affected Strata

Stratigraphic tops noted during drilling of all four study area wells include Pennsylvanian to Cambrian strata. The Oread Limestone Formation, Heebner Shale Member of the Oread Limestone Formation, Lansing Group, Base of the Kansas City Group, Altamont Limestone Formation, Cherokee Group, “Mississippi Lime,” Chattanooga Shale Formation, “Hunton Group,” Maquoketa (Sylvan) Shale Formation, and Viola (Kimmswick) Limestone Formation were encountered without any anomalies. However, quartz sand grains that appeared to be shocked were recovered from the Simpson Group (George Petersen, personal communication), an Ordovician geologic unit notable for the economically valuable St. Peter Sandstone Formation (Benson and Wilson, 2015). If the Echo Cliff Structure is indeed an Ordovician impact structure, formed during deposition of the Simpson Group, then some of the geologic units below the

Simpson Group may have been affected, either by complete destruction or brecciation (Carpenter and Carlson, 1997). However, if the St. Peter Sandstone formation of the Simpson Group was the target of the Echo Cliff impact, then the kinetic energy of the impactor may have been partially absorbed by the water and soft sand leading to a diminished crater topography (Wong et al., 2001). Also, the low strength of the unconsolidated sand may have reduced the potential for shock metamorphism to occur (Buchanan et al., 1998). Infilling of the resulting crater would directly affect geologic units post-dating the impact, likely represented by atypically thick strata (Carpenter and Carlson, 1997). Due to the possibility of the Ames structure and the Echo Cliff structure forming from the same multiple impact event (Vastag, 2013), and the Maquoketa (Sylvan) Shale being the lowest reliably mappable unit above the Ames structure (Koger and Wiley, 1997), our stratigraphic description will focused on the Precambrian basement to the Maquoketa (Sylvan) Shale (Figure 5).

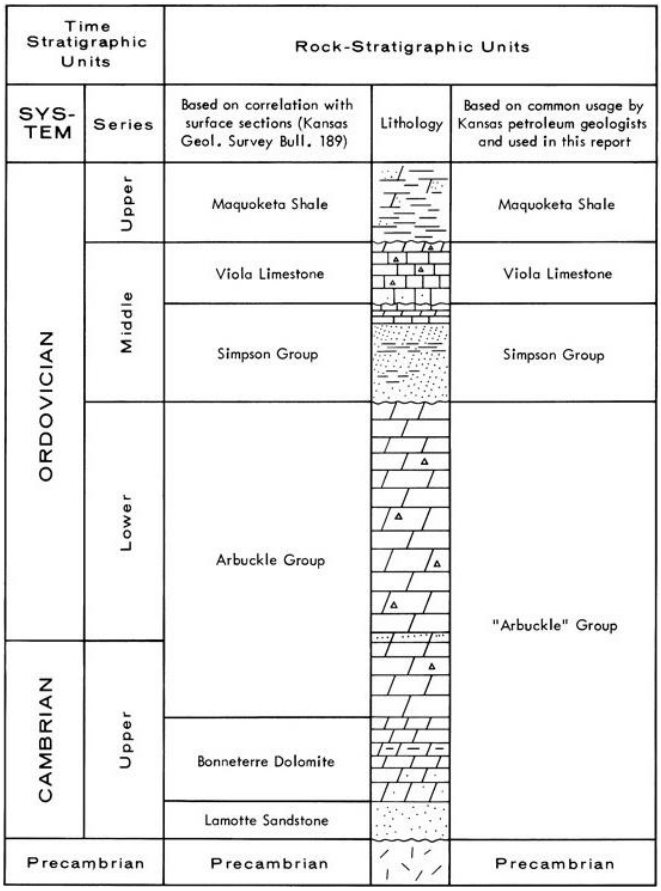

Figure 5: A stratigraphic column of Precambrian, Cambrian, and Ordovician strata found in Kansas. From Cole (1975).

Description of the Possibly Affected Strata

Relief on the Precambrian basement of Kansas ranges from ~ 9500 feet in depth in the Hugoton Embayment to ~ 600 feet over the Nemaha ridge (Merriam, 1963). The composition of the Precambrian basement also varies widely with granite, gneiss, schist, and quartzite often reported (Merriam, 1963). The overall distribution of compositions remains ambiguous in most of the state due to wells reaching the Precambrian being mainly on structural highs (Zeller et al., 1968), leaving the deep basinal areas mostly unmapped (Merriam, 1963). Granite is the most often reported rock type in wells that reach the Precambrian (Merriam, 1963), and in the study area, this is the basement rock ascertained from inversion of gravity and magnetic data (Figure 6). However, it is important to note that areas of exposed basement, for example the shield areas

of the world, exhibit significant variations in composition (Gay, 1995) and that most likely the pure granite composition of the study area is an oversimplification. An intricate pattern of faulting is also revealed on the exposed areas (Figure 7), which divides the basement into blocks of varying shapes and sizes (Gay, 1995). The complexity is due to the basement being formed by multiple tectonic, intrusive, and metamorphic episodes during the Archean and Proterozoic (Gay, 1995). The basement faulting, termed as shear zones by Gay (1995), are zones of weakness that can become reactivated by tectonic stresses or gravitational loading. The reactivated shear zones and basement topography have a direct effect on the overlying sedimentary cover (Gay, 1995). The shear zones, if reactivated, can be the locus of faulting that propagates into the sedimentary cover (Gay, 1995). Also, shear zones erode to topographic lows relative to surrounding areas due to intense fracturing, which creates more surface area for erosion (Gay, 1995), and may provide additional accommodation space for deposition (Domenico, 1967). The basement lows created by eroded shear zones or down-dropped blocks within the shear zone can create synclines in the sedimentary cover by gravitational compaction into the basement low (Gay, 1995). Topographic highs on the basement rocks can affect later sedimentary cover through sediment onlap (Carr, 1995), and by gravitational compaction of sediment deposited on top of the high, forming anticlines (Gay, 1995). The anticlines formed through gravitational compaction can influence later deposition if exhibited on the surface (Gay, 1989). The exhibited highs may be the locus for winnowing of sediment and reef development (Gay, 1989).

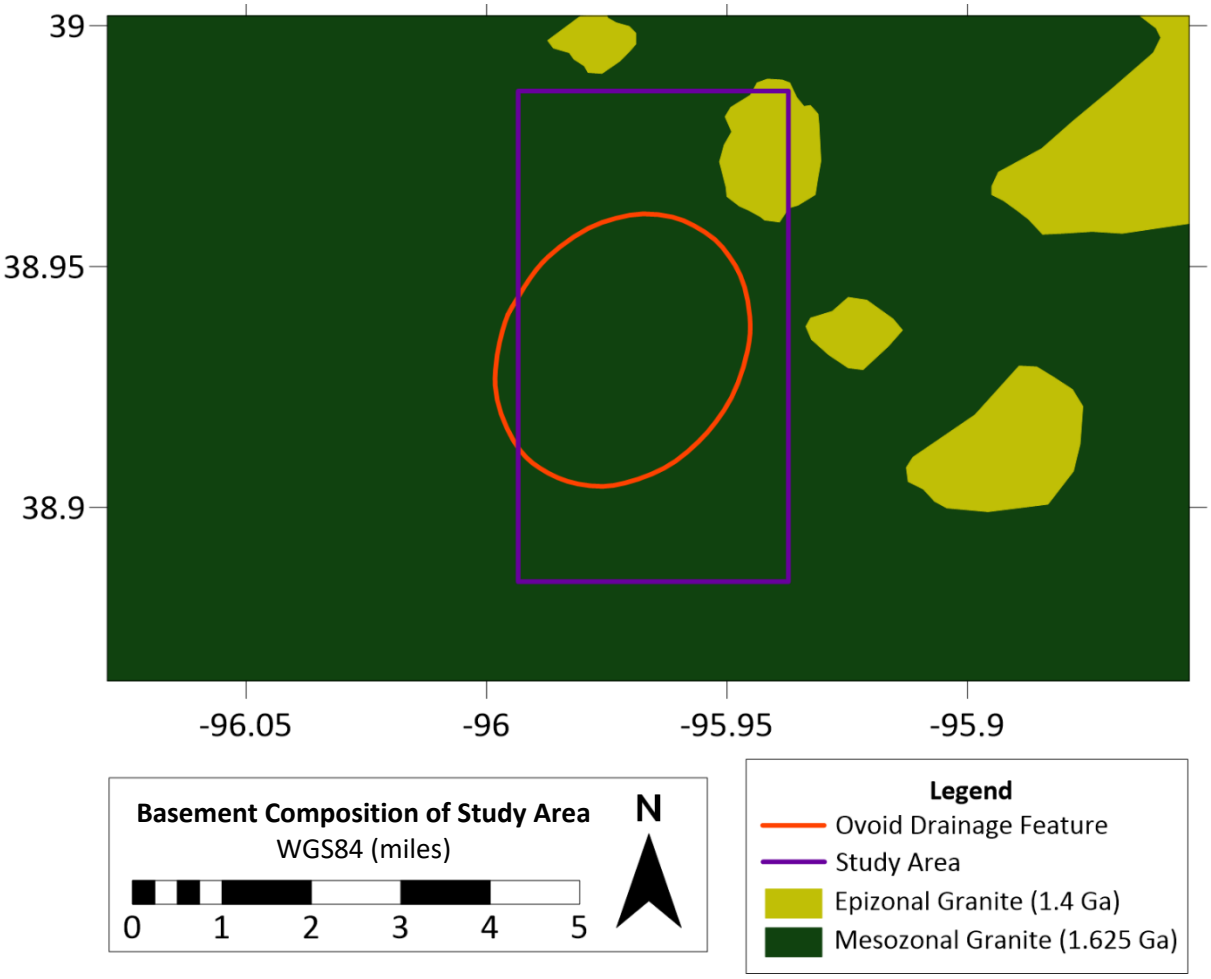

Figure 6: Postulated Precambrian basement composition of the study area based on inversion of gravity and aeromagnetic data. Based on Xia et al. (1995).

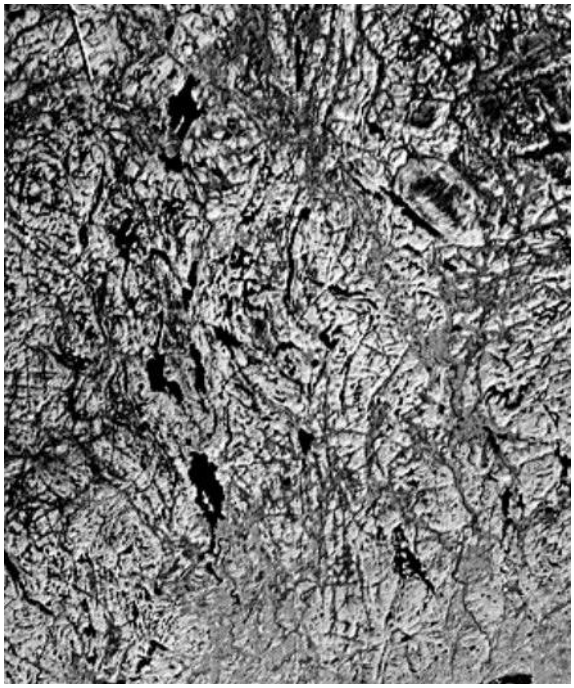

Figure 7: Landsat image of exposed basement in the Canadian Shield. Note the extensive fracturing. From Short et al. (1976).

In most of Kansas, basal Paleozoic sandstones overlie the basement (Scott and McElroy, 1964). These basal sandstones have been called the "Reagan," "Lamotte," "Paleozoic basal sandstone," and "granite wash" depending on the ascertained age of the sand (Scott and McElroy, 1964). The composition of the sands is influenced by the underlying basement but generally is described as arkosic with a grain size ranging from fine to coarse (Newell et al., 1987). The average thickness of these sandstones is ~ 40 feet (Zeller et al., 1968), but the thickness greatly depends on the topography of the basement during deposition. Approximately 1000 feet of basal sandstone was reported in a graben on the Kansas-Missouri state line (Kisvarsanyi, 1984).

The Cambro-Ordovician Arbuckle Group in Kansas is primarily represented by dolomite, cherty dolomite, and dolomitic limestone deposited in a shallow subtidal to intertidal environment (Franseen et al., 2004). The dolomitic nature of the Arbuckle Group in Kansas is possibly due to low rainfall and high evaporation which resulted in magnesium-rich, hypersaline,

shallow waters (Ross, 1976). The upper boundary of the Sauk sequence is represented by a major unconformity at the top of the Arbuckle Group (Franseen et al., 2004). A vast landscape of mostly carbonates and residual Precambrian basement was exposed, and an extensive system of caves and sinkholes developed (Kerans, 1988). Many of the sinkholes are filled with Simpson Group material, often represented by an abnormally thick St. Peter Sandstone (Merriam and Atkinson, 1956).

During the Ordovician, Kansas (Figure 8) was likely a marine shoreface environment (Benson and Wilson, 2015) located approximately between 20 - 30° south of the equator (Franseen et al,. 2004). The environmental interpretation is due to the exceptionally pure, well sorted, well rounded, and highly spherical quality of the St. Peter Sandstone (Figure 9). The St. Peter Sandstone is one of a number of lower Paleozoic sheet sandstones that was formed through cyclical reworking of older Cambrian and Proterozoic sandstones or weathered basement rock (Benson and Wilson, 2015). A minor unconformity separates the Simpson Group from the overlying Viola (Kimmswick) Limestone (Lee, 1956).

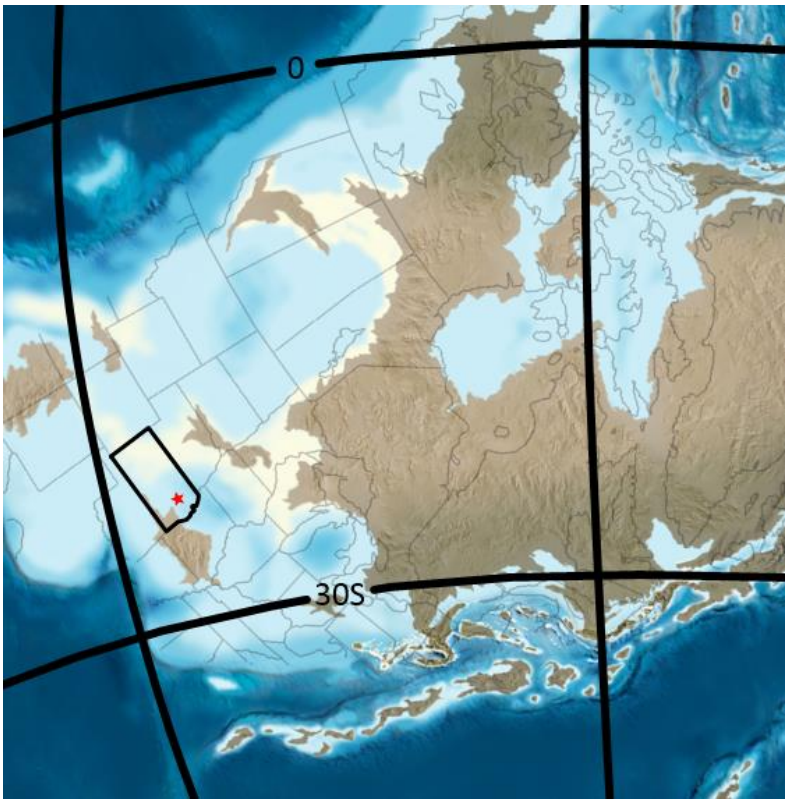

Figure 8: Paleoenvironmental interpretation of North America during the middle Ordovician (470 Ma). The black outline is Kansas with the study area represented by a red star. Based on Franseen et al. (2004) and Blakey (2011).

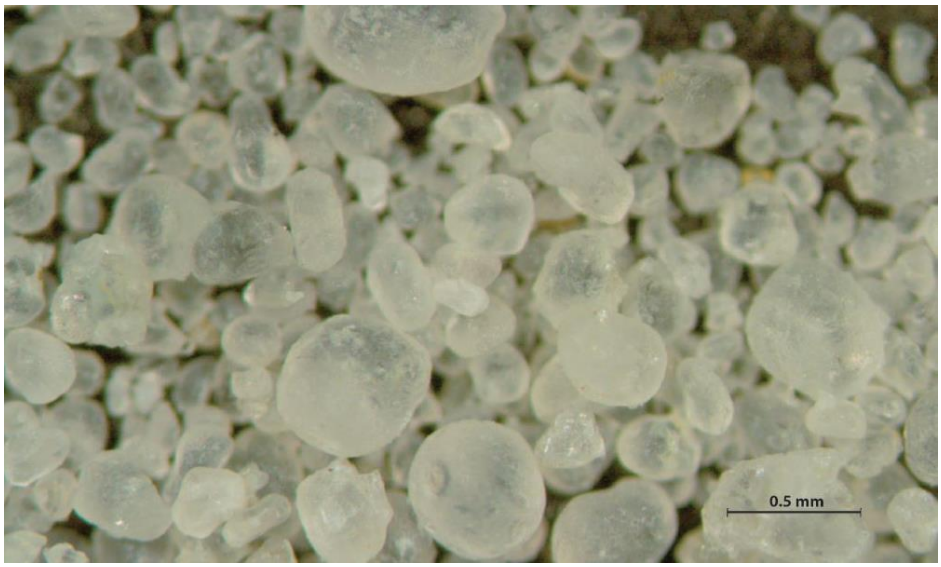

Figure 9: Unsorted sample of St. Peter sandstone. From Benson and Wilson (2015).

The Middle Ordovician Viola (Kimmswick) Limestone, consists mostly of dolomite, with some limestone, and chert beds (Zeller et al., 1968). The Viola (Kimmswick) Limestone in Kansas has been correlated, at least in part, to the Viola Limestone type locality in Oklahoma and the Kimmswick Limestone of Missouri (Adkison, 1972). Facies within the Viola (Kimmswick) Limestone are highly variable and do not lend themselves to accurate regional mapping (Lee, 1956). Subaerial exposure of the Viola (Kimmswick) limestone resulted in an unconformity on which the Maquoketa (Sylvan) Shale now lies (Zeller et al., 1968).

The upper Ordovician Maquoketa (Sylvan) Shale is the youngest Ordovician formation in northeastern Kansas and is considered equivalent to the Sylvan Shale in Oklahoma (Lee, 1956). The composition of the Maquoketa typically varies from silty dolomitic shale to cherty, silty dolomite (Zeller et al., 1968). Due to deposition on an uneven, unconformable surface, environments of deposition varied and in some areas, the Maquoketa can be nearly indistinguishable from the underlying Viola (Kimmswick) Limestone (Adkison, 1972). However, the impure dolomite of the Maquoketa usually contrasts sharply with the clean coarsely crystalline dolomite of the Viola (Lee, 1956).

Chapter 3 - Formation, Classification, and Identification of Impact Craters

Hypervelocity impact craters form when an impactor, usually a meteorite or comet, of sufficient size and velocity to survive passage through the target body's atmosphere, with little deceleration, strikes the surface of the target body (French, 1998). Impactors that survive to hit the surface of the Earth are typically large > 20 m and are traveling at near their initial cosmic velocity > 11 km/s at impact (French, 1998).

Immediately after an impactor strikes a target body, a complex series of events begins. The process of hypervelocity impact crater formation is not duplicatable in a laboratory, and no significant impact crater has formed in recorded human history, so the formation process is not entirely understood (French, 1998). Formation hypotheses based on indirect observations of previously formed impact craters on Earth and other celestial bodies are the norm (French, 1998).

Hypervelocity crater formation is not a mechanical process; the impactor does not excavate the feature produced (French, 1998). Penetration craters such as the Haviland crater, the only confirmed impact crater in Kansas (Suchy, 2007), are mechanically produced by a low-velocity impactor (French, 1998) and are equivalent to dropping a rock in the mud. In contrast, shockwaves emanating from the center of the impact site excavate hypervelocity impact craters (French, 1998). There are three stages of hypervelocity impact crater formation: contact and compression, excavation, and modification (French, 1998).

Contact and Compression

The contact and compression stage lasts no more than a few seconds and involves the transfer of kinetic energy of the impactor into shockwaves that excavate the crater (French,

1998). At the point of contact, the impactor only penetrates up to twice its diameter before being vaporized by the shockwave reflected back into the impactor by the target surface (French, 1998). The initial shockwave pressures generated by the impact may exceed 100 GPa and then dissipate with distance to form concentric zones of disturbed material (French, 1998). Figure 10 illustrates the zoning produced by shockwave dissipation during the contact and compression stage. The shockwave is intense compared to anything that can happen naturally on Earth and permanent deformation results in rocks that the shock waves pass through (French, 1998).

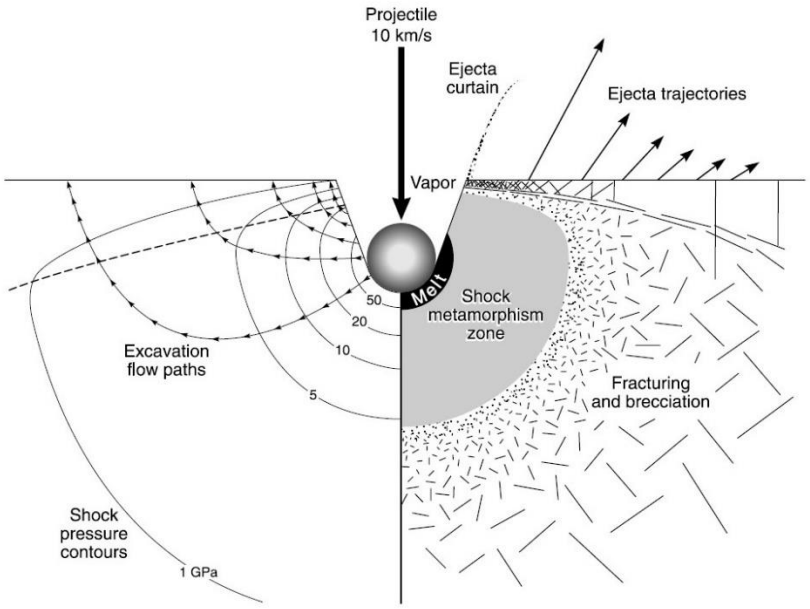

Figure 10: Illustration of zoning produced by shockwave dissipation during the contact and compression stage of crater formation. From Melosh (1989).

Excavation

Excavation begins concurrently with the later portion of the contact and compression stage (French, 1998). Shockwaves produced by the impact form two zones of excavation, the ejection and displacement zones (French, 1998). In the ejection zone, target material moves upward and away from the point of contact to form an ejecta curtain (French, 1998).

Displacement zone material moves downward and away from the point of contact to form the transient crater (French, 1998). The excavation stage lasts from a few seconds to minutes with more substantial impacts (Melosh, 1989) and ends when the shockwaves lose enough energy to stop displacing material (French, 1998).

Modification

Modification of the transient crater begins as soon as the maximum size of the transient crater is reached (French, 1998). The modification stage involves the collapse of overstepped sides of the transient crater and possible rebound of target rocks (French, 1998). Simple and complex craters are distinct final products of the modification stage (French, 1998). The modification stage has no definite end and continues with mass wasting, isostatic uplift, erosion, and sedimentation of the impact site (French, 1998).

Impact Crater Classification

The type of hypervelocity impact crater produced (Figure 11) is primarily a function of the size and velocity of the impactor and the gravitational pull and composition of the target body (French, 1998). Angle of incidence may have a minor affect, with ovoid or elongated craters postulated to form from a near horizontal trajectory. However, due to crater excavation occurring from shockwaves radiating from the point of impact, nearly all craters are essentially circular (Elbeshausen et al, 2013). Typically, hypervelocity impact craters are 20 - 30x the diameter of the impactor with a depth approximately one-third of the crater diameter (French, 1998). On Earth, simple craters are bowl-shaped and typically < 2 - 4 km in diameter (French, 1998). Simple craters are very similar to the previous transient crater with the only modification being deposition of crater-fill breccia consisting of fallback ejecta and slumping of the crater rim

(French, 1998). Crater-fill breccia may fill half the original depth of the crater (French, 1998). An excellent example of a simple crater is Meteor crater in Arizona (French, 1998).

On Earth, complex craters are typically > 2 - 4 km in diameter and distinguished from simple craters by possessing a centrally uplifted region, a relatively flat floor, and extensive inward collapse of the crater rim to form ring grabens (French, 1998). The formation of complex craters is most similar to a drop of liquid hitting a liquid surface (Melosh, 1989). Within the central uplift, stratigraphic units rise one-tenth the diameter of the complex crater (French, 1998). As complex craters increase in diameter, the structures present within the crater become more complicated and eventually convert the central uplift into a ring structure (French, 1998). Complex craters that possess two or more concentric ring structures are called multi-ring basins (Melosh, 1989).

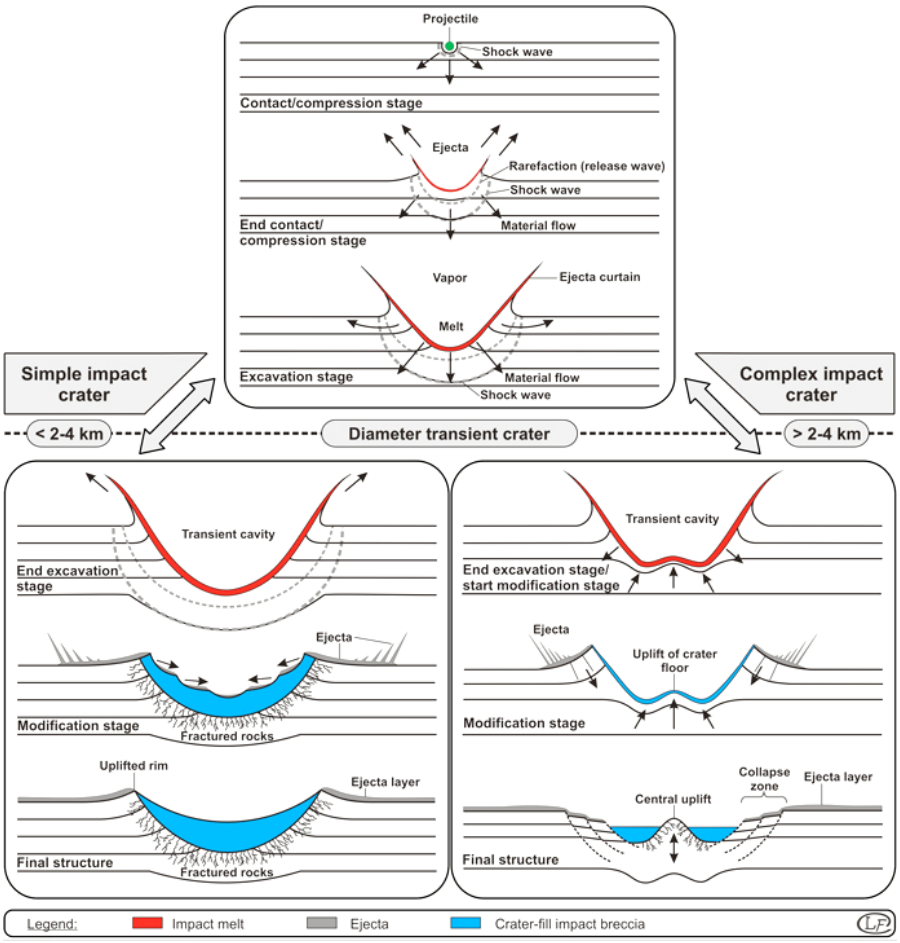

Figure 11: Cross-sectional diagrams illustrating the formation of simple and complex hypervelocity impact craters. From Ferrière (2014).

Impact Crater Identification

The ease of identifying impact craters is directly related to the degree of preservation (Grieve and Pilkington, 1996). Terrestrial impact craters will immediately begin to be deformed by erosion while infilling of sediment occurs in underwater impact craters (French, 1998). Impact structure is the term used in this study when the original topographic features of an impact crater are destroyed or masked due to weathering. Detection of new impact structures is becoming increasingly dependent on geophysical techniques due to their degree of preservation which may impair surface expression (French, 1998). Identifying impact structures is a two-stage process consisting of identification of a candidate impact structure and verification of the impact structure (French, 1998).

Selecting the Candidate Impact Site

Selecting candidate impact sites is dependent upon detection of a roughly circular anomaly in the topography of an area or a circular anomaly in geophysical data such as magnetic and gravity data (French, 1998). Due to the subsurface changes induced at the impact site, utilization of geophysical data is key (Grieve and Pilkington, 1996).

Magnetic Surveys

Magnetic surveys are utilized to observe local modifications of the Earth's magnetic field due to proximity to a magnetic body (Mussett and Khan, 2000). Magnetic data is the least reliable for associating anomalies with features of an impact structure due to wide variation in magnetic signature (Pilkington and Grieve, 1992). Negative or random anomalies have been interpreted as impact breccias formed during crater formation (Scott et al., 1997). Positive anomalies are possibly uplifted magnetic basement rock or impact melt with remnant magnetization. (Hart et al., 1995). Unfortunately, volcanic structures can also have a range of

magnetic signatures and can be roughly circular (French, 1998). Volcanic activity is often proposed as the cause of candidate impact structures after initial discovery (French, 1998).

Gravity Surveys

Gravity surveys are used to observe lateral density differences in the subsurface (Mussett and Khan, 2000) and to estimate the relative size of an impact structure (French, 1998). During the excavation stage, a massive amount of material is fractured and brecciated which lowers the overall density of the impact site (French, 1998). Subsequent modification of the impact crater by crater-fill breccia and sediment deposition will also reduce the density of the impact site relative to the surrounding area (French, 1998). Due to its low density, an impact structure will typically express a negative gravity anomaly that extends to the borders of the impact structure (French, 1998). Simple impact structures often exhibit an entirely negative gravity anomaly (French, 1998) while complex impact structures may exhibit a positive anomaly in the central uplift and then a negative anomaly throughout the rest of the structure (Pilkington and Grieve, 1992). Uplifted basement rocks may cause the positive central anomaly found in some complex impact structures (Pilkington and Grieve, 1992).

Verifying the Impact Structure

Observing shock metamorphism in thin section is the most common way of verifying impact structures (French, 1998). The only option for subsurface impact structures is the utilization of drill cuttings or cores for this process.

Shock Metamorphism

Shock metamorphism is the permanent deformation of rocks and crystal lattices by the intense pressures of the shock wave generated by impact (French, 1998). Depending on the pressures experienced by the target rocks, different features of shock metamorphism will result

(French, 1998). Shatter cones (Figure 12) require the least amount of pressure to form 2 - < 10 GPa and are superficially similar in appearance to cone-in-cone structures (French, 1998). Typically, shatter cones are the first shock metamorphic effects observed at an impact structure due to their extensive formation pressure range and resistance to further metamorphism (French, 1998).

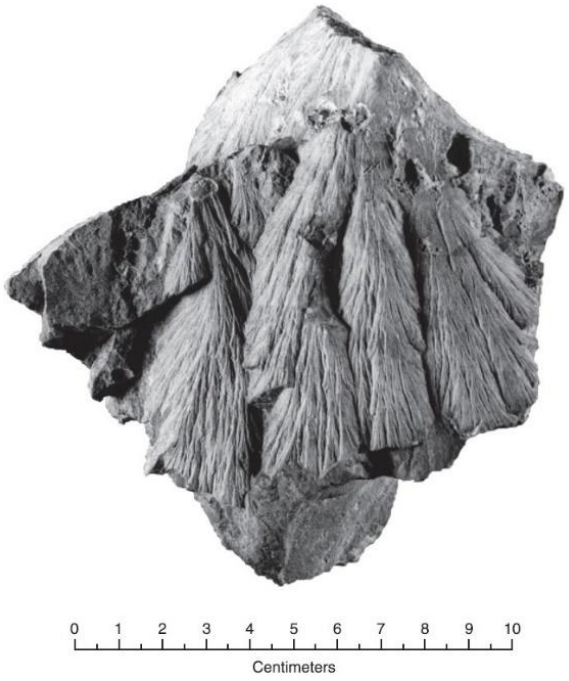

Figure 12: Small well-developed shatter cones in fine-grained limestone. From French (1998).

High-pressure mineral polymorphs are another reliable indicator of an impact event (French, 1998). Usually diamond, stishovite, and coesite form deep in the Earth's mantle under high static pressures (French, 1998). The discovery of these minerals in relatively shallow rocks within impact structures suggests that they also can be formed by the sudden and intense pressures of an impact event (French, 1998). Diamonds and coesite are less reliable than stishovite for verifying an impact structure since they can be transported to the surface by

tectonics and kimberlite pipes respectively (French, 1998). Observation of stishovite has never occurred in any geological setting other than an impact structure (French, 1998).

Planar deformation features (PDFs) are the most widely used shock metamorphic effects for verifying impact structures (French, 1998). Shockwave pressures 8 - 25 GPa deform the crystal lattice of minerals at the impact site (French, 1998). Typically, PDFs (Figure 13) are observed in quartz since it is abundant in both sedimentary and crystalline rocks (French, 1998). PDFs in thin section consist of multiple sets of linear features that extend across the observed surface (French, 1998). The orientation of PDFs relative to planes with the crystal lattice is used to distinguish these features from non-shock deformation (French, 1998).

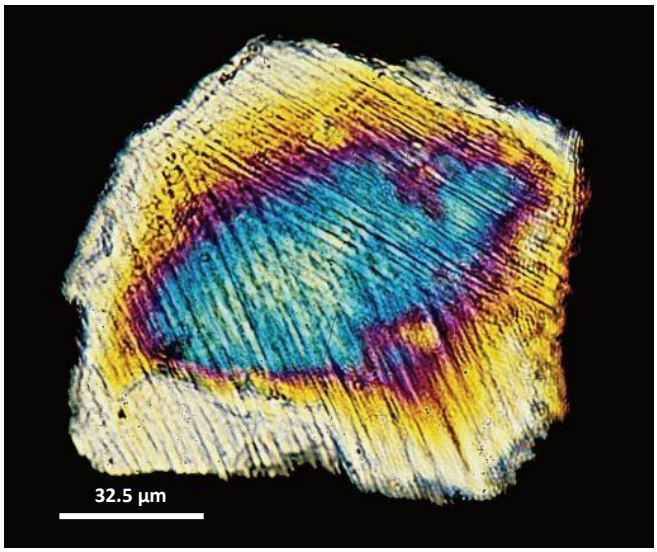

Figure 13: PDF in quartz grain from the USGS-NASA Langley core of the Chesapeake Bay crater. Modified from Horton et al. (2005).

Chapter 4 - Methods of Investigation

Methods of investigation for this study included a gravity survey, geophysical modeling of the A - A' and B - B' transects, well log correlation, and petrographic analysis of drill cuttings for shock metamorphism. This study also incorporated the previously mentioned surface magnetic survey in the study area (Daniel Merriam, unpublished data) to bolster the amount of data useful for geophysical modeling.

Surface Magnetic Survey

In 2008, a surface magnetic survey was conducted along two local roads (Figures 1 and 2) that divided the study area (Daniel Merriam, personal communication). Due to lack of metadata, the type of magnetometer used and the methods of processing and residualizing the data are unknown. For the purpose of this study, it is assumed that the methods for this survey are similar to those used for the surface magnetic survey undertaken at the Edgerton structure, an unconfirmed impact structure near Edgerton, Kansas (Merriam et al., 2009). For the Edgerton structure, a Geometrics G-858 MagMapper magnetometer was utilized along two local roads that divided the structure. A Geometrics G-856 Proton Precession magnetometer measured diurnal magnetic field fluctuations every 10 minutes at the confluence of the two roads. The raw measurements were corrected for diurnal variation, and the cultural noise was either manually removed and replaced by a normal earth field value or removed by wavelet analysis. The processed data were then residualized using a linear trend.

Scanned copies of the Echo Cliff structure surface magnetic survey from Daniel Merriam (personal communication) were digitized using WebPlotDigitizer Version 3.1 (Rohatgi, 2016). The digitized data (Figure 2) were then imported into Oasis montaj® 9 from Geosoft, Inc. and used as the magnetic data for the A - A' and B - B' geophysical models within GM-SYS®.

Gravity Survey

A gravity survey (Figure 14) was conducted along the same transects as the previous surface magnetic survey using a Worden gravimeter (Figure 15A). However, two sections of the previous transects were not surveyed due to hazardous conditions along a paved road and difficulties in keeping equal station spacing along a significant curve in the road. The stations were spaced every 164 feet (~ 50 meters) and were located using an open reel tape measure and marking flags (Figure 15B). The base station was located at the confluence of the two roads and was revisited approximately every hour for drift correction. At each station, the gravity measurement and time were recorded along with any special circumstances regarding that station such as proximity to bridges, ditches, or pipes.

Latitudes and longitudes of the stations were located after the survey using Google Earth Pro® 7 from Google, LLC. The WGS84 station coordinates from Google Earth Pro® were then converted to NAD83 using the West Virginia Department of Environmental Protection - Coordinate Conversion Tool Application (WVDEP, 2018). The NAD83 coordinates were then used to query The National Map - Bulk Point Query Service Version 2.0 (USGS, 2018) to output station elevations in meters.

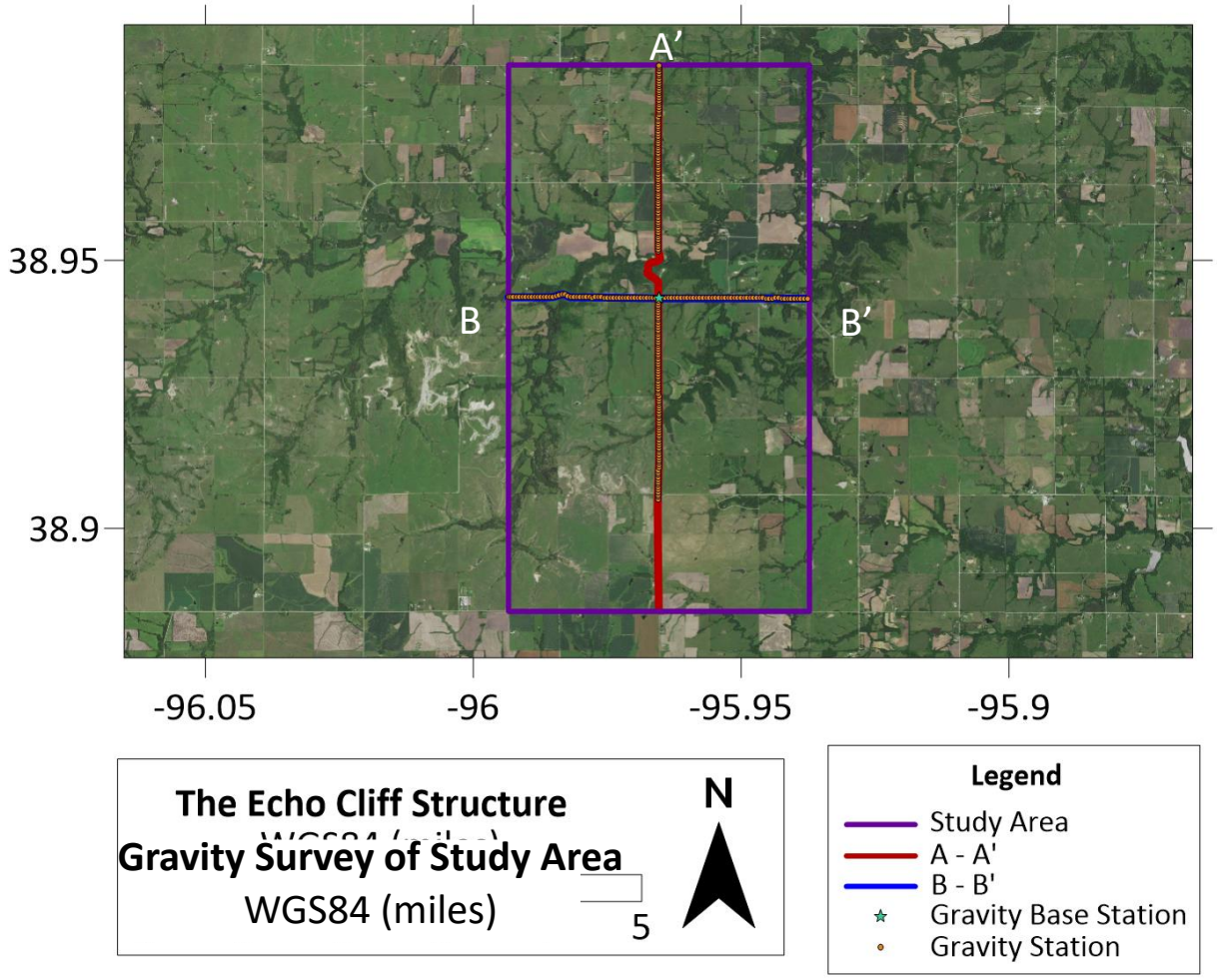

Figure 14: Study area with gravity survey base station and stations overlain. Note gaps in survey indicated by the unobstructed A - A’ transect.

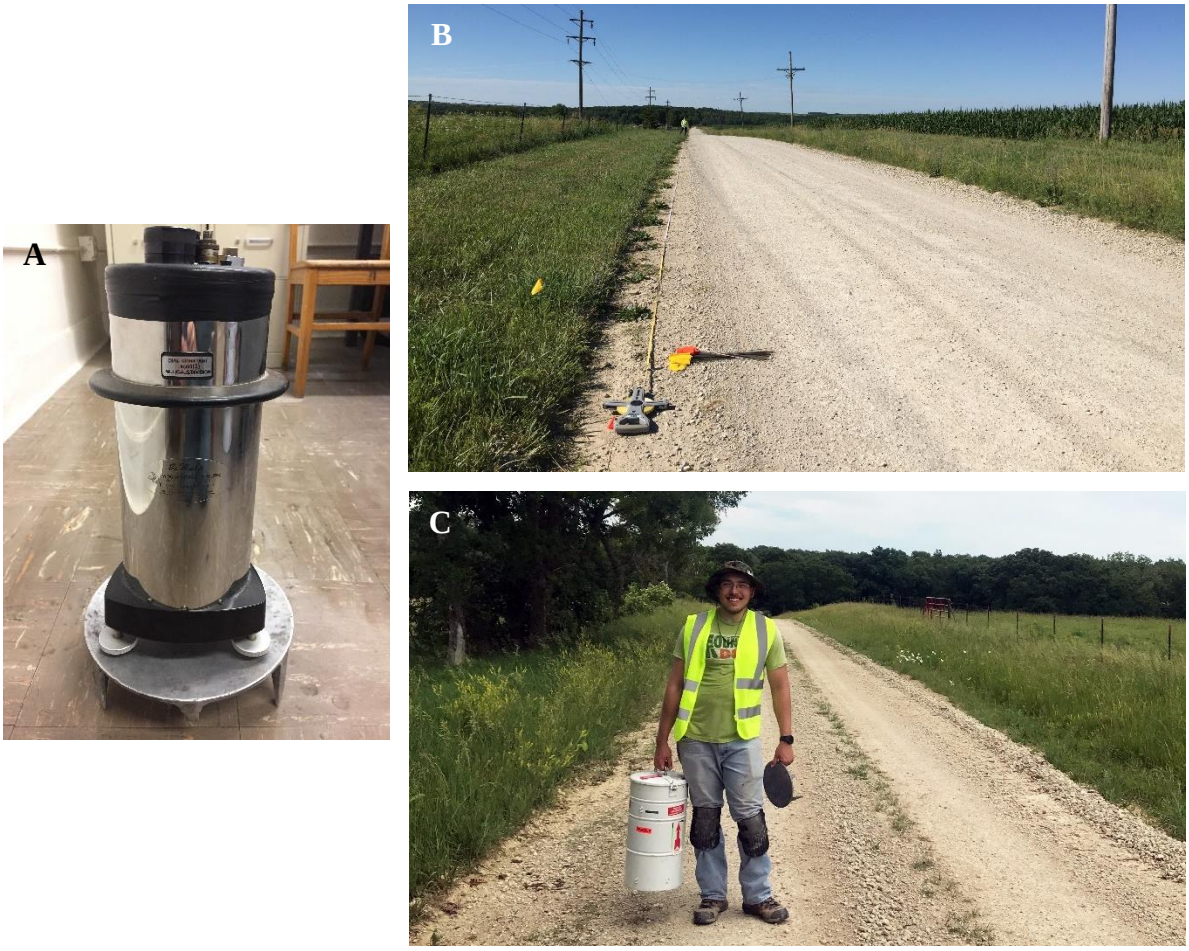

Figure 15: Equipment and methods used for the gravity survey. (A) Worden gravimeter. (B) Open reel tape measure, marking flags, and field assistant (fiancée). (C) The author conducting the gravity survey.

The raw gravity measurements (Figure 16), time and date of measurements, and station latitude, longitude, and elevation were imported into Oasis montaj® for processing. Latitude and longitude of the stations were converted from WGS84 to WGS84 UTM zone 15N within Oasis montaj®. The gravity processing mostly followed the workflow outlined in the montaj Gravity and Terrain Correction How-To Guide (Geosoft Inc., 2015). However, the gravity measurements were not converted to absolute gravity, and the free air and Bouguer anomalies were referenced to the lowest station elevation rather than sea level. The lowest station was used as a datum due to the possibility of anomaly originators being between the lowest station and sea level. For the

Bouguer anomaly, Earth density was assumed to be 2.34 g/cc. This density was arrived at using the method outlined in (Nettleton, 1939) on a hill in the northern portion of the A - A' transect.

For the terrain correction, a local DEM was created by combining the USGS NED 1/3 arc-second N39W97, N40W97, N39W96, and N40W96 1 x 1 degree ArcGrid formatted grids from The National Map Download Version 1.0 (USGS, 2018) in VTBuilder from Virtual Terrain Project. After combination, the grid was exported as an ArcInfo ASCII Grid and then converted to USGS ASCII DEM using MyGeodata Converter (GeoCzech Inc., 2018). The local DEM was then converted from NAD83 to WGS84 UTM zone 15N within Oasis montaj®. For the regional DEM, a section of the Shuttle Radar Topography Mission (SRTM) 1 Arc-Second Global elevation data between 38.77 N, -95.8W and 39.09N, -96.14W was downloaded using the Seeker tool in Oasis montaj®. The SRTM data was then converted from WGS84 to WGS84 UTM zone 15N in Oasis montaj®. For terrain correction, the local DEM was utilized for the first kilometer around a station with the regional DEM coming into effect between 1 kilometer and 166.735 kilometers. The terrain density was assumed to be 2.34 g/cc.

After processing was finished, the complete Bouguer anomalies (Figure 17) were upward continued by 385.71 meters to a 700 meter plane using the Forward Fourier Transformation Continuation Filter in Oasis montaj®. The upward continuation attenuated noise and possible data distortion from topographic relief (Xia et al., 1993). The upward continued complete Bouguer gravity anomalies (Figure 18) were not residualized due to the ability of GM-SYS® to use complete Bouguer anomalies for modeling purposes. Also, further residualization was complicated by the gap in the A - A' transect of the data and the possible addition of edge-effects in the area of interest if residualization techniques such as low-order polynomial removal were utilized.

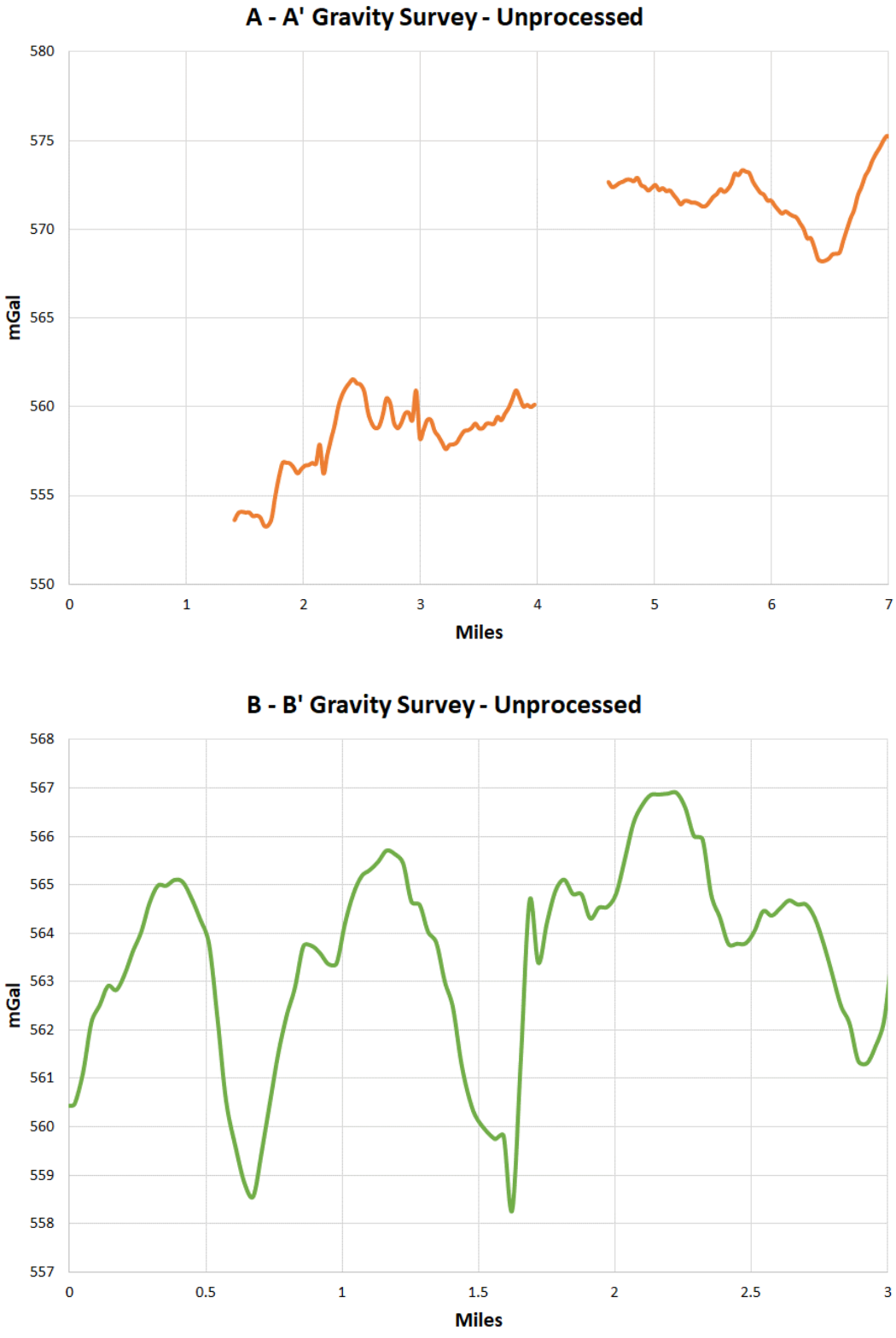

Figure 16: Unprocessed A - A' and B - B' transects of the gravity survey in the study area. The A - A' and B - B' transects intersect at ~ 4 miles and ~ 1.5 miles respectively. See Appendix B for data.

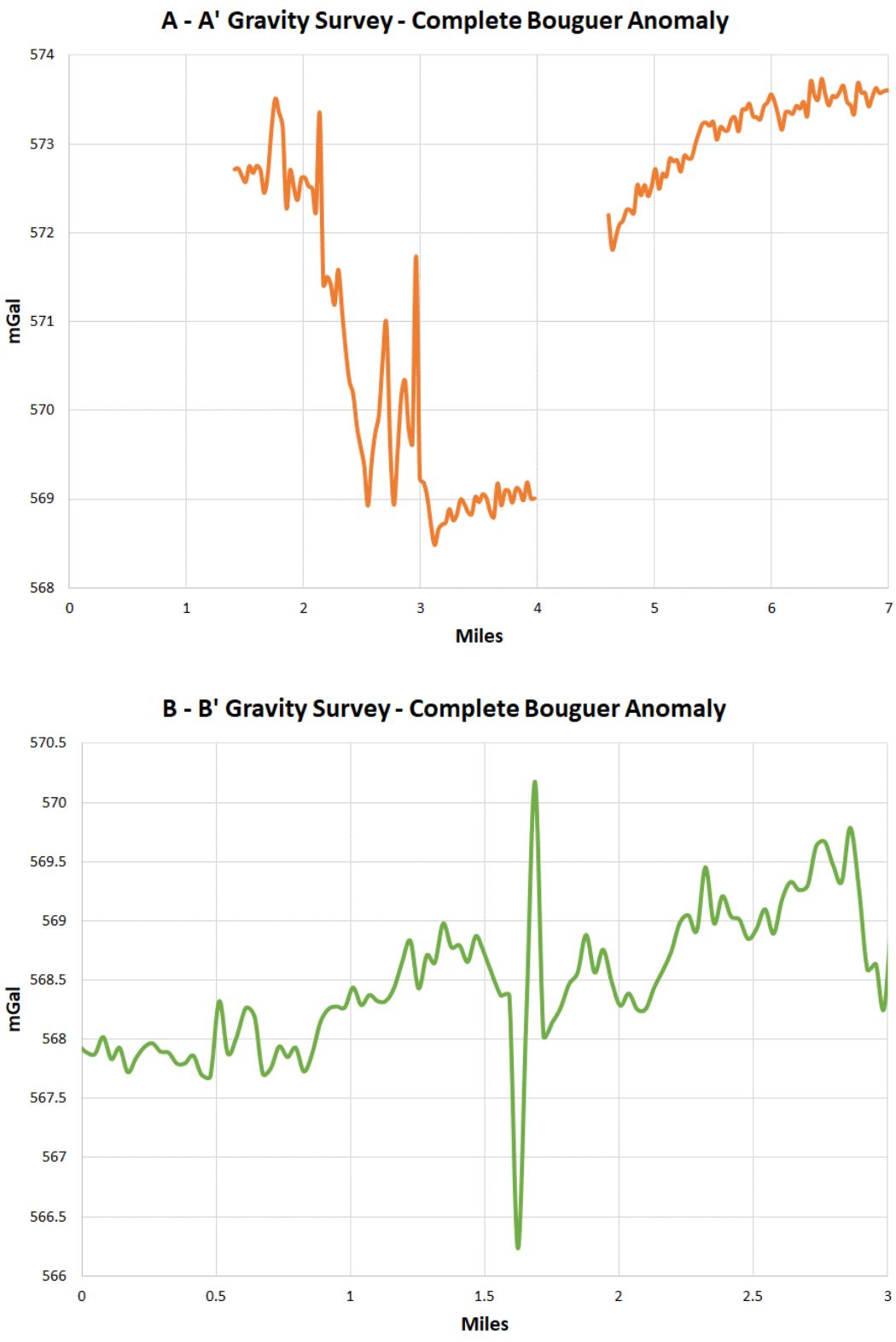

Figure 17: Complete Bouguer anomalies of the A - A' and B - B' transects of the gravity survey in the study area. The A - A' and B - B' transects intersect at ~ 4 miles and ~ 1.5 miles respectively. See Appendix B for data.

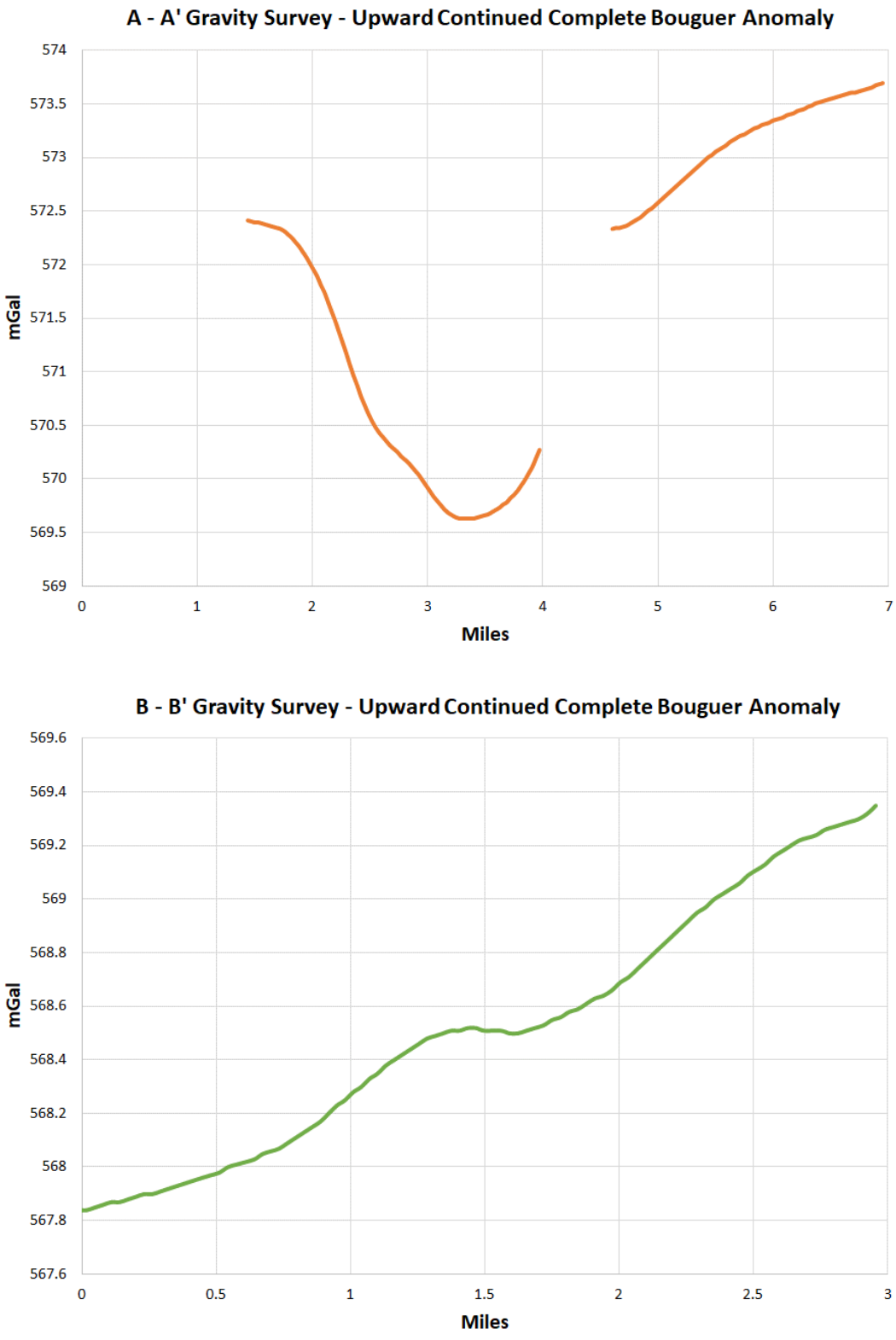

Figure 18: Upward continued complete Bouguer anomalies of the A - A' and B - B' transects of the gravity survey in the study area. The A - A' and B - B' transects intersect at ~ 4 miles and ~ 1.5 miles respectively. See appendix B for data.

Quality Control of the Surface Magnetic Survey

It was immediately apparent upon loading both the surface magnetic survey and upward continued Bouguer gravity anomalies into GM-SYS® that there were significant differences between the data (Figures 2 and 18). Significant differences are not unusual since rocks have relatively low differences in density but can have widely different magnetic susceptibilities (Hinze et al., 2012). However, some amount of correlation was expected. There were also significant differences between the surface magnetic survey and Kansas Geological Survey (KGS) aeromagnetic data of the area (Figure 19), most notably the drastic negative anomalies on the profiles in areas of positive anomalies in the aeromagnetic data. Even with the large sampling distance differences between the surveys, more correlation was expected. As a result, the surface magnetic survey was carefully inspected for possible issues.

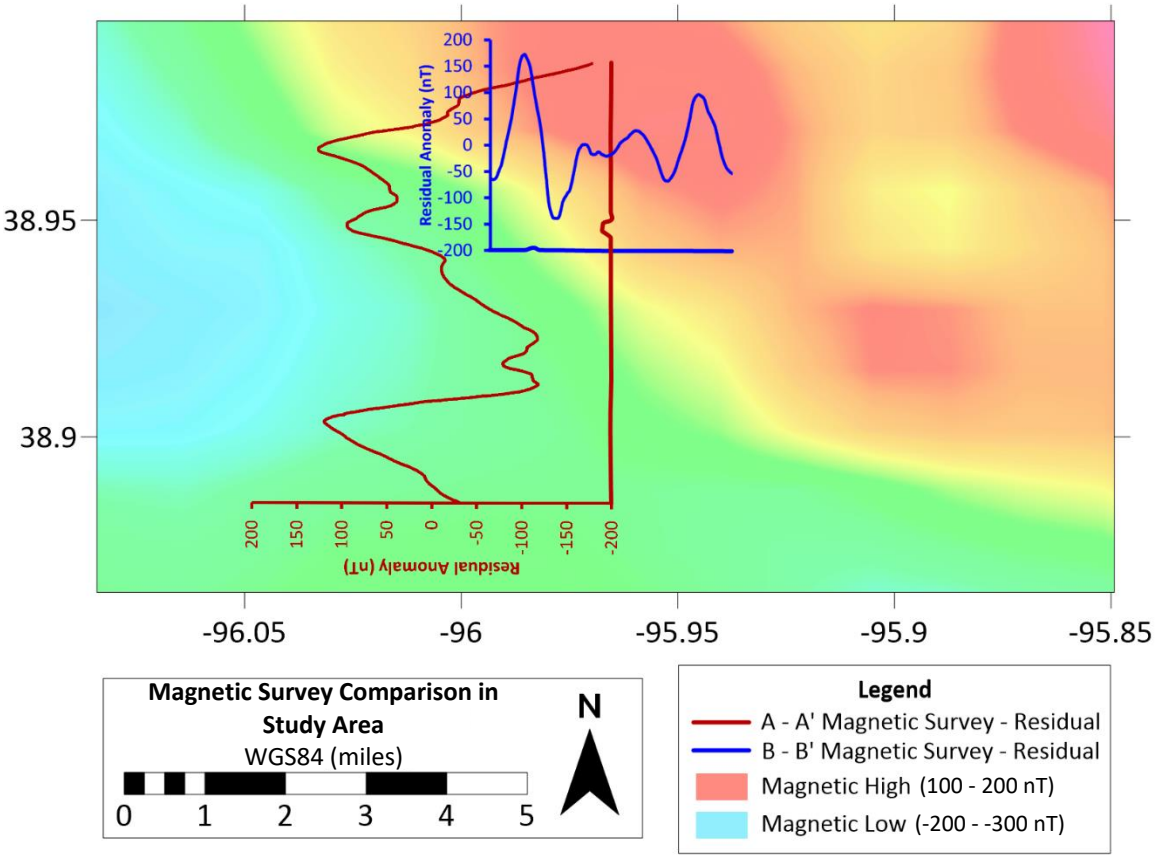

Figure 19: Comparison of A - A' and B - B' residual magnetic surveys and KGS aeromagnetic data. Note the extreme negative anomalies in the profiles and their location on the aeromagnetic data.

The first issue is the discrepancy between the graph of the A - A' transect (Figure 20A) and map of the A - A' residual magnetic data (Figure 20B). The graph of the A - A' magnetic data shows a total distance of 11,263 meters. This distance was used for plotting the surface magnetic survey on the Landsat MSS and TM analysis product, with that product used for planning the gravity survey. However, the mapped A - A' transect (Figure 20B) is only ~ 8,867 meters when measured in Google Earth Pro®. It is unknown which distance is correct for the A - A' transect, but the most likely candidate is the 11,263 meter long transect, since the magnetic data were probably recorded, processed, and plotted by the same person. The 11,263 meter long

transect was used for the purposes of this study. There was no discrepancy with the B - B' transect.

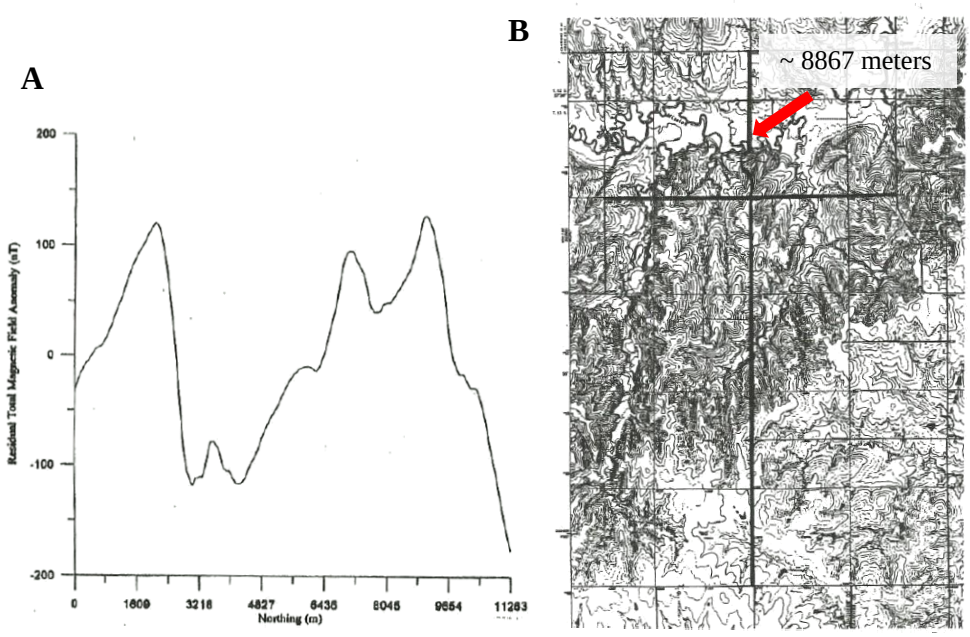

Figure 20: Discrepancy between the distance of the plotted A - A' residual magnetic survey (A) and the distance mapped for the A - A' transect (B). Modified from Daniel Merriam (unpublished data).

The second problem is the suspiciously high correlations of most relative positive anomalies with possible sources of cultural noise such as bridges and powerlines when the profiles are imported into Surfer® (Figure 21). The G-858 MagMapper magnetometer is described as highly sensitive and able to locate a variety of items including pipelines and utilities (Geometrics Inc., 2001). Again, it is unknown whether the G-858 was used for this survey. However, this magnetometer was used at the Edgerton structure (Merriam et al., 2009) and to locate abandoned brine wells in Hutchinson, Kansas (Xia, 2002). Therefore, it is very likely that the G-858 was the magnetometer used in the Echo Cliff magnetic survey and would have been sensitive enough to detect any ferric object or electromagnetic source along the transects. The noise from the ferric objects and electromagnetic sources has apparently piggybacked on the

magnetic signature of the underlying geologic structure and was not removed during processing. These positive anomalies from cultural noise were then interpreted as originating from an impact structure by (Daniel Merriam, personal communication) and (George Petersen, personal communication).

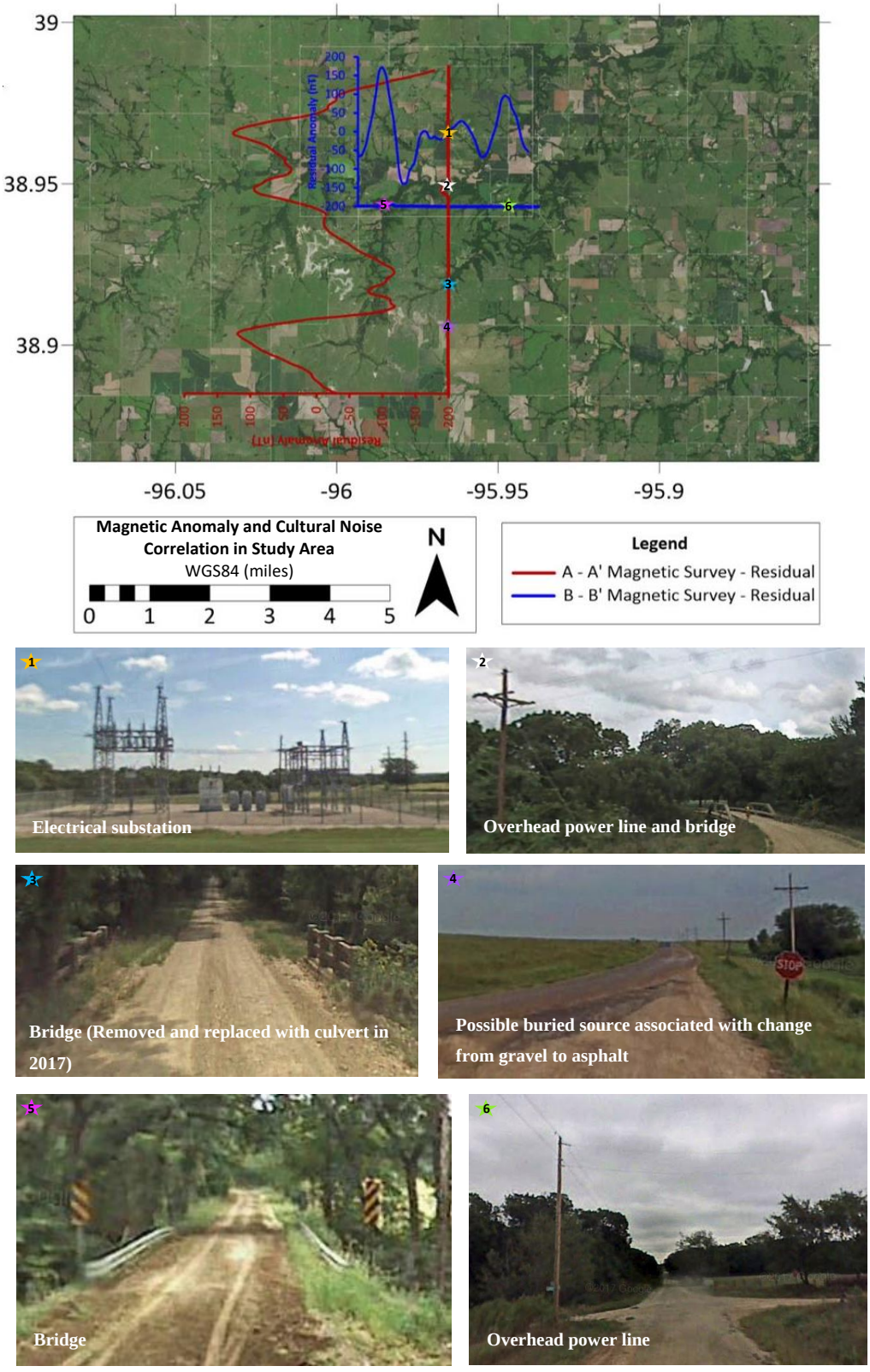

Figure 21: Suspicious correlations between residual magnetic survey relative positive anomalies and sources of possible cultural noise. Road images from Google Maps.

The final problem is the significant edge effects at the edges of the transects (Figure 22). Edge effects are artifacts introduced during the residualization process and are typically avoided during interpretation (Hinze et al., 2012). However, these edge effects were interpreted as the edges of an impact structure by (Daniel Merriam, personal communication) and (George Petersen, personal communication) and subsequently influenced later exploration. The edge effects should have been removed or at least indicated in the profiles after processing. Due to the apparent issues with the surface magnetic survey, it was abandoned for further use in modeling in GM-SYS® and replaced with an aerial magnetic survey.

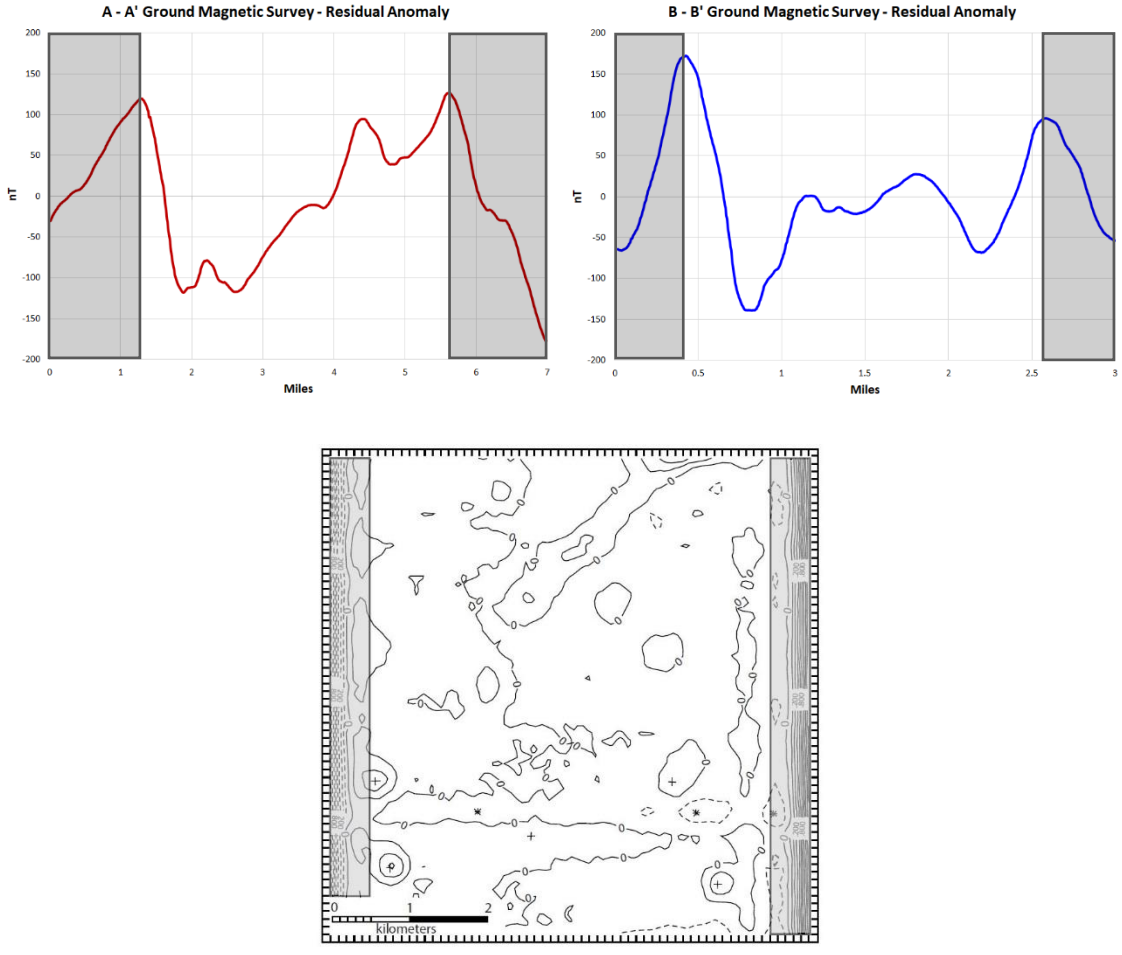

Figure 22: Edge effects in the A - A’ and B - B’ residual magnetic survey profiles with a comparison to edge effects displayed on a residual gravity anomaly map. Modified from Daniel Merriam (unpublished data) and Hinze et al. (2012).

Aeromagnetic Survey

A request was granted for aeromagnetic data by Applied Geophysics, Inc. of Salt Lake City, Utah. The donated maps (Parker Gay, unpublished data) consist of a reduced to the pole total intensity contour map, a reduced to the pole NewMag® residual contour map, and a basement shear zone interpretation map. The aeromagnetic data were collected in 1983 with a proton magnetometer with a flight elevation of 2500 feet and E - W flight lines 0.5 miles apart. The total intensity data were residualized and a basement shear zone map was produced using proprietary algorithms and techniques.

In Surfer® a scan of the residual contour map was georeferenced, converted from WGS72 UTM zone 15N to WGS84 UTM zone 15N, and study area contours were digitized. A grid was produced from the contours and exported as a GRD Geosoft Binary Grid. The grid was imported into Oasis montaj®, converted into a map, and paths of the A - A’ and B - B’ transects were overlain. Profiles of the data along the transects (Figure 23) were extracted and used as the replacement magnetic data for the A - A’ and B - B’ geophysical models within GM-SYS®.

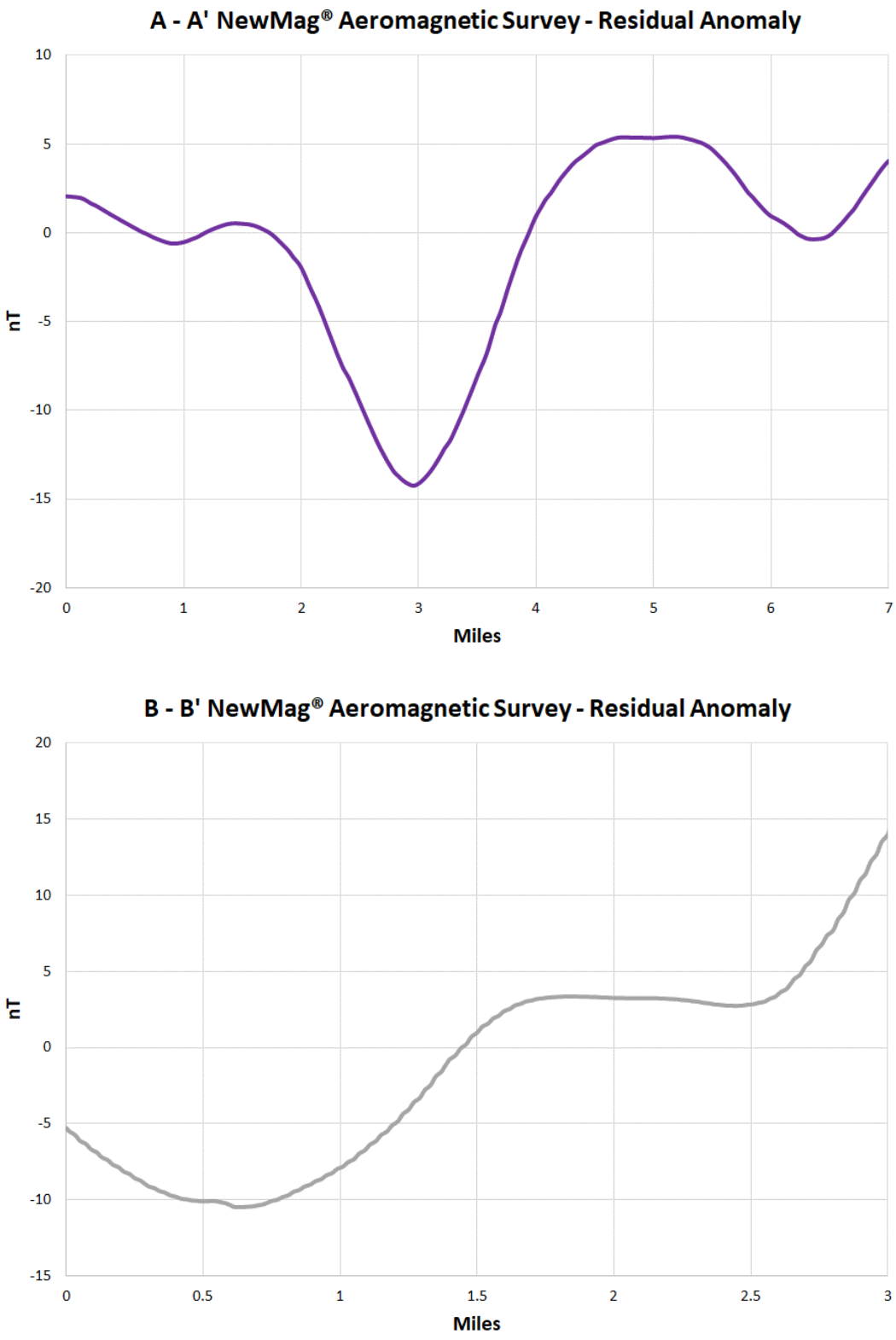

Figure 23: NewMag® residual aeromagnetic survey of the A - A' and B - B' transects. The A - A' and B - B' transects intersect at ~ 4 miles and ~ 1.5 miles respectively. Based on Parker Gay (unpublished data). See Appendix B for data.

Geophysical Models in GM-SYS®

Both A - A' and B - B' geophysical models were created using the upward continued complete Bouguer gravity anomaly data (Figure 18) and NewMag® residual aeromagnetic data (Figure 23). Modeling in GM-SYS® is done through creating and manipulating surfaces and the blocks between them. Surfaces are usually based on geologic horizons and blocks are assigned geophysical values that are presumed to be close to reality. For our model, only densities, magnetic susceptibilities, and the size and shape of blocks were manipulated. Once a density and magnetic susceptibility is assigned to a block, the geophysical response from that block is automatically calculated using previously set modeling parameters and displayed. The purpose of the modeling is to create a model that is geologically realistic and with a calculated geophysical response within an acceptable error to the measured data. It is important to remember that assigning one geophysical parameter for an entire block is an oversimplification. Rock is heterogeneous, and it is impractical to model at that level of detail. Also, geophysical responses are not unique. Many different plausible geologic scenarios can have the same geophysical response (Hinze et al., 2012).

Modeling parameters were calculated from the latitude, longitude, and elevation of the confluence of the transects and an arbitrary date of May 11, 1983, for the date of the aerial magnetic survey. A density of 2.34 g/cc was utilized for background density and everything between the topography and the elevation of the lowest station in the gravity survey. The topography was based on profiles extracted from the local correction grid previously used in the terrain correction during gravity data processing. The surfaces within the sedimentary strata were based on the adjusted well tops from the well log stratigraphic cross-section. The strata between each top were considered the block for assigning densities and magnetic susceptibilities during

modeling. For example, the Base of the Kansas City Group was the top reported above the Cherokee Group. The strata between the reported Base of the Kansas City Group and Cherokee Group is now all the Base of the Kansas City Group block for modeling purposes. The densities of the blocks were taken from the average of the average bulk density (RHOB) well log measurement between the tops in each well from the study area. For example, each bulk density measurement within the Simpson Group was noted, totaled, and averaged, and then the Simpson Group bulk density average from each well was subsequently totaled and averaged. The magnetic susceptibilities were assigned using the average magnetic susceptibly of each sedimentary rock type from the GM-SYS® User's Guide Version 4.9 (Northwest Geophysical Associates Inc., 2004).

Modeling parameters for rock below the sedimentary strata were not as constrained. No wells in the study area penetrated below the Arbuckle Group. However, basement rocks in the study area were assumed to be granite based on Xia et al. (1995). Also, basal sandstone was assumed to be between the Arbuckle Group and underlying granite due to the SS Farms "WD" 8-23 well, ~ 5 miles northwest of the study area, penetrating 20 feet into it. The density of the granite was assumed from a geophysical model within Yarger (1989), and the magnetic susceptibility was assigned from an assumption of 1% magnetite content (Xia et al., 1992) using Hemant (2003) as a reference. The density and magnetic susceptibility of the basal sandstone were assumed from an average sandstone in the GM-SYS® User's Guide Version 4.9 (Northwest Geophysical Associates Inc., 2004). Starting depth to basement parameters were based on a georeferenced and digitized Kansas Precambrian basement map (Cole, 1976) with basal sandstone filling the area between the Arbuckle Group and granite. The Arbuckle Group thickness was based on the extent of the Arbuckle Group in the SS Farms "WD" 8-23 well.

Shear Zone Analysis

The donated basement shear zone interpretation map was scanned and then georeferenced in Surfer®. The coordinate system was converted from WGS72 UTM zone 15N to WGS84 UTM zone 15N. The scanned and georeferenced shear zone interpretation map was then used as the basis for polylines for mapping purposes. The Kansas Earthquake Database, a record of earthquakes in Kansas from 1977 to Aug. 5, 2017 (KGS, 2017), was downloaded and converted into a KML file using the Excel to KML tool on the Earth Point website (Earth Point, 2018). The earthquake epicenters were then imported into Surfer® and displayed as point vectors. Geologic structure maps of Kansas and Missouri were also georeferenced and displayed in Surfer® to facilitate in mapping tectonic zones near the study area.

Well Log Stratigraphic and Structural Cross-section

Digital (LAS) files from three wells in the study area (Dorothy Wendland 1, Phillip Wendland 1, and Andrew Wendland 1) were imported into Petrel® 2016 from Schlumberger Limited. Additionally, LAS files from a well North of the study area (Adams "A" 1) and a well south of the study area (Thompson 1-33) were also imported. The Thompson 1-33 LAS file was produced from a scanned well log image that was digitized in Didger® 5 from Golden Software, LLC. All the LAS files and the scanned well log were downloaded from the Kansas Geological Survey database (KGS, 2018).

The reported formation tops from the imported wells were entered into Petrel®, compared to the gamma ray curve, and adjusted accordingly. The matched curve deflections were then utilized to pick formation tops from the Adam "A" 1 and Thompson 1-33 gamma ray logs. The wells and corresponding gamma ray curves were then displayed in a Petrel® well cross-section window from the southernmost to northernmost well and hung off of the Maquoketa (Sylvan)

Shale top to create a stratigraphic cross-section. A structural cross-section was also produced by hanging the geologic units off of sea level.

Binocular and Petrographic Analysis of Drill Cuttings

Drill cuttings were donated by George Petersen for both the Andrew Wendland 1 and Dorothy Wendland 1 wells (Figure 24A). The Simpson Group interval plus an additional two bags from above and below the interval were identified and separated for cleaning. The usual increments for the drill cutting bags were 10 foot intervals unless a sample circulation occurred or total depth (TD) was reached. Each of the separated bags of drill cuttings was then washed and wet sieved into > 1 millimeter (coarse sand), > 125 microns (medium sand), and > 63 microns (fine sand) sizes (Figure 24B). No solvents were used during the washing and grain sizes < 63 microns were not captured, due to difficulties in saving the material. The sieved cuttings were then washed into labeled, folded paper towel cones for drying. After drying, the sieved cuttings were placed in labeled manilla envelopes (Figure 24C) and examined for PDFs (Figure 24D).

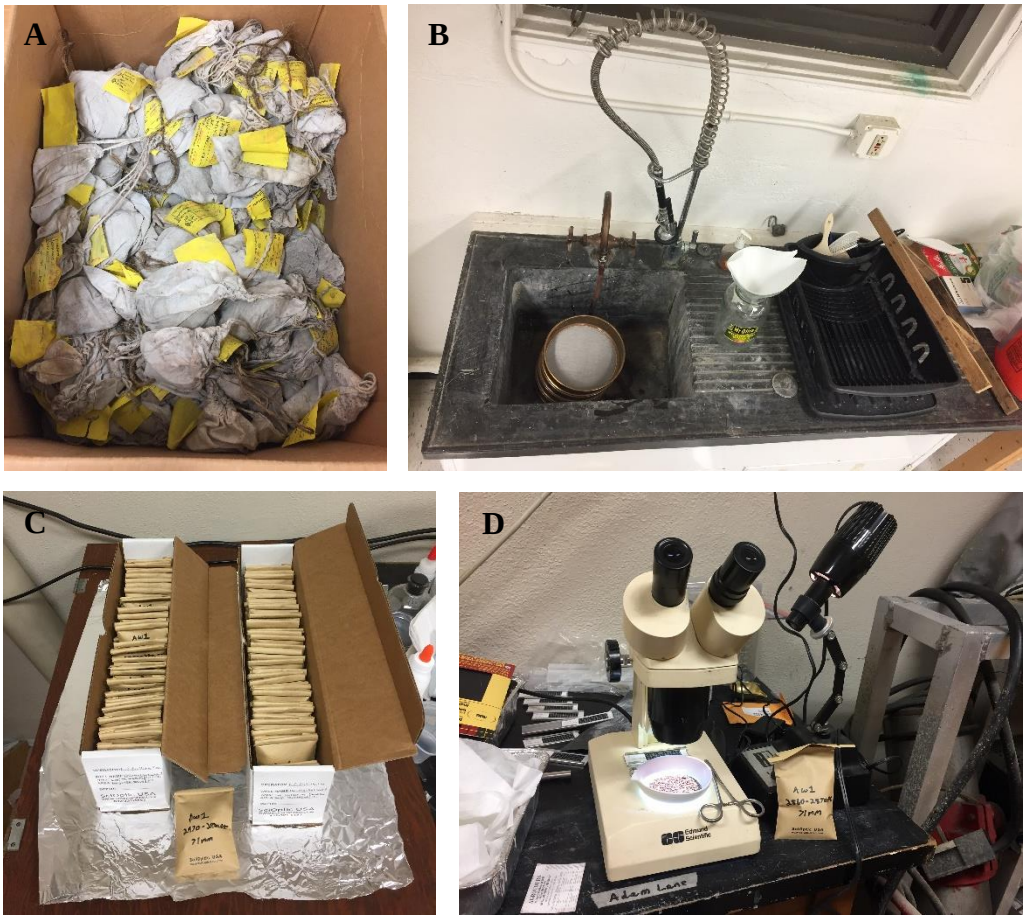

Figure 24: The drill cutting cleaning and sorting process. (A) Unprocessed drill cuttings. (B) Area of washing and wet sieving. (C) Sorted and packed drill cuttings. (D) Stereo microscope used for examination.

In a similar process to Herrmann (2009), clove oil was placed on quartz sand aggregates from the > 1mm cuttings and examined for planar deformation features using an Edmund Scientific 1x - 3x stereo microscope (Figure 25). Clove oil has a similar refractive index to quartz. In clove oil the quartz grains appear translucent, leaving anything within the grain such as fractures and inclusions readily observable. Due to limitations in the power of the stereo microscope, it was decided that thin sections were needed for conclusive analysis.

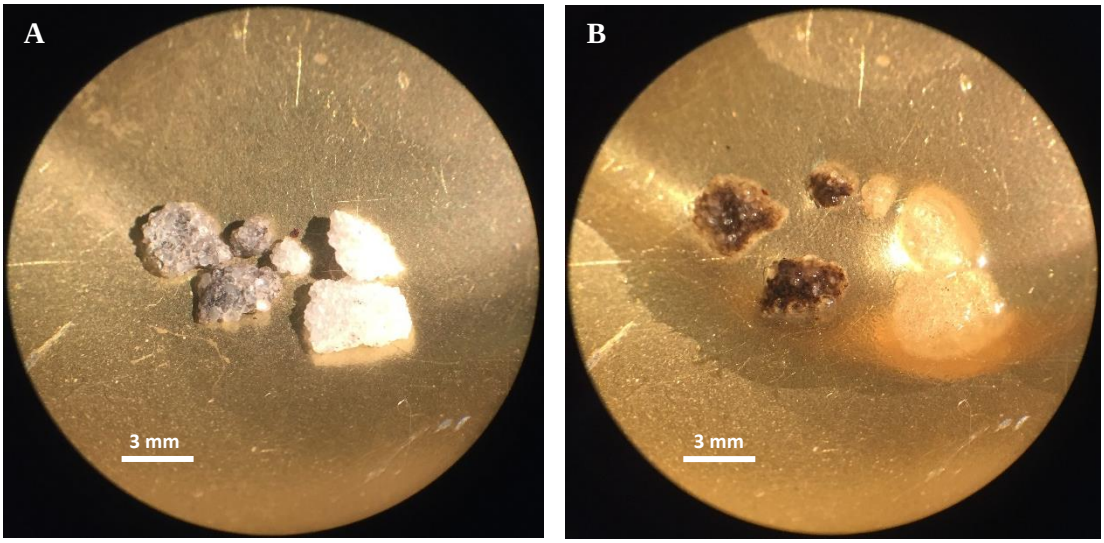

Figure 25: Quartz sand aggregates from Andrew Wendland 1. (A) Before clove oil droplet. (B) After clove oil droplet.

For each bag of drill cuttings from the Simpson Group interval of Andrew Wendland 1, six to seven thin sections were produced. Five from the > 63 microns (fine sand), one from the > 125 microns (medium sand), and one from the > 1 millimeter (coarse sand). The > 1 millimeter (coarse sand) thin section was only produced if sand aggregates were found in that size range. The variation in sand aggregates is due to the amount of sand varying within the analyzed interval. For the Dorothy Wendland 1 cuttings, the sandiest 10 foot interval was targeted to produce 12 thin sections of > 63 micron and two thin sections of > 125 micron cuttings.

To produce the thin sections, two different processes were used for mounting the cuttings. For the Dorothy Wendland 1 thin sections, the drill cuttings were placed directly on the frosted slides and resin was poured over top of them. For the Andrew Wendland 1 thin sections, the drill cuttings were placed in labeled plastic ice cube trays and immersed in epoxy (Figure 26A). After the resin set, the drill cutting plugs were labeled and removed from the trays. The bottoms of each plug were then sanded using 400 grit sandpaper to flatten the plug bottom and decrease the chances of the plug being plucked off during grinding. Glass slides were then

frosted using the grinder on a Hillquist thin section machine to decrease plucking of the epoxy plugs. After drying, the frosted glass slides were labeled using a diamond tipped engraver, and the sanded epoxy plugs were attached using more fiberglass resin (Figure 26B). Later, the excess resin was cut off using the thin section machine saw (Figure 26C).

Both sets of thin sections were finished by grinding to the point that light could pass through any quartz grains but not to the standard 30 micron thickness. The nonstandard grinding was due to the impossibility of grinding all cuttings within the thin section down to the same thickness at the same time; some quartz grains were “deeper” in the thin section than others. The thin sections were then finished by attaching a coverslip using more fiberglass resin. Finally, the finished thin sections were examined using a Leica DM EP 5x - 40x polarizing microscope (Figure 26D).

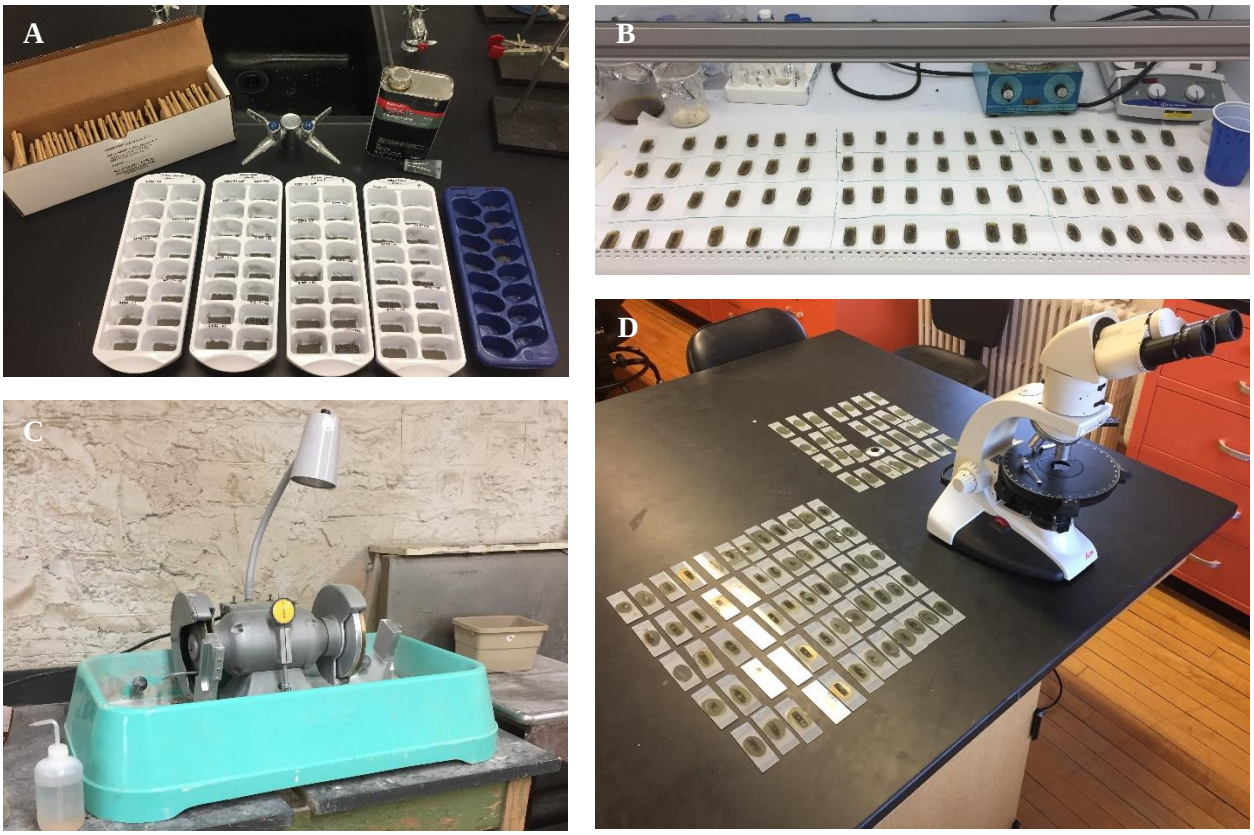

Figure 26: The thin section production process. (A) Drill cuttings in ice cube trays ready to be immersed in resin. (B) Drill cutting plugs drying in a fume hood after attachment to frosted slide. (C) The Hillquist thin section machine used for frosting slides, sawing, and grinding. (D) The finished thin sections ready for examination.

Chapter 5 - Results and Discussion

Well Log Structural and Stratigraphic Cross-Sections

The structural cross-section (Figure 28) provides a view of the current relationship of geologic units in the study area and beyond. It is important to note the general lack of relief in the structural cross-section. Within the study area, the maximum relief observed is ~ 20 feet between well tops in adjacent wells. The thickness of the geologic units also stays consistent along the transect. There are also no geologic units unique to the study area that could be interpreted as material deposited immediately after an impact event.

Using the smallest diameter of the ovoid drainage feature as a reference (~ 1.65 miles) and a third of that diameter for crater depth (French, 1998), an approximately half-mile-deep crater should have been excavated by such an impact. This ~ 0.55-mile-deep crater could then have been modified through slumping of the rim and deposition of crater-fill breccia (French, 1998). The final result would be a ~ 1.65 mile wide crater with a total depth of ~ 0.55 miles and an apparent depth of ~ 0.28 miles due to infilling. If the Echo Cliff structure is Ordovician (same age as Ames and associated events) and struck during deposition of the Simpson Group, then the Arbuckle Group, ~ 70 feet below the Simpson Group, would have been completely obliterated. This ~ 0.28-mile-deep crater would have significantly affected sediment deposition postdating the impact.

A stratigraphic cross-section hanging off the Maquoketa (Sylvan) Shale (Figure 29) reveals what the study area and beyond may have looked like immediately after deposition of the Maquoketa, the geologic unit that would have immediately postdated the impact. There is no significant thickness change within the Maquoketa, and relief of lower lying units within the study area is between 2 - 3 feet. At the Ames structure, a preburial stratigraphic cross-section

(Figure 30A) exhibits significant relief and complete annihilation and mixing of geologic units within the structure. Figure 30B documents geologic units at the Ames structure that were destroyed upon impact and post-impact units that were affected by infilling and compaction within and over the structure. The Ingalls structure, a proposed impact structure near Ingalls, Oklahoma (Herrmann, 2009), also exhibits significant relief stratigraphic changes within the proposed structure (Figure 31).

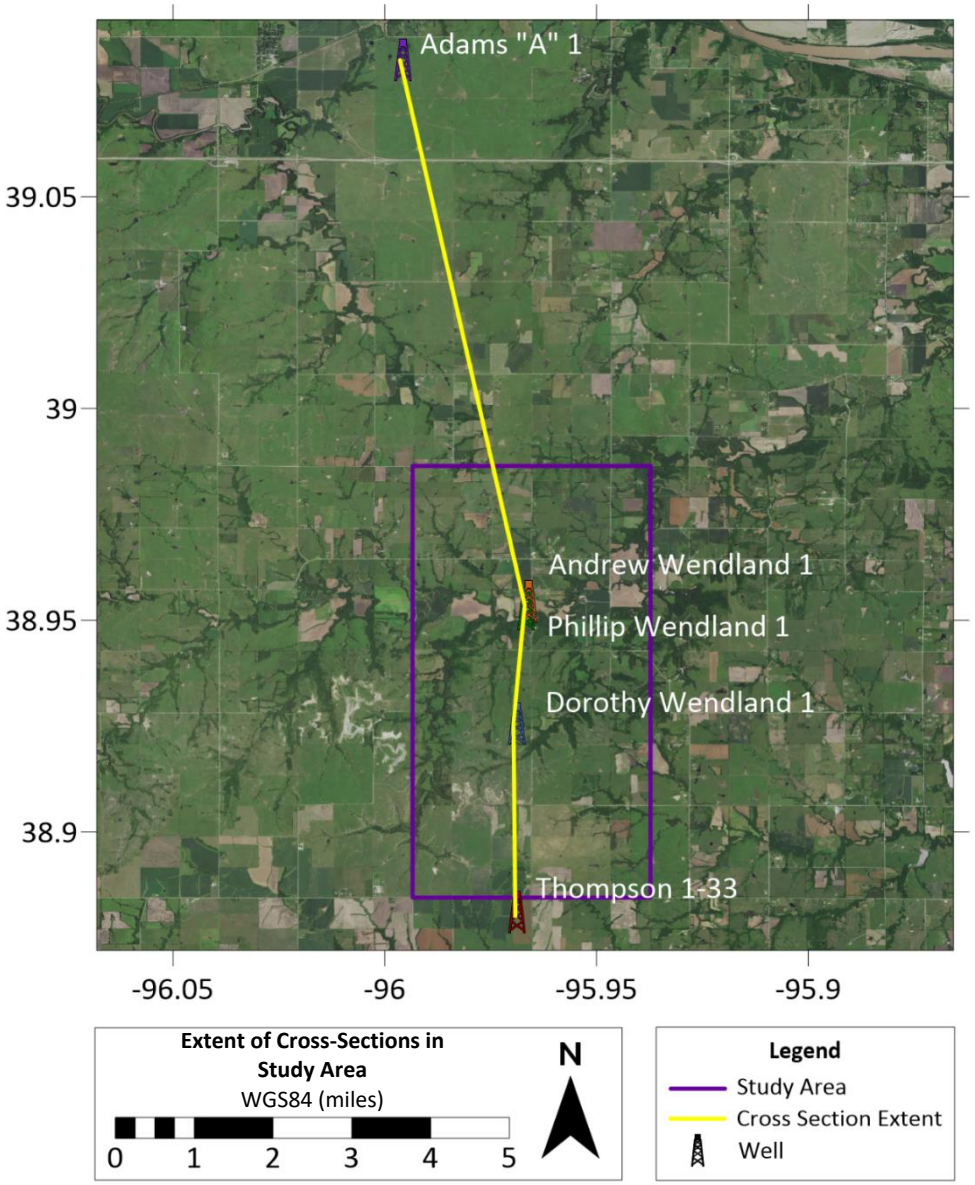

Figure 27: Extent of the cross-sections (Figures 27 and 28) within and beyond the study area.

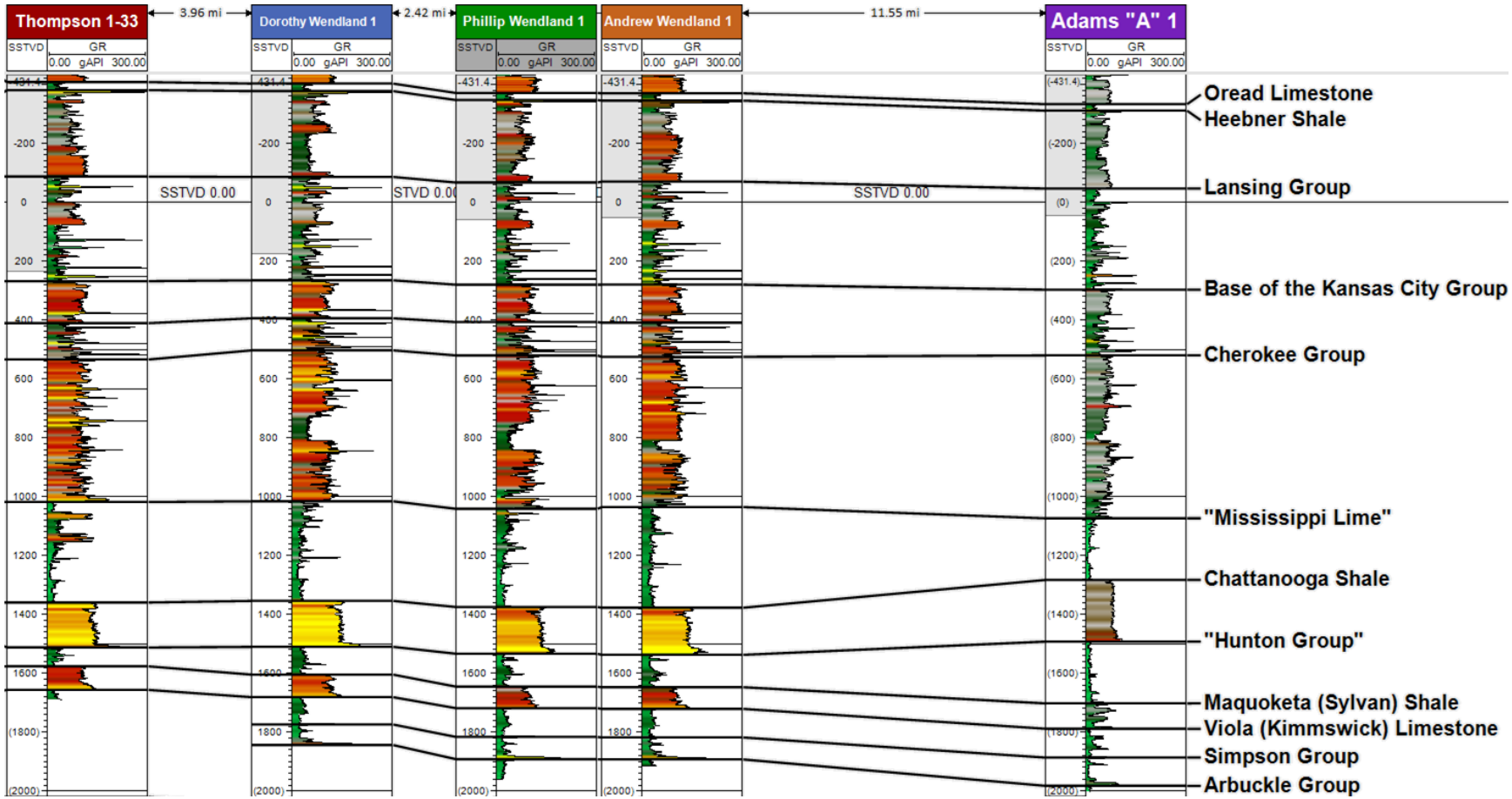

Figure 28: Structural cross-section within and beyond the study area. See Appendix A for tops data.

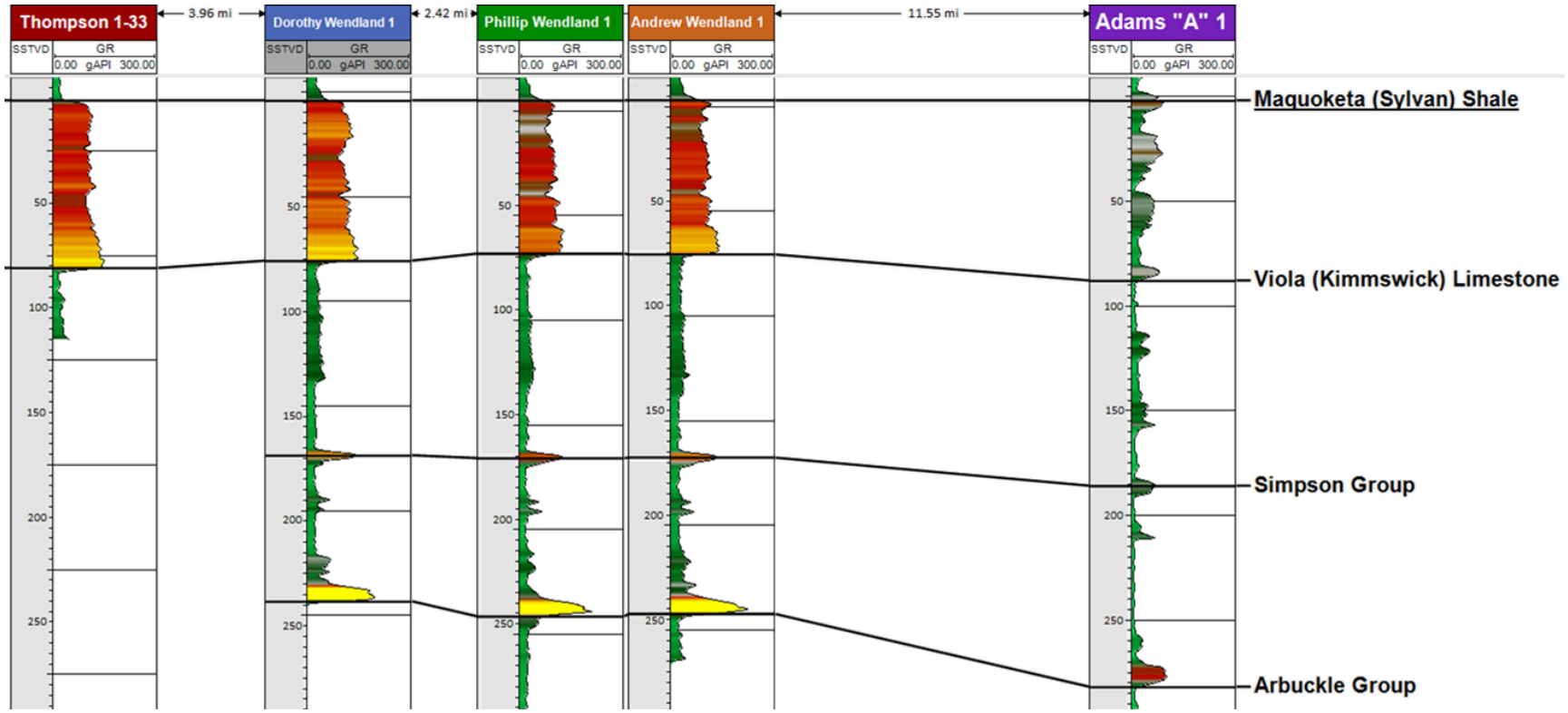

Figure 29: Stratigraphic cross-section, hung off the Maquoketa (Sylvan) Shale, within and beyond the study area. See Appendix A for tops data.

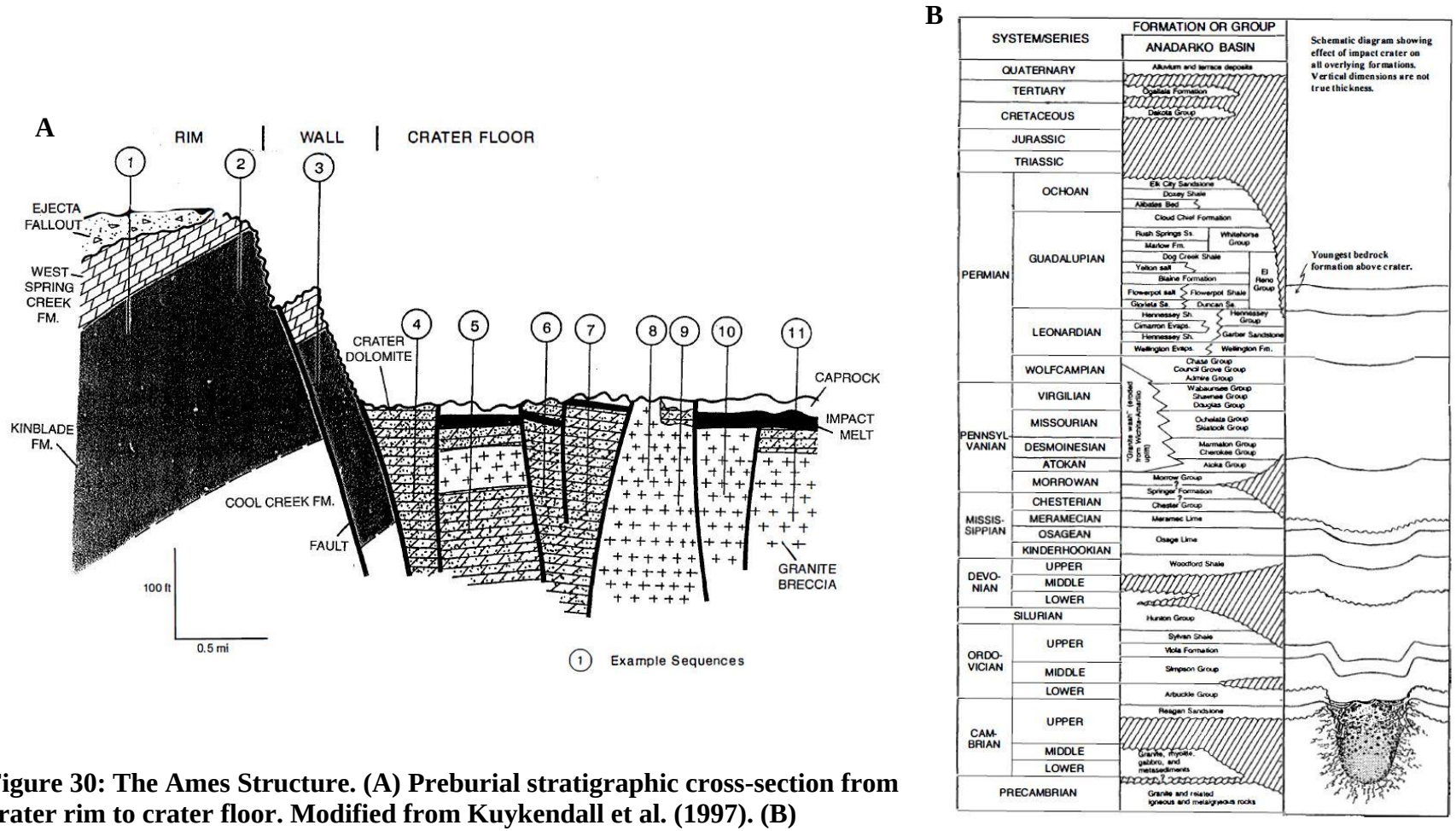

Figure 30: The Ames Structure. (A) Preburial stratigraphic cross-section from crater rim to crater floor. Modified from Kuykendall et al. (1997). (B) Stratigraphic column for the Anadarko basin modified to show formations affected by the Ames Structure. Modified from Carpenter and Carlson (1997)

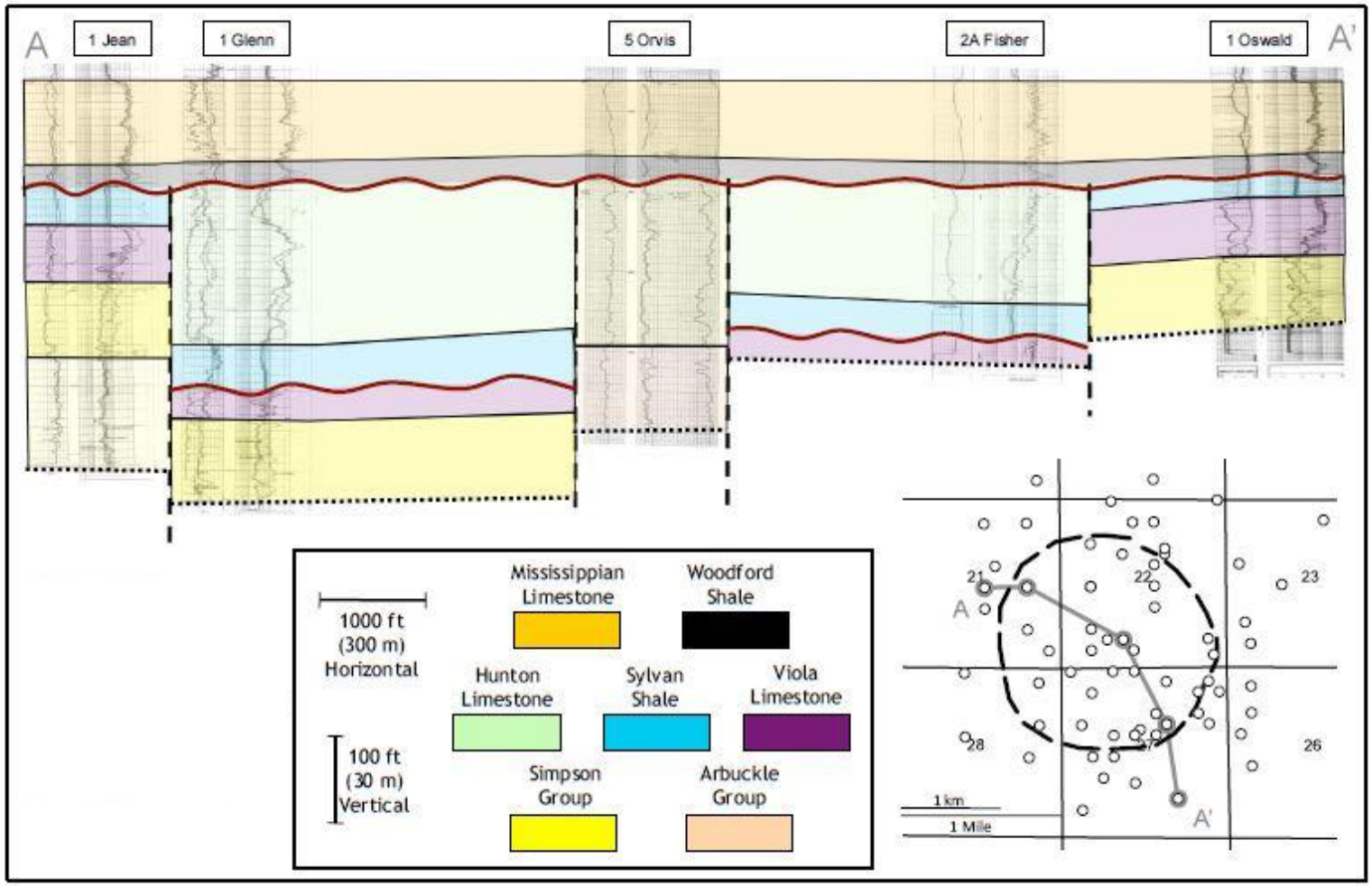

Figure 31: Cross-section through the proposed Ingalls structure. The structure is outlined on the inset map. Modified from Herrmann (2009).

Shear Zone Analysis

The georeferenced and digitized basement shear zone interpretation map revealed some possible basement shear zones that cross the study area (Figure 32). The proximity of the overlain earthquake epicenters to the interpreted basement shear zones presumably indicates faults that have been recently active, within the last ~ 40 years. More of these shear zones are presumably active but have not been recorded historically. Observations of stream polylines in the area seem to indicate a weak correlation between stream drainages and interpreted basement shear zones. The correlation is inferred to indicate faulting in the Permian surface rocks that have weathered and become the path of least resistance for surface runoff. Also, the pattern of shear zones in the study area seems to resemble en echelon faulting (Figure 33) which is indicative of a strike-slip system (Grechishnikova, 2017).

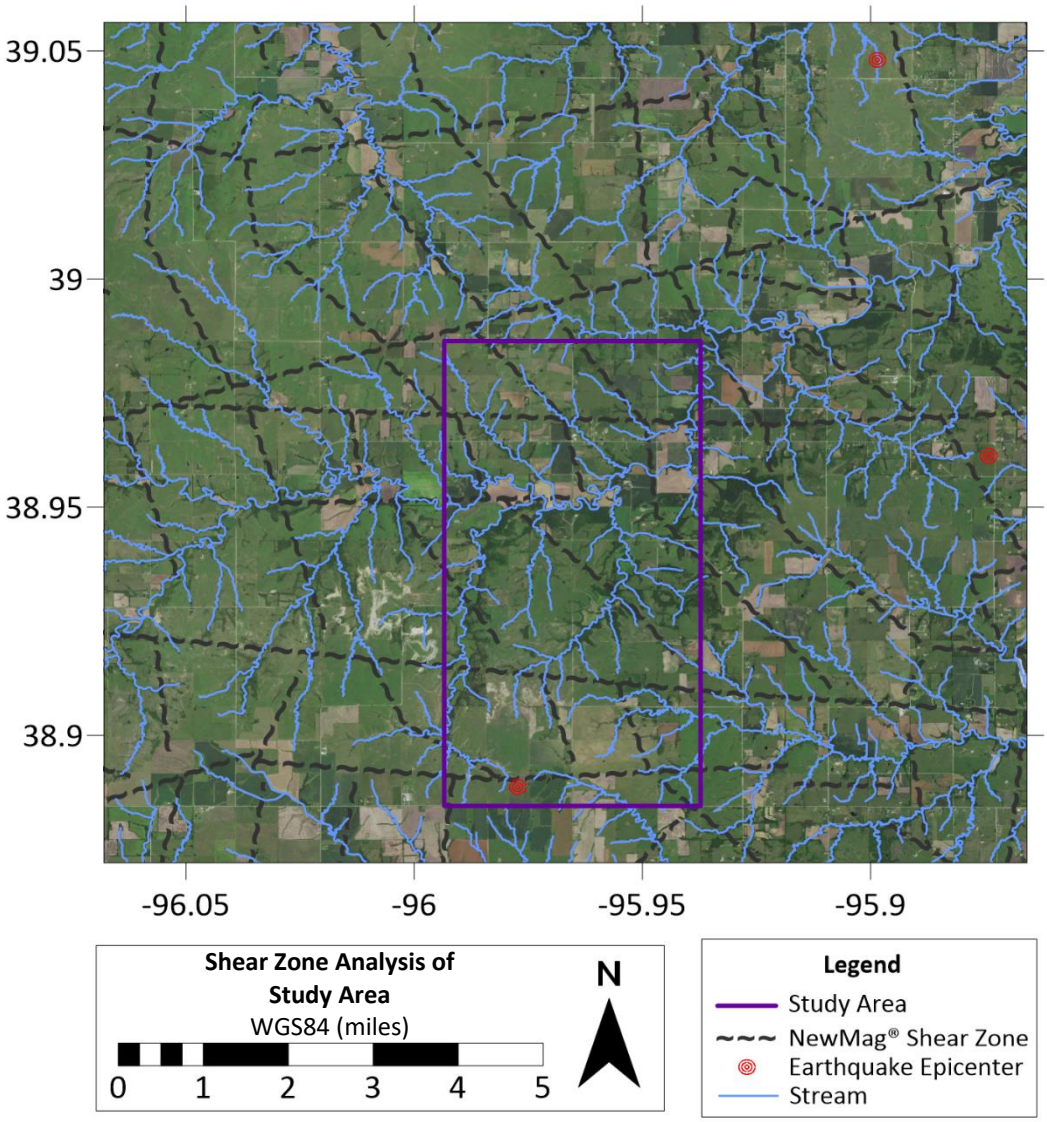

Figure 32: NewMag® basement shear zones, earthquake epicenters, and streams in and around the study area. Based on Parker Gay (unpublished data).

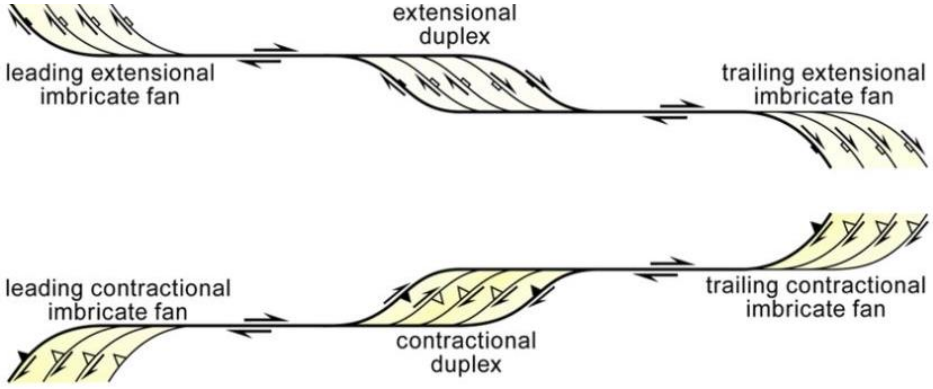

Figure 33: Idealized strike-slip system. Modified from Grechishnikova (2017)

The Bolivar-Mansfield Tectonic Zone (BMTZ) is a complex zone of faults and folds mapped in Paleozoic (McCracken, 1971) and basement rocks in western Missouri (Kisvarsanyi, 1974) and eastern Kansas (Cole, 1976). At the Kansas-Missouri state line, the BMTZ is the northern boundary of a 50 km-wide graben filled with ~ 1000 feet of basal sandstone (Kisvarsanyi, 1984). The extent of the BMTZ is defined by the previously mentioned mapped faults and folds, but also by high magnetic anomalies presumed to be intrusions emplaced along faulting in the zone (Kisvarsanyi, 1984) and by a low gravity anomaly (Cox 1988). En echelon faulting occurs in Paleozoic rocks above the BMTZ, with earthquakes recently occurring along the trend (Cox, 1988). The trend of the BMTZ in relation to the study area (Figures 34 and 35) reveals that the BMTZ passes directly through the southern portion of the study area (Baars, 1995) and is presumably the cause of the en echelon faulting observed in the NewMag® basement shear zone interpretation map. Presumably geophysical effects of the BMTZ are recorded in the NewMag® residual aeromagnetic survey and gravity survey of the A - A' and B - B' transects.

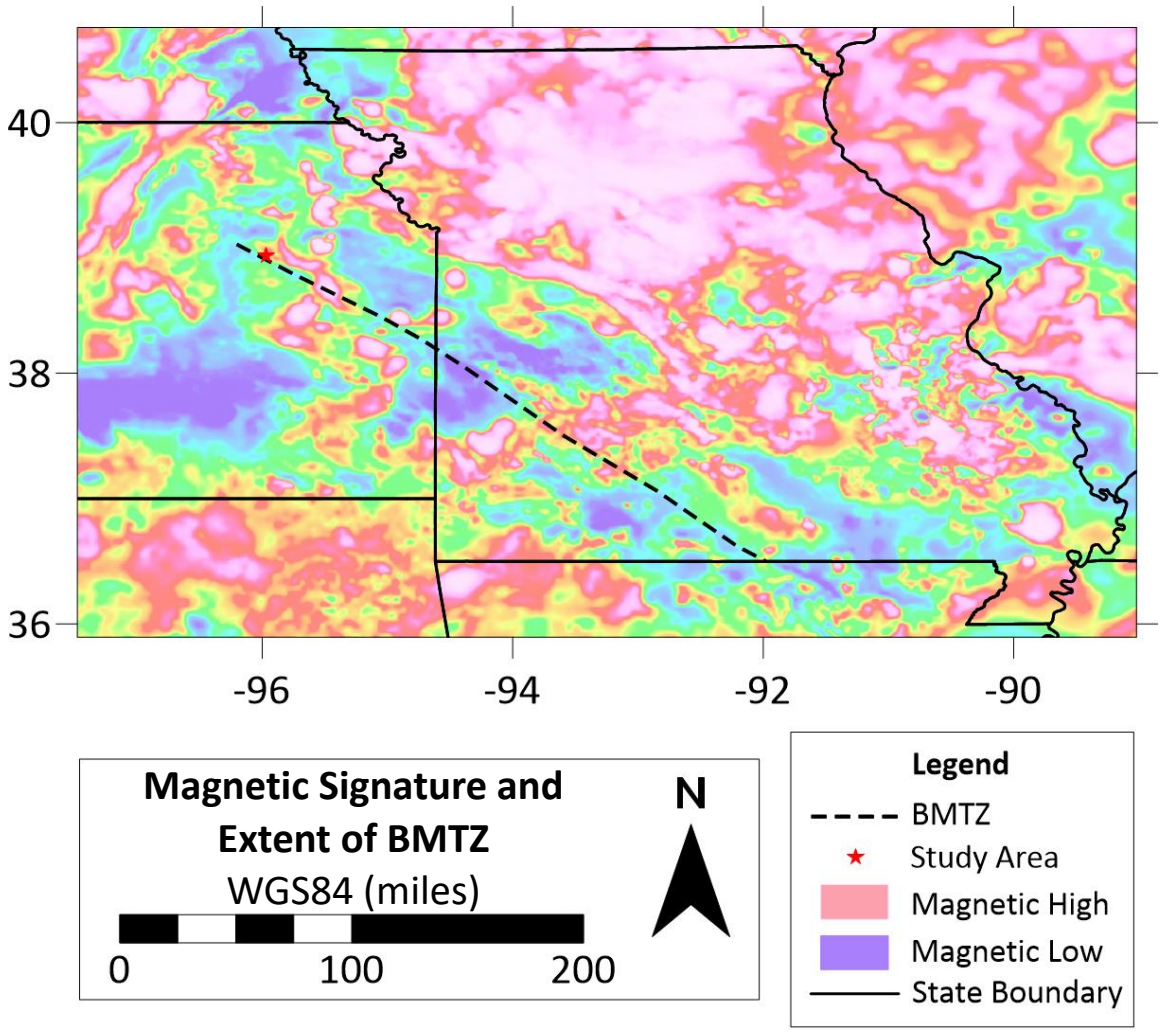

Figure 34: The BMTZ in relation to the study area. Residual magnetic anomalies are also displayed. Based on Baars (1995) and Kisvarsanyi (1984).

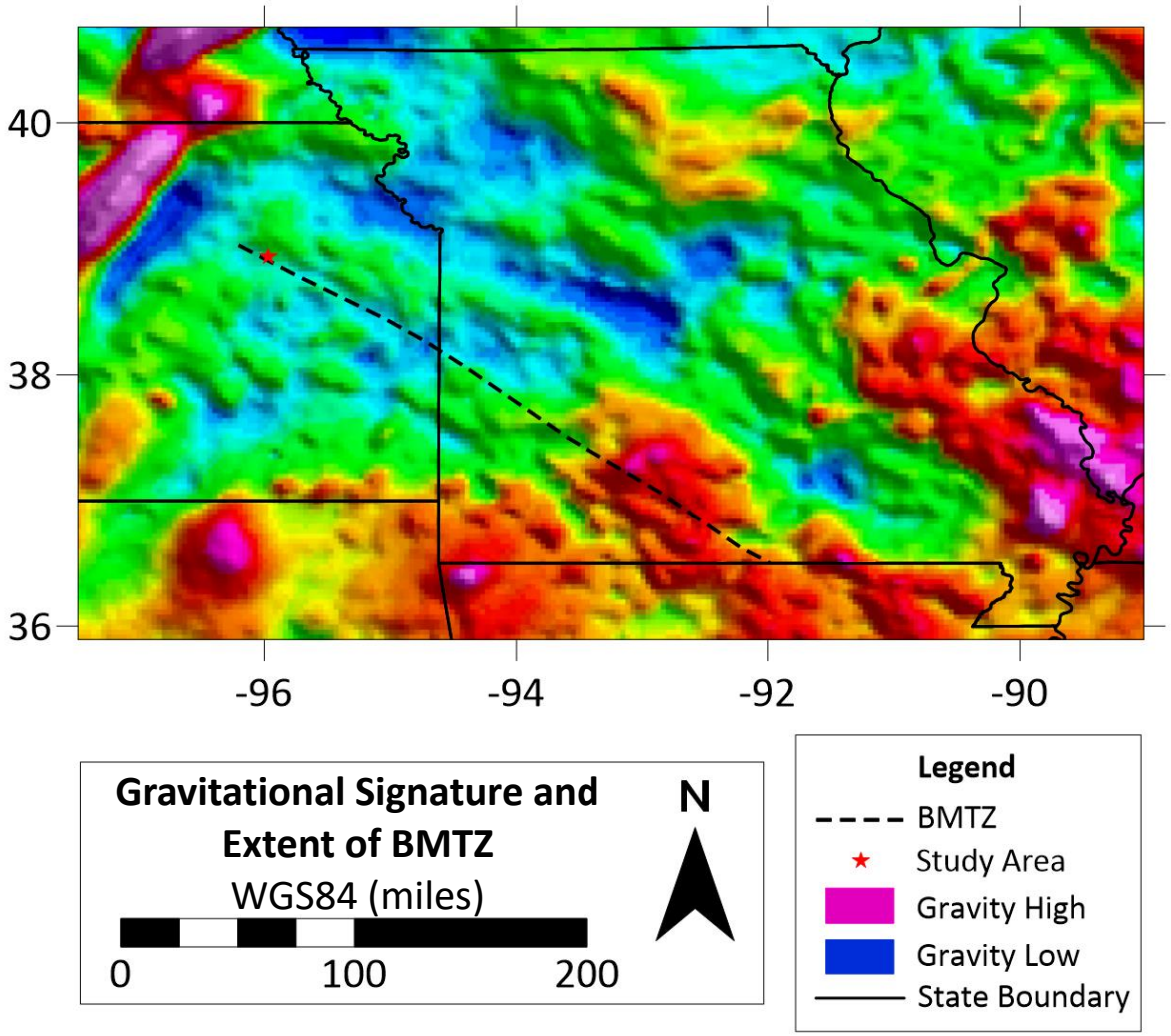

Figure 35: The BMTZ in relation to the study area. Isostatic gravity anomalies are also displayed. Based on Baars (1995) and Kisvarsanyi (1984).

Geophysical Models in GM-SYS®

The geophysical models in GM-SYS® (Figures 36 and 37) indicate that the gravitational and magnetic anomalies recorded along the A - A' and B - B' transects are possibly caused by variation in basement topography, cataclastic granulation of basement rocks due to faulting, and deposition of a thick basal sandstone over the basement. This contrasts with the geophysical model of the Ames structure (Figure 38), whose geophysical profile is primarily caused by brecciation of sedimentary and basement rocks by a confirmed impact event. The sedimentary cover observed in the structural cross-section (Figure 28) has a minimal effect on modeling of the observed anomalies. The offset of geologic units observed in the cross-section was imported into the model, but the offset is essentially nonexistent due to the scale of the model. The low-density area in the basement rocks along the A - A' transect is presumed to be less dense due to faulting and cataclasis of the rocks in the BMTZ. Magnetic susceptibility of this area was presumably not affected, resulting in the basement topography in that area to be deeper to accommodate for the magnetic low. This low basement topography is possibly caused by erosion of the faulted basement rock, which accommodated deposition of the thick basal sandstone layer. The basement in the B - B' model was assumed to be the same density as the less dense area of A - A' due to intersection of the B - B' transect at that location. The step-wise pattern of the basement observed in the B - B' model may be due to down dropped blocks from the en echelon faulting observed in the NewMag® shear zone map (Figure 32). The greater depth to basement in the western portion of the transect is consistent with the previously mapped interpretation of the Precambrian in the area (Cole, 1976), which is a general increase in depth from east to west. It is important to note that the magnetic highs on the A' and B' end members of the models match with observed magnetic highs on the regional magnetic map (Figures 34, 36, and 37) and are

presumably caused by the epizonal granite observed in (Figure 6). This epizonal granite is consistent with areas of high magnetic anomalies along the trend of the BMTZ which are interpreted as intrusions intruded along faults. The gravitational low observed in the A - A' model is also in general agreement with the low gravitational trend observed along the BMTZ (Figures 35 and 36).

It is important to note that the observed geophysical anomalies are not unique and could be created by a different subsurface interpretation. For example, the densities and magnetic susceptibilities assigned to blocks and the general shape of the blocks could vary and still approximate the same anomaly. It is possible that an impact structure below the Arbuckle Group exists and is influencing the geophysical anomalies observed. However, until a seismic survey or a well to basement is drilled in the study area, the geophysical models will remain unconfirmed.

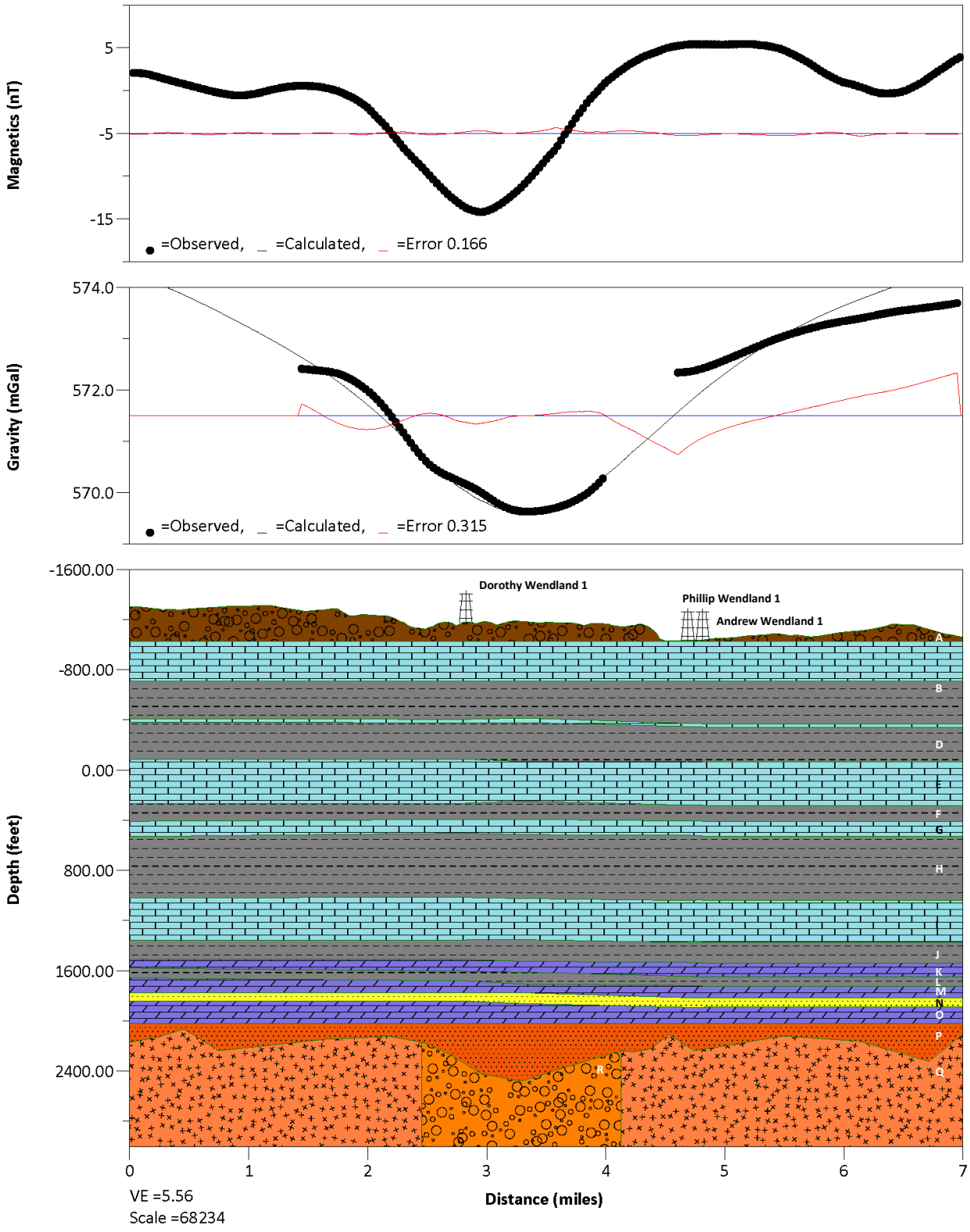

Figure 36: A - A' GM-SYS® geophysical model. Letters represent blocks. See Appendix C for model parameters.

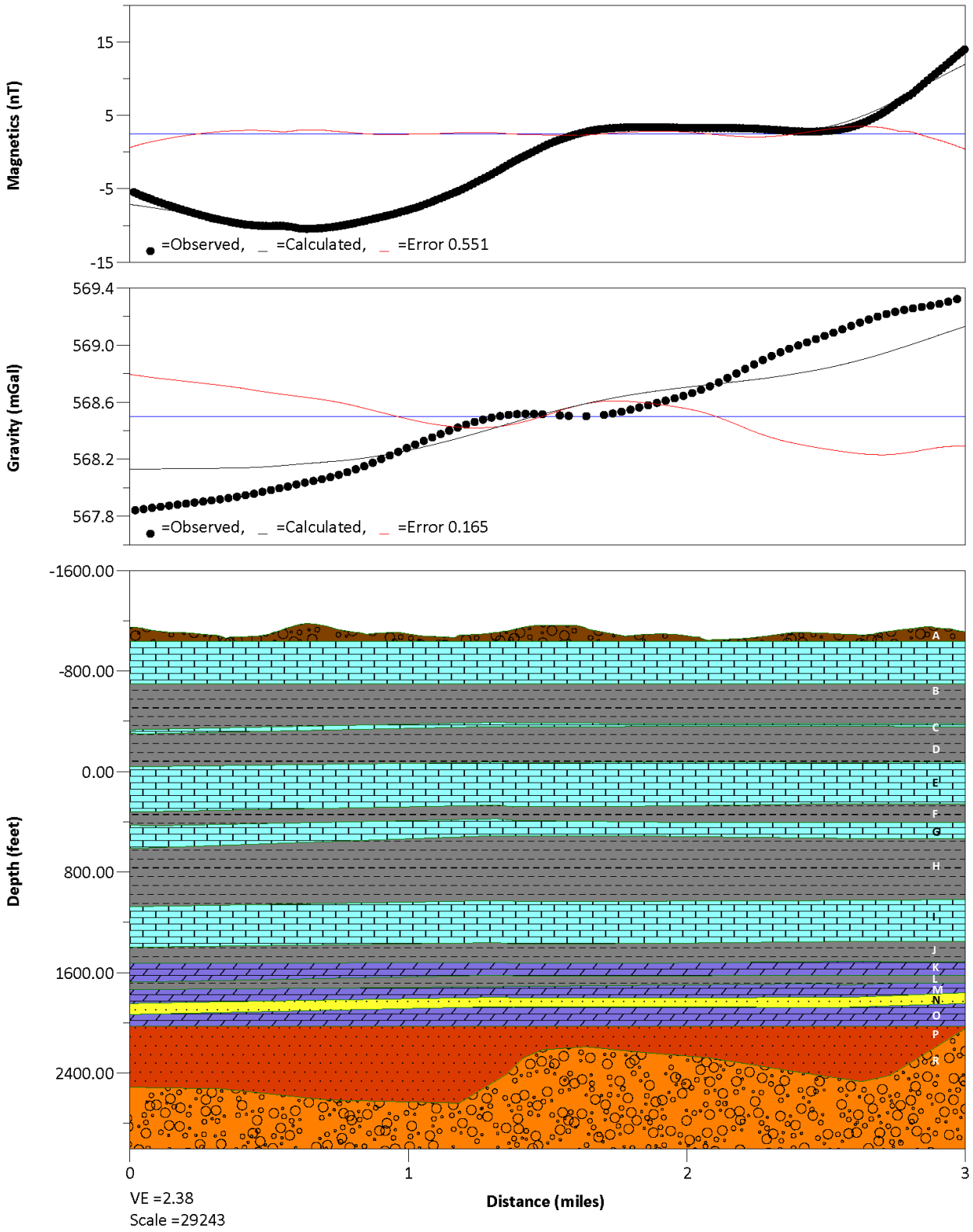

Figure 37: B - B' GM-SYS® geophysical model. Letters represent blocks. See Appendix C for model parameters.

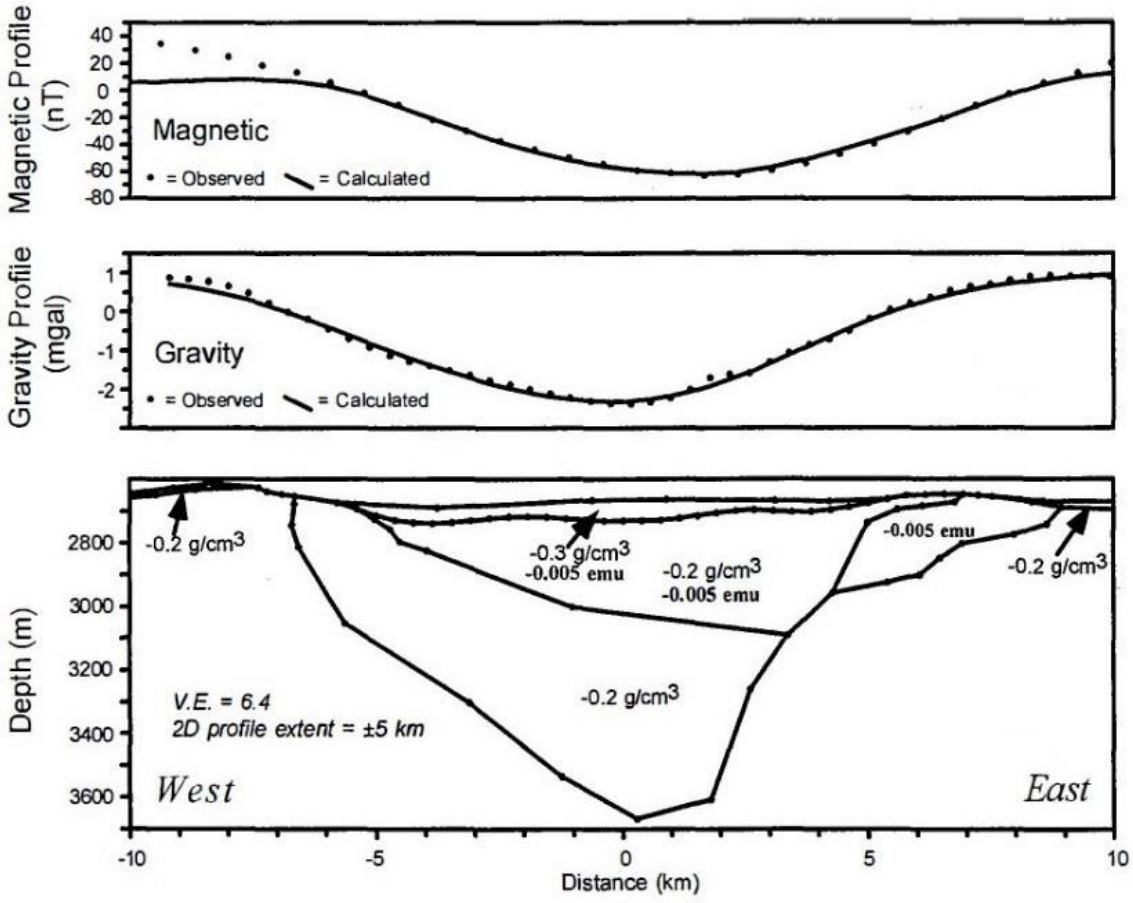

Figure 38: Geophysical model of the Ames structure. Modified from Ahern (1997).

Binocular and Petrographic Analysis of Drill Cuttings

After examining 103 thin sections and > 11,000 quartz grains for PDFs (Figure 13), none were observed (Appendix D). Cracks were observed in a few grains, but these could have been introduced at any point during the life of the grain. Representative examples of quartz grains observed are shown in Figures 39.

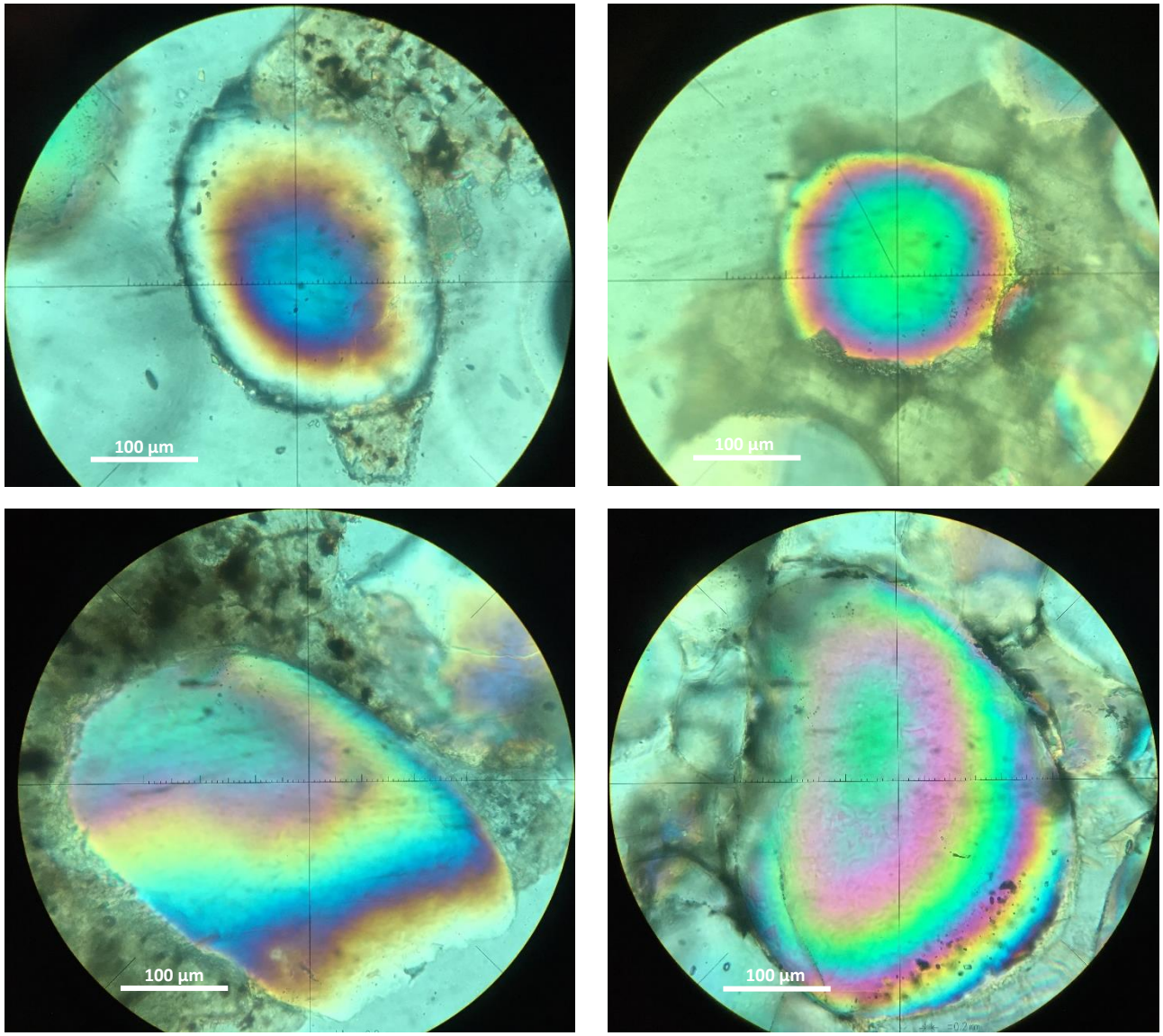

Figure 39: Thin sections of quartz sand grains in cross-polarized light. Note lack of PDFs (Figure 13).

Chapter 6 - Conclusions

From the results of our study, the questions proposed previously in the thesis objective can be answered as follows.

1. The subsurface of the study area as revealed by the structural and stratigraphic cross-sections is not consistent with the effects of an impact structure such as the Ames. The subsurface has no significant variation in depth or thickness for the units of interest.
2. Rather than the effects of an impact structure, the geophysical anomaly models seem to correlate with effects of basement topographic relief and rock density changes from faulting associated with the BMTZ.
3. None of the examined grains exhibit shock metamorphism.
4. There is not enough evidence to verify the proposed identity of the Echo Cliff structure as an Ordovician impact structure. It is possible that the structure is older than the Ordovician and shocked quartz may be found in basal sandstone in the study area. However, currently no wells in the study area penetrate through the Arbuckle Group into the underlying basal sandstone so this cannot be tested. Most likely the ovoid drainage feature proposed as the Echo Cliff structure is a natural culmination of faulting associated with the BMTZ and subsequent erosion.

Chapter 7 - References

Ahern JL. 1997. Gravity and Magnetic Investigation of the Ames Structure, North-Central Oklahoma. OGS. Circ. 100:330-333.

Anderson KH, Wells JS. 1968. Forest City Basin of Missouri, Kansas, Nebraska, and Iowa. AAPG. Bull. 52(2):264-281.

Baars DL. 1995. Basement Tectonic Configuration in Kansas. KGS. Bull. 237:7-9.

Benson ME, Wilson AB. 2015. Frac Sand in the United States - A Geological and Industry Overview. USGS. OFR. 2015(1107).

Blakey R. 2011. Paleogeography and Geologic Evolution of North America. Department of Geology, Northern Arizona University. [accessed 2018 Mar 24]; http://jan.ucc.nau.edu/rcb7/nam.html.

Buchanan PC, Koeberl C, Reid AM. 1998. Impact into Unconsolidated, Water-Rich Sediments at the Marquez Dome, Texas. Meteorit. Planet. Sci. 33:1053-1064.

Carpenter BN, Carlson R. 1997. The Ames Meteorite-Impact Crater. OGS. Circ. 100:104-119.

Carr TR, Hopkins J, Anderson NL, Hedke DE. 1995. Case History of Hampton Field (Arbuckle Group), Rush County, Kansas. KGS. Bull. [accessed 2018 Mar 24];237:145-152. http://www.kgs.ku.edu/Publications/Bulletins/237/Carr1/hampton.pdf

Castaño JR, Clement JH, Kuykendall MD, Sharpton VL. 1997. Source-Rock Potential of Impact Craters. OGS. Circ. 100:100-103.

Cole VB. 1975. Subsurface Ordovician-Cambrian Rocks in Kansas: With Maps Showing the Thickness of Potentially Oil-Bearing Formations. KGS. Subsurf. Geol. Ser. [accessed 2018 Mar 24];2. http://www.kgs.ku.edu/Publications/Bulletins/Sub2/.

Cole VB, cartographer. 1976. Configuration of the Top of Precambrian Rocks in Kansas [subsurface map]. Lawrence (KS). Kansas Geological Survey.

Cox RT. 1988. Evidence of Late Cenozoic Activity Along the Bolivar-Mansfield Tectonic Zone, Midcontinent, USA. In: The Compass: The Earth-Science Journal of Sigma Gamma Epsilon. 65(4):207-213.

Domenico SN. 1967. Detail Gravity Profile Across San Andreas Fault Zone. Geophysics. 32(2):297-301.

Donofrio RR. 1997. Survey of Hydrocarbon-Producing Impact Structures in North America: Exploration Results to Date and Potential for Discovery in Precambrian Basement Rock. OGS. Circ. 100:17-29.

Earth Point. 2018. Excel to KML - Display Excel Files on Google Earth. [accessed 2018 Mar 24]; https://www.earthpoint.us/ExcelToKml.aspx.

Elbeshausen D, Wünnemann K, Collins GS. The Transition from Circular to Elliptical Impact Craters. Journal of Geophyical Research: Planets. 118:2295-2309.

Ferrière L. 2014. Excavation and Modification. Dr. Ludovic Ferrière. [accessed 2016 Nov 06]; http://www.meteorimpactonearth.com/modification.html.

Franseen EK, Byrnes AP, Cansler JR, Steinhaeff DM, Carr TR. 2004. The Geology of Kansas: Arbuckle Group. KGS. Bull. [accessed 2018 Mar 24];250(2).

French BM. 1998. Traces of Catastrophe: A Handbook of Shock-Metamorphic Effects in Terrestrial Meteorite Impact Structures. Houston (TX): Lunar and Planetary Institute.

Gay SP, Jr. 1989. Gravitational Compaction, A Neglected Mechanism in Structural and Stratigraphic Studies: New Evidence from Mid-Continent, USA. AAPG. Bull. 73(5):641-657.

Gay SP, Jr. 1995. The Basement Fault Block Pattern: Its Importance in Petroleum Exploration, and Its Delineation with Residual Aeromagnetic Techniques. In: Ojakangas RW, Dickas AB, Green JC, editors. Basement Tectonics 10: Proceedings of the International Conferences on Basement Tectonics. Dordrecht (NL): Springer. p. 159-207.

GeoCzech Inc. 2018. MyGeodata Converter: Online GIS / CAD Data Conversion and Transformation Tool. [accessed 2018 Mar 24]; https://mygeodata.cloud/converter/.

Geometrics Inc. 2001. G-858 MagMapper Manual. [accessed 2018 Mar 24]; ftp://geom.geometrics.com/pub/mag/Manuals/858Manual_D2.pdf.

Geosoft Inc. 2015. Montaj Gravity and Terrain Correction How-To Guide. [accessed 2018 Mar 24]; http://updates.geosoft.com/downloads/files/how-to-guides/Gravity%20and%20Terrain%20Correction%20Formulas.pdf.

Grechishnikova A. 2017. Niobrara Discrete Fracture Network: From Outcrop Surveys to Subsurface Reservoir Models. [dissertation]. [Golden (CO)]: Colorado School of Mines.

Grieve RAF, Pilkington M. 1996. The Signature of Terrestrial Impacts. AGSO J. Austral. Geol. Geophys. 16:399-420.

Grieve RAF. 1997. Terrestrial Impact Structures: Basic Characteristics and Economic Significance, with Emphasis on Hydrocarbon Production. OGS. Circ. 100:3-16.

Hart RJ, Hargraves RB, Andreoli MAG, Tredoux M, Doucouré CM. 1995. Magnetic Anomaly near the Center of the Vredefort Structure: Implications for Impact-Related Magnetic Signatures. Geology. 23:277-280.

Hatch JR, Newell KD. 1999. Geochemistry of Oils and Hydrocarbon Source Rocks from the Forest City Basin, Northeastern Kansas, Northwestern Missouri, Southwestern Iowa, and Southeastern Nebraska. KGS. Techn. Ser. [accessed 2018 Mar 23];13. http://www.kgs.ku.edu/Publications/Bulletins/TS13/.

Hemant K. 2003. Modelling and Interpretation of Global Lithospheric Magnetic Anomalies. [dissertation]. [Berlin (DE)]: Free University of Berlin.

Herrman BJ. 2011. Impact at Ingalls? Evidence for a Subsurface Ordovician Meteorite Impact Near Ingalls, Oklahoma. [thesis]. [Fort Worth (TX)] Texas Christian University.

Hinze WJ, von Frese RRB, Saad AH. 2012. Gravity and Magnetic Exploration: Principles, Practices, and Applications. Cambridge (UK): Cambridge University Press.

Horton JW, Powars DS, Jr., Gohn GS. 2005. Studies of the Chespeake Bay Impact Structure - The USGS-NASA Langley Corehole, Hampton, Virginia, and Related Coreholes and Geophysical Surveys. USGS Prof. Pap. 1688.

Kerans C. 1988. Karst-controlled Reservoir Heterogeneity in Ellenburger Group Carbonates of West Texas. AAPG. Bull. 72(10):1160-1183.

KGS. 2017. Kansas Earthquake History. [accessed 2018 Mar 24]; http://www.kgs.ku.edu/Geophysics/Earthquakes/historic.html.

KGS. 2018. Kansas Oil and Gas Interactive Map. [accessed 2018 Mar 24]; http://maps.kgs.ku.edu/oilgas/.

Kisvarsanyi EB. 1974. Operation Basement: Buried Precambrian Rocks in Missouri - their Petrography and Structure. AAPG. Bull. 58(4):674-684.

Kisvarsanyi EB. 1984. The Precambrian Tectonic Framework of Missouri as Interpreted from the Aeromagnetic Anomaly Map. MODNR. Contrib. Precam. Geol. 14.

Koger DG, Wiley MA. 1997. Correlation of Landsat MSS (Multi-Spectral Scanner) and TM (Thematic Mapper) Images with Subsurface Structure, Ames, Oklahoma. OGS. Circ. 100:260-264.

Kuykendall MD, Johnson CL, Carlson RA. 1997. Reservoir Characterization of a Complex Impact Structure: Ames Impact Structure, Northern Shelf, Anadarko Basin. OGS. Circ. 100:199-206.

Lee W. 1943. The Stratigraphy and Structural Development of the Forest City Basin in Kansas. AAPG. Bull. [accessed 2016 Nov 07];51. http://www.kgs.ku.edu/Publications/Bulletins/51/02_intro.html.

Lee W. 1956. Stratigraphy and Structural Development of the Salina Basin Area. KGS. Bull. 121.

McCracken MH. 1971. Structural Features of Missouri. MGS&WR. Rep. Inves. 49.

Melosh HJ. 1989. Impact Cratering: A Geologic Process. New York (NY): Oxford University Press.

Merriam DF, Atkinson WR. 1956. Simpson Filled Sinkholes in Eastern Kansas. KGS. Bull. 119(2).

Merriam DF. 1963. The Geologic History of Kansas. KGS. Bull. [accessed 2018 Mar 24];162. http://www.kgs.ku.edu/Publications/Bulletins/162/index.html.

Merriam DF, Xia J, Harbaugh J. 2009. The Edgerton Structure: A Possible Meteorite Impact Feature in Eastern Kansas. International Journal of Geophysics [accessed 2016 Nov 05];2009. doi:10.1155/2009/621528.

Mussett AE, Khan MA. 2000. Looking into the Earth: An Introduction to Geological Geophysics. Cambridge (UK): Cambridge University Press.

Nettleton LL. 1939. Determination of Density for Reduction of Gravimeter Observations. Geophys. 4(3):176-183.

Newell KD, Watney WL, Cheng SWL, Brownrigg RL. 1987. Stratigraphic and Spatial Distribution of Oil and Gas Production in Kansas. KGS. Subsurf. Geol. Ser. [accessed 2018 Mar 24];9.

Newell KD, Sawin RS, Brady LL. 2001. Natural Gas from Coal in Eastern Kansas. KGS. PIC. [accessed 2018 Mar 23];19. http://www.kgs.ku.edu/Publications/pic19/PIC19.pdf.

Northwest Geophysical Associates Inc. 2004. GM-SYS® Gravity/Magnetic Modeling Software: User's Guide Version 4.9. [accessed 2018 Mar 24]; http://pages.geo.wvu.edu/~wilson/gmsys_49.pdf

Pilkington M, Grieve RAF. 1992. The Geophysical Signature of Terrestrial Impact Craters. Rev. Geophys. 30:161-181.

Rohatgi A. 2016. WebPlotDigitizer: Web Based Tool to Extract Data from Plots, Images, and Maps. [accessed 2018 Mar 24]; https://automeris.io/WebPlotDigitizer/.

Ross RJ, Jr. 1976. Ordovician Sedimentation in the Western United States. In: Bassett MG, editor. The Ordovician System: Proceedings of a Paleontologic Association Symposium, Birmingham, September 1974. Cardiff (UK): University of Wales Press and Natural Museum of Wales. p. 73-106.

Scott RG, Pilkington M, Tanczyk EI. 1997. Magnetic Investigations of the West Hawk, Deep Bay and Clearwater Impact Structures, Canada. Meteorites & Planet. Sci. 32:293-308.

Scott RW, McElroy MN. 1964. Precambrian-Paleozoic Contact in Two Wells in Northwestern Kansas. KGS. Bull. [accessed 2018 Mar 24];170(2)

Short NM, Lowman PD, Jr., Fredan SC. 1976. Mission to Earth: Landsat Views the World. Washington (DC): NASA

Smith RK, Anders, EL, Jr. 1951. The Geology of the Davis Ranch Oil Pool, Wabaunsee County, Kansas. KGS. Bull. [accessed 2018 Mar 23];90(2). http://www.kgs.ku.edu/Publications/Bulletins/90_2/.

Spray J. 2018. Earth Impact Database. Planetary and Space Science Centre. [accessed 2018 Feb 07]; http://www.passc.net/EarthImpactDatabase/.

Suchy DR. 2007. Meteorites in Kansas. KGS. PIC. [accessed 2016 Nov 26];26 http://www.kgs.ku.edu/Publications/PIC/pic26.html.

USGS. 1995. 1995 National Assessment of United States Oil and Gas Resources: Overview of the 1995 National Assessment of Potential Additions to Technically Recoverable Resources of Oil and Gas - Onshore and State Waters of the United States. USGS. Circ. 1118.

USGS. 2018. The National Map: Bulk Point Query Service (V 2.0). [accessed 2018 Mar 24]; https://viewer.nationalmap.gov/apps/bulk_pqs/.

USGS. 2018. The National Map: Download (V 1.0). [accessed 2018 Mar 24]; https://viewer.nationalmap.gov/basic/.

Vastag B. 2013. Crater Found in Iowa Points to Asteroid Break-Up 470 Million Years Ago. The Washington Post. [accessed 2016 Nov 27]. https://www.washingtonpost.com/national/health-science/crater-found-in-iowa-points-to-asteroid-break-up-470-million-years-ago/2013/02/18/545131f8-76d5-11e2-aa12-e6cf1d31106b_story.html?wprss=rss_national.

Wong AM, Reid AM, Hall SA, Sharpton VL. 2001. Reconstruction of the Subsurface Structure of the Marquez Impact Crater in Leon County, Texas, USA, Based on Well-Log and Gravity Data. Meteorit. Planet. Sci. 36:1443-1455.

WVDEP. 2018. Coordinate Conversion Tool. [accessed 2018 Mar 24]; https://tagis.dep.wv.gov/convert/.

Xia J, Sprowl DR, Steeples DW. 1992. Lithological Distribution in the Basement of Kansas, Based on Potential-Field Data. In: SEG Technical Program Expanded Abstracts 1992. Society of Exploration Geophysicists. p. 564-567.

Xia J, Sprowl DR, Adkins-Heljeson D. 1993. Correction of Topographic Distortions in Potential-Field Data: A Fast and Accurate Approach. Geophys. 58(4):515-523.

Xia J, Sprowl D, Steeples D, Miller R, cartographers. 1995. Model of Precambrian Geology of Kansas from Gravity and Aeromagnetic Data [geologic map]. Lawrence (KS): Kansas Geological Survey.

Xia J. 2002. Using the High-Resolution Magnetic Method to Locate Abandoned Brine Wells in Hutchinson, Kansas. KGS. OFR. 2002(43).

Yarger HL. 1989. Major Magnetic Features in Kansas and their Possible Geologic Significance. KGS. Bull. [accessed 2018 Mar 24]; 226:197-213. http://www.kgs.ku.edu/Publications/Bulletins/226/Yarger/13_yarger.pdf.

Zeller DE, Jewett JM, Bayne CK, Goebel ED, O'Connor HG, Swineford A. 1968. The Stratigraphic Succession in Kansas. KGS. Bull. [accessed 2018 Mar 24];189. http://www.kgs.ku.edu/Publications/Bulletins/189/index.html

Appendix A - Cross-Section Data

	Thompson 1-33	Dorothy Wendland 1	Phillip Wendland 1	Andrew Wendland 1	Adams "A" 1
Datum	1318	1229	1031	1040	1038
Oread Limestone	910	819	670	665	705
Heebner Shale	942	845	694	690	727
Lansing Group	1233	1136	974	965	990
Base of the Kansas City Group	1586	1486	1320	1314	1335
Cherokee Group	1852	1725	1561	1560	1558
"Mississippi Lime"	2336	2238	2082	2046	2108
Chattanooga Shale	2680	2576	2416	2412	2485
"Hunton Group"	2830	2732	2574	2572	2533
Maquoketa (Sylvan) Shale	2894	2826	2686	2682	2740
Viola (Kimmswick) Limestone	2974	2903	2759	2756	2826
Simpson Group		2996	2857	2853	2924
Arbuckle Group		3063	2930	2924	3020

Appendix B - Geophysical Data

A - A' Geophysical Data											
Distance (Miles)	Elevation (Feet)	Latitude (WGS84)	Longitude (WGS84)	Station Number	Date (DD-MM-YY)	Time	Gravity Reading * 0.4008	Complete Bouguer Anomaly (CBA)	Upward Continued CBA	Surface Magnetic Data	NewMag® Residual Magnetic Data
0	0	38.88481277	-95.9653478							-30.481	2.0855
0.017516448	0.057468665	38.88506657	-95.96535324							-29.203	2.06674
0.048460724	0.158991883	38.88551494	-95.96536048							-23.062	2.04664
0.079703258	0.261493638	38.88596755	-95.96537135							-18.631	2.02586
0.111045211	0.364321571	38.88642157	-95.96538041							-14.628	1.99157
0.142088907	0.466170968	38.88687136	-95.96538947							-10.697	1.90864
0.17333144	0.568672723	38.88732397	-95.96539128							-8.03	1.79048
0.204480769	0.670868685	38.88777517	-95.96540215							-5.835	1.67142
0.235530678	0.772738468	38.88822496	-95.96540577							-3.356	1.55235
0.266673792	0.874914044	38.88867616	-95.96541302							-0.367	1.43332
0.297624282	0.976457648	38.88912454	-95.96542027							2.619	1.31431
0.328860602	1.078939017	38.88957715	-95.9654257							4.579	1.19531
0.359898083	1.180768027	38.89002694	-95.96543114							6.201	1.07654
0.391034984	1.282923217	38.89047797	-95.96544035							7.096	0.96056
0.422078679	1.384772614	38.89092776	-95.96544579							7.975	0.84805
0.45321558	1.486927803	38.89137896	-95.96545122							10.313	0.73629
0.484458114	1.589429558	38.89183157	-95.96545666							13.674	0.62449
0.515700648	1.691931313	38.89228418	-95.96545666							16.874	0.51274
0.546750557	1.793801096	38.89273397	-95.96546209							21.609	0.40153
0.577694832	1.895324314	38.89318235	-95.96546753							26.361	0.29155
0.608639108	1.996847532	38.89363073	-95.96547297							32.528	0.1824
0.639981061	2.099675466	38.89408474	-95.96548021							38.11	0.07378
0.671217382	2.202156834	38.89453735	-95.96548021							42.788	-0.03546
0.702453702	2.304638203	38.89498996	-95.96549109							47.493	-0.13993
0.733621671	2.406895324	38.89544155	-95.96549706							51.308	-0.2353
0.764864205	2.509397078	38.89589416	-95.96549525							56.044	-0.32099
0.796032174	2.611654199	38.89634577	-95.96549455							62.058	-0.39944
0.827169075	2.713809389	38.89679697	-95.96550361							67.131	-0.46895
0.858318403	2.816005351	38.89724817	-95.9655181							72.348	-0.53031
0.889554724	2.918486719	38.89770078	-95.96552173							77.154	-0.57327
0.920878036	3.021253495	38.89815467	-95.96552319							81.979	-0.5774
0.952014937	3.123408684	38.89860587	-95.96552863							85.847	-0.56192
0.983151837	3.225563874	38.89905707	-95.96553044							89.132	-0.52733
1.014388158	3.328045243	38.89950968	-95.96552682							92.707	-0.47867
1.045525058	3.430200432	38.89996088	-95.96552319							95.909	-0.41033
1.076661959	3.532355622	38.90041208	-95.96552682							98.737	-0.32246
1.107898279	3.634836991	38.90086469	-95.96552863							102.115	-0.22559
1.139134599	3.737318359	38.90131729	-95.96552682							106.046	-0.1184
1.17037092	3.839799728	38.9017699	-95.96553045							109.929	-0.00379
1.201514034	3.941975304	38.9022211	-95.9655232							113.015	0.10072
1.232607439	4.04398779	38.9026715	-95.96552353							116.294	0.19136
1.263756767	4.146183752	38.9031227	-95.96552353							118.808	0.27184
1.29481289	4.248073921	38.90357249	-95.96552896							119.728	0.34699
1.326260476	4.35124842	38.90402792	-95.96552897							116.983	0.41968
1.357409804	4.453444382	38.90447912	-95.96553259							111.41	0.48336
1.388465927	4.555334552	38.90492891	-95.96552897							103.428	0.52987
1.411754912	4.631741985	38.90538333	-95.96553131	3001	26-06-17	12:29	553.46472	572.7133154		97.146	0.55315
1.44338891	4.73552807	38.90584146	-95.96553437	3002	26-06-17	12:22	553.86552	572.7236277	572.41	84.204	0.55715

1.475029121	4.839334541	38.90629959	-95.96551003	3003	26-06-17	12:19	553.94568	572.6392914	572.4	72.091	0.54967
1.506644477	4.943059467	38.90675772	-95.96551036	3004	26-06-17	12:16	553.9056	572.5739062	572.39	54.924	0.53379
1.538290902	5.046886324	38.90721585	-95.96548876	3005	26-06-17	12:14	553.9056	572.7500831	572.39	40.058	0.50995
1.569912473	5.150631637	38.90767398	-95.96548176	3006	26-06-17	12:11	553.7052	572.6734616	572.38	23.839	0.47412
1.601527829	5.254356563	38.90813211	-95.96547381	3007	26-06-17	12:08	553.74528	572.7550897	572.37	10.774	0.42208
1.633149399	5.358101875	38.90859024	-95.96547206	3008	26-06-17	12:06	553.62504	572.7056333	572.36	-13.197	0.352
1.664770969	5.461847188	38.90904837	-95.96546667	3009	26-06-17	12:00	553.18416	572.4486824	572.35	-37.288	0.263
1.69639254	5.5655925	38.9095065	-95.96546667	3010	26-06-17	11:57	553.18416	572.6624725	572.34	-56.975	0.16385
1.728045178	5.669439743	38.90996463	-95.96543999	3011	26-06-17	11:53	553.58496	573.1763268	572.33	-79.656	0.05575
1.759778595	5.773552007	38.91042276	-95.96542761	3012	26-06-17	11:50	554.86752	573.5095306	572.31	-95.177	-0.07748
1.791592791	5.877929291	38.91088089	-95.96541346	3013	26-06-17	11:46	555.94968	573.3557019	572.28	-104.327	-0.25469
1.823332421	5.982061941	38.91133902	-95.96540351	3014	26-06-17	11:43	556.75128	573.1851512	572.25	-110.931	-0.44977
1.855059625	6.086153819	38.91179715	-95.96539012	3015	26-06-17	11:40	556.75128	572.2800583	572.21	-115.61	-0.64587
1.886718477	6.190021448	38.91225528	-95.96537973	3016	26-06-17	11:36	556.7112	572.7045949	572.17	-118.192	-0.84194
1.918340047	6.29376676	38.91271341	-95.96536785	3017	26-06-17	11:33	556.47072	572.5112863	572.12	-115.155	-1.07194
1.949967831	6.397532459	38.91317154	-95.96535939	3018	26-06-17	11:12	556.19016	572.3693841	572.07	-112.343	-1.35774
1.981583188	6.501257385	38.91362967	-95.96535443	3019	26-06-17	11:08	556.43064	572.6141078	572.01	-111.882	-1.65711
2.013204758	6.605002697	38.9140878	-95.96535055	3020	26-06-17	11:06	556.63104	572.6200771	571.95	-111.422	-1.97656
2.044832542	6.708768396	38.91454593	-95.96533392	3021	26-06-17	11:03	556.67112	572.5232106	571.89	-110.38	-2.40339
2.076447898	6.812493322	38.91500407	-95.9653351	3022	26-06-17	10:59	556.79136	572.4971931	571.81	-104.804	-2.86978
2.108069468	6.916238634	38.9154622	-95.96533867	3023	26-06-17	10:56	556.75128	572.2456293	571.74	-96.187	-3.30413
2.139684825	7.019963561	38.91592033	-95.96534492	3024	26-06-17	10:52	557.83344	573.3428881	571.65	-86.244	-3.72061
2.171318822	7.123749645	38.91637846	-95.96535592	3025	14-06-17	12:13	556.5108	571.4111717	571.56	-80.395	-4.17715
2.203033598	7.22780075	38.91683659	-95.96535838	3026	14-06-17	12:09	557.5128	571.5044768	571.47	-78.898	-4.67992
2.234767015	7.331913014	38.91729472	-95.96535067	3027	14-06-17	12:06	558.39456	571.4104157	571.37	-79.532	-5.19497
2.26651286	7.43606605	38.91775285	-95.96535266	3028	14-06-17	12:03	559.19616	571.1916373	571.27	-82.566	-5.71294
2.298190353	7.539994838	38.91821098	-95.9653637	3029	14-06-17	12:00	560.23824	571.5843976	571.17	-85.577	-6.23338
2.32997348	7.644270192	38.91866911	-95.9653581	3030	14-06-17	11:55	560.87952	571.1312308	571.06	-92.023	-6.75764
2.361682042	7.748300911	38.91912724	-95.96534738	3031	14-06-17	11:52	561.28032	570.6776448	570.96	-99.422	-7.23705
2.393347108	7.852188926	38.91958537	-95.96534292	3032	14-06-17	11:49	561.56088	570.3283887	570.87	-103.565	-7.68049
2.424987319	7.955995397	38.9200435	-95.96535826	3033	14-06-17	11:46	561.76128	570.1872492	570.77	-105.217	-8.11985
2.456602676	8.059720323	38.92050163	-95.96536019	3034	14-06-17	11:43	561.5208	569.8269306	570.69	-105.63	-8.55759
2.488261528	8.163587953	38.92095976	-95.96536613	3035	14-06-17	11:40	561.44064	569.5945927	570.61	-107.075	-9.00186
2.519939022	8.267516741	38.92141789	-95.96536463	3036	14-06-17	11:37	561.03984	569.3711652	570.54	-110.447	-9.46446
2.55169108	8.371690163	38.92187602	-95.96540072	3037	14-06-17	11:33	559.87752	568.9281429	570.48	-113.692	-9.92992
2.583499062	8.476047061	38.92233415	-95.96540124	3038	14-06-17	11:29	559.23624	569.4290116	570.43	-116.408	-10.3829
2.615170341	8.579955463	38.92279228	-95.96540296	3039	14-06-17	11:26	558.95568	569.7513676	570.39	-117.17	-10.8319
2.646791912	8.683700775	38.92325041	-95.96540344	3040	14-06-17	11:22	559.03584	569.967456	570.35	-116.891	-11.2763
2.678407268	8.787425701	38.92370854	-95.9654023	3041	14-06-17	11:18	559.67712	570.5864138	570.31	-115.503	-11.7145
2.710059907	8.891272945	38.92416667	-95.96540543	3042	14-06-17	11:14	560.59896	570.9716619	570.28	-113.333	-12.1221
2.741830606	8.995507526	38.9246248	-95.96539793	3043	14-06-17	11:10	560.3184	569.6192722	570.25	-109.659	-12.4872
2.773483245	9.099354769	38.92508293	-95.96541063	3044	14-06-17	11:02	559.19616	568.9383138	570.21	-104.838	-12.8432
2.805235303	9.203528191	38.92554106	-95.96542117	3045	14-06-17	10:57	558.87552	569.5423198	570.18	-100.609	-13.1728
2.836875514	9.307334662	38.92599919	-95.96542418	3046	14-06-17	10:53	559.15608	570.1657675	570.15	-97.158	-13.4731
2.868503298	9.411100361	38.92645732	-95.96543128	3047	14-06-17	10:49	559.67712	570.336986	570.11	-93.97	-13.7262
2.900168364	9.514988376	38.92691545	-95.96543872	3048	14-06-17	10:45	559.7172	569.7832281	570.07	-89.833	-13.9154
2.931796148	9.618754075	38.92737358	-95.96544614	3049	14-06-17	10:37	559.27632	569.6277759	570.03	-85.628	-14.0585
2.963448787	9.722601318	38.92783171	-95.96543917	3050	14-06-17	10:33	560.9196	571.7322247	569.98	-80.827	-14.1654
2.995070357	9.82634663	38.92828984	-95.96543998	3051	06-06-17	15:26	558.43464	569.2297861	569.93	-75.423	-14.2303
3.026716782	9.930173487	38.92874797	-95.96544781	3052	06-06-17	15:23	558.9156	569.1908619	569.88	-71.156	-14.1793

3.058400489	10.03412266	38.9292061	-95.96544086	3053	06-06-17	15:20	559.47672	569.0271074	569.83	-66.775	-14.0493
3.090028273	10.13788836	38.92966423	-95.96544225	3054	06-06-17	15:16	559.47672	568.712061	569.79	-62.931	-13.8661
3.121674698	10.24171522	38.93012236	-95.96545574	3055	06-06-17	15:12	558.87552	568.4840729	569.75	-59.11	-13.6489
3.153333551	10.34558285	38.93058049	-95.96546667	3056	06-06-17	15:08	558.59496	568.6592298	569.71	-55.594	-13.4019
3.184973762	10.44938932	38.93103862	-95.96546667	3057	06-06-17	15:05	558.23424	568.7156828	569.68	-52.632	-13.1171
3.216613973	10.55319579	38.93149675	-95.96547065	3058	06-06-17	15:02	557.87352	568.7387808	569.66	-49.511	-12.797
3.248235544	10.6569411	38.93195488	-95.96547982	3059	06-06-17	14:59	558.114	568.8905221	569.64	-46.55	-12.459
3.2798509	10.76066603	38.93241301	-95.96548001	3060	06-06-17	14:56	558.15408	568.7635924	569.63	-42.847	-12.1098
3.311478684	10.86443173	38.93287114	-95.96546667	3061	06-06-17	14:53	558.27432	568.8282955	569.63	-38.415	-11.7422
3.34309404	10.96815665	38.93332927	-95.96546667	3062	06-06-17	14:50	558.63504	568.9968986	569.63	-34.812	-11.3462
3.374721824	11.07192235	38.9337874	-95.96546667	3063	06-06-17	14:33	558.9156	568.9497895	569.63	-31.266	-10.9087
3.406337181	11.17564728	38.93424553	-95.96546667	3064	06-06-17	14:30	558.95568	568.8565396	569.63	-27.627	-10.4535
3.437958751	11.27939259	38.93470366	-95.96546667	3065	06-06-17	14:27	559.07592	568.8326101	569.64	-24.063	-9.99648
3.469574108	11.38311751	38.93516179	-95.96546667	3066	06-06-17	14:24	559.3164	569.0277311	569.65	-21.145	-9.50539
3.501195678	11.48686283	38.93561992	-95.96546667	3067	06-06-17	14:21	559.03584	568.9696853	569.66	-18.529	-9.01047
3.532817248	11.59060814	38.93607805	-95.9654713	3068	06-06-17	14:17	559.03584	569.0574189	569.67	-16.686	-8.51247
3.564438818	11.69435345	38.93653618	-95.96547246	3069	06-06-17	14:14	559.27632	569.0142304	569.69	-14.768	-7.99997
3.596054175	11.79807838	38.93699431	-95.96547212	3070	06-06-17	14:10	559.27632	568.8583544	569.71	-12.93	-7.52494
3.627675745	11.90182369	38.93745244	-95.96546667	3071	06-06-17	14:01	559.23624	568.8010612	569.73	-12.117	-7.07246
3.659291101	12.00554862	38.93791057	-95.96547255	3072	06-06-17	13:18	559.5168	569.1788666	569.76	-10.973	-6.49422
3.690906458	12.10927354	38.9383687	-95.96547105	3073	06-06-17	13:15	559.3164	568.9323869	569.78	-10.535	-5.82083
3.722528028	12.21301886	38.93882683	-95.96546667	3074	06-06-17	13:11	559.67712	569.0954907	569.82	-10.524	-5.1517
3.754155812	12.31678455	38.93928496	-95.96545574	3075	06-06-17	13:08	559.99776	569.0906172	569.85	-10.56	-4.52669
3.785820878	12.42067257	38.93974309	-95.96545492	3076	06-06-17	13:05	560.47872	568.9627055	569.89	-11.511	-3.89968
3.817448662	12.52443827	38.94020122	-95.96545171	3077	06-06-17	13:01	560.95968	569.1219605	569.94	-12.741	-3.25405
3.849095087	12.62826512	38.94065935	-95.96545826	3078	06-06-17	12:59	560.5188	569.0932221	569.99	-14.305	-2.64219
3.880729085	12.73205121	38.94111748	-95.96545819	3079	06-06-17	12:55	560.03784	568.9903274	570.05	-13.88	-2.05974
3.912350655	12.83579652	38.94157561	-95.96546167	3080	06-06-17	12:51	560.118	569.1906185	570.11	-11.293	-1.47729
3.943966011	12.93952145	38.94203374	-95.96546092	3081	06-06-17	12:48	559.99776	569.0102628	570.19	-7.496	-0.95765
3.975581368	13.04324637	38.94249187	-95.96546667	3082	06-06-17	12:43	560.118	569.0127307	570.27	-2.796	-0.51337
4.038414403	13.24939151	38.943402	-95.965454							8.886	-0.05642
4.069582373	13.35164863	38.943853	-95.965458							16.538	0.43046
4.100508007	13.45311069	38.944301	-95.965465							24.473	0.87714
4.131501993	13.554797	38.94475	-95.965462							33.112	1.24411
4.162831519	13.65758416	38.945204	-95.965465							40.361	1.58043
4.19403677	13.7599636	38.945656	-95.965456							49.32	1.92581
4.2245523	13.86008017	38.9461	-95.965538							58.425	2.24073
4.248655281	13.93915819	38.946446	-95.9659							67.075	2.54065
4.26860129	14.00459786	38.94674	-95.966336							72.769	2.84328
4.288907694	14.07121992	38.947032	-95.96677							79.59	3.12106
4.308853704	14.13665958	38.94732	-95.96721							84.823	3.36669
4.33562858	14.22450367	38.947706	-95.967483							89.5	3.60489
4.366740626	14.32657732	38.948155	-95.967425							92.93	3.84029
4.396839837	14.42532801	38.948601	-95.967369							94.486	4.03771
4.427889746	14.52719779	38.949046	-95.967288							94.446	4.18991
4.456205622	14.62009765	38.949459	-95.967077							93.839	4.34227
4.468670325	14.66099235	38.949637	-95.966547							92.624	4.50046
4.477456511	14.68981842	38.949767	-95.965993							91.068	4.66339
4.486062499	14.71805329	38.949891	-95.965648							90.262	4.83047
4.509040799	14.79344141	38.950226	-95.96526							86.641	4.98152

4.539674389	14.89394532	38.950668	-95.965163							83.097	5.07513
4.57042604	14.99483657	38.951111	-95.965267							80.087	5.14834
4.607130887	15.1152593	38.95163333	-95.96544315	3083	24-06-17	12:04	572.66304	572.1998617	572.33	75.667	5.22104
4.638005771	15.21655485	38.95208056	-95.96545856	3084	24-06-17	12:08	572.38248	571.8157695	572.34	70.927	5.29253
4.668869841	15.31781493	38.95252778	-95.96545938	3085	24-06-17	12:11	572.46264	571.9479624	572.34	63.445	5.35654
4.699736179	15.41908245	38.95297501	-95.96545139	3086	24-06-17	12:14	572.62296	572.0895917	572.35	53.203	5.39594
4.730598824	15.52033785	38.95342223	-95.96545002	3087	24-06-17	12:17	572.70312	572.1356999	572.36	45.66	5.40744
4.76146262	15.62159702	38.95386946	-95.96544755	3088	24-06-17	12:20	572.82336	572.2558608	572.38	42.121	5.40388
4.792325669	15.72285375	38.95431668	-95.96544962	3089	24-06-17	12:23	572.82336	572.2572146	572.4	39.388	5.39821
4.823190476	15.82411624	38.95476391	-95.96545277	3090	24-06-17	12:26	572.7432	572.2206934	572.42	39.07	5.39449
4.854058204	15.92538832	38.95521113	-95.965447	3091	24-06-17	12:30	572.9436	572.5374567	572.44	39.069	5.39482
4.884936938	16.0266965	38.95565836	-95.96544571	3092	24-06-17	12:33	572.5428	572.4210785	572.47	39.745	5.3896
4.915813469	16.12799746	38.95610558	-95.96545551	3093	24-06-17	12:45	572.46264	572.5372773	572.5	42.944	5.38298
4.946682502	16.22927382	38.95655281	-95.96544666	3094	24-06-17	12:48	572.26224	572.4114265	572.52	46.283	5.37578
4.97754527	16.33052962	38.95700003	-95.9654487	3095	24-06-17	12:51	572.42256	572.5359108	572.55	47.192	5.36784
5.008409766	16.4317911	38.95744726	-95.96544511	3096	24-06-17	12:54	572.58288	572.7183955	572.58	47.768	5.37043
5.039275762	16.53305749	38.95789448	-95.96545152	3097	24-06-17	12:57	572.30232	572.4941744	572.61	47.751	5.38447
5.070141716	16.63432375	38.95834171	-95.96545693	3098	24-06-17	13:01	572.42256	572.6640873	572.64	48.776	5.40096
5.101010713	16.73559999	38.95878893	-95.96545005	3099	24-06-17	13:04	572.26224	572.6328831	572.67	51.199	5.41856
5.131880385	16.83687844	38.95923616	-95.9654509	3100	24-06-17	13:08	572.30232	572.8355081	572.7	54.32	5.43137
5.162752521	16.93816498	38.95968338	-95.96544856	3101	24-06-17	13:11	572.06184	572.805462	572.73	57.273	5.43692
5.193628594	17.03946444	38.96013061	-95.96545063	3102	24-06-17	13:15	571.82136	572.8148787	572.76	60.046	5.43735
5.224499641	17.1407474	38.96057783	-95.96545822	3103	24-06-17	13:18	571.5408	572.6889388	572.79	63.297	5.42383
5.25536403	17.24200852	38.96102506	-95.9654535	3104	24-06-17	13:20	571.7412	572.8687488	572.82	66.289	5.38747
5.286227999	17.34326827	38.96147228	-95.96545886	3105	24-06-17	13:23	571.7412	572.8375107	572.85	69.095	5.3389
5.317093875	17.44453427	38.96191951	-95.96546093	3106	24-06-17	13:26	571.66104	572.841234	572.88	72.466	5.28833
5.347963301	17.54581192	38.96236673	-95.96546667	3107	24-06-17	13:28	571.66104	572.9913685	572.91	75.75	5.23311
5.378835884	17.64709992	38.96281396	-95.96546667	3108	24-06-17	13:31	571.58088	573.12192	572.94	79.714	5.16684
5.409708557	17.74838822	38.96326118	-95.96546667	3109	24-06-17	13:33	571.46064	573.2253991	572.97	85.048	5.07837
5.440571899	17.84964591	38.96370841	-95.96546667	3110	24-06-17	13:36	571.50072	573.2396832	573	91.105	4.97909
5.471442057	17.95092596	38.96415563	-95.96546667	3111	24-06-17	13:38	571.7412	573.2042834	573.02	97.918	4.85736
5.502350171	18.05233053	38.96460286	-95.96543762	3112	24-06-17	13:41	572.02176	573.2474736	573.05	104.184	4.69834
5.533266665	18.1537626	38.96505008	-95.96546667	3113	24-06-17	13:43	572.18208	573.0475565	573.07	112.25	4.50815
5.564135054	18.25503685	38.96549731	-95.96547601	3114	24-06-17	13:47	572.46264	573.1907224	573.09	119.687	4.30737
5.59500556	18.35631804	38.96594453	-95.96546667	3115	24-06-17	14:06	572.3424	573.1568526	573.11	125.053	4.1018
5.625874752	18.45759492	38.96639176	-95.96547557	3116	24-06-17	14:09	572.50272	573.1527628	573.14	126.224	3.88091
5.656741044	18.55886229	38.96683898	-95.9654732	3117	24-06-17	14:12	572.82336	573.2755575	573.16	125.485	3.64975
5.687643354	18.66024782	38.96728621	-95.96548196	3118	24-06-17	14:16	573.38448	573.2979718	573.18	121.713	3.40695
5.718512682	18.76152515	38.96773343	-95.96549379	3119	24-06-17	14:19	573.30432	573.1406058	573.2	117.752	3.14735
5.749381915	18.86280216	38.96818066	-95.96548257	3120	24-06-17	14:22	573.58488	573.383789	573.21	110.641	2.86903
5.780247752	18.96406803	38.96862788	-95.96547802	3121	24-06-17	14:24	573.50472	573.3872525	573.23	102.883	2.58521
5.811118943	19.06535147	38.96907511	-95.96548561	3122	24-06-17	14:27	573.42456	573.4530721	573.25	93.268	2.30578
5.842003228	19.16667787	38.96952233	-95.9654865	3123	24-06-17	14:32	572.9436	573.3124579	573.27	82.356	2.03877
5.8728852	19.26799668	38.96996956	-95.96548295	3124	24-06-17	14:34	572.62296	573.3029147	573.28	74.092	1.80312
5.903760619	19.36929399	38.97041678	-95.96548496	3125	24-06-17	14:36	572.3424	573.2778435	573.3	63.568	1.57932
5.934639605	19.470603	38.97086401	-95.96547818	3126	24-06-17	14:38	572.22216	573.4214221	573.31	47.593	1.36604
5.965532472	19.57195756	38.97131123	-95.96546667	3127	24-06-17	14:41	571.90152	573.466729	573.32	31.68	1.15873
5.99639827	19.6732233	38.97175846	-95.96546667	3128	24-06-17	14:43	571.90152	573.5573879	573.34	19.933	0.99143
6.027268743	19.77450438	38.97220568	-95.96546667	3129	24-06-17	14:46	571.62096	573.4687593	573.35	8.21	0.87992
6.058134545	19.87577014	38.97265291	-95.96546667	3130	24-06-17	14:49	571.38048	573.3156037	573.36	0.666	0.77612

6.089003394	19.97704589	38.97310013	-95.96545624	3131	24-06-17	14:51	571.18008	573.1597508	573.37	-6.413	0.66318
6.119869053	20.07831118	38.97354736	-95.9654537	3132	24-06-17	14:54	571.30032	573.3554864	573.39	-10.566	0.53955
6.150740476	20.17959538	38.97399458	-95.96544361	3133	24-06-17	14:57	571.18008	573.3603316	573.4	-15.038	0.40246
6.181609582	20.28087198	38.97444181	-95.96543555	3134	24-06-17	15:00	571.05984	573.3398313	573.41	-17.215	0.25057
6.212478858	20.38214914	38.97488903	-95.96543539	3135	24-06-17	15:03	570.97968	573.4279668	573.43	-16.782	0.086
6.243357813	20.48345805	38.97533626	-95.9654375	3136	24-06-17	15:06	570.65904	573.3974058	573.44	-18.497	-0.07439
6.274252634	20.58481901	38.97578348	-95.96542732	3137	24-06-17	15:08	570.3384	573.4730852	573.45	-21.531	-0.20611
6.305140073	20.68615576	38.97623071	-95.96542161	3138	24-06-17	15:10	569.81736	573.3128398	573.47	-25.502	-0.29627
6.336030366	20.78750187	38.97667793	-95.96541805	3139	24-06-17	15:12	569.81736	573.7064371	573.48	-28.572	-0.32896
6.366924251	20.88885976	38.97712516	-95.96540464	3140	24-06-17	15:15	569.29632	573.543561	573.5	-29.57	-0.33898
6.397846653	20.99031121	38.97757238	-95.96539877	3141	24-06-17	15:17	568.65504	573.4991708	573.51	-29.818	-0.32699
6.42873834	21.09166189	38.97801961	-95.96538746	3142	24-06-17	15:20	568.5348	573.7335585	573.52	-29.826	-0.31474
6.459608637	21.1929424	38.97846683	-95.96539626	3143	24-06-17	15:23	568.57488	573.5560753	573.53	-32.771	-0.27075
6.490479586	21.29422504	38.97891406	-95.96538943	3144	24-06-17	15:25	568.69512	573.4339664	573.54	-38.224	-0.17851
6.521348307	21.39550038	38.97936128	-95.96537927	3145	24-06-17	15:28	568.9356	573.5370059	573.55	-44.066	-0.04197
6.552211806	21.49675858	38.97980851	-95.96538101	3146	24-06-17	15:31	568.97568	573.526104	573.56	-50.368	0.14648
6.583074788	21.59801509	38.98025573	-95.96537888	3147	24-06-17	15:34	569.05584	573.5876888	573.57	-58.683	0.35278
6.61398507	21.69942678	38.98070296	-95.96537867	3148	24-06-17	15:36	569.7372	573.6545359	573.58	-68.279	0.56561
6.644933968	21.80096516	38.98115018	-95.96537634	3149	24-06-17	15:39	570.37848	573.4751301	573.59	-79.742	0.79319
6.675846391	21.90238387	38.98159741	-95.96537518	3150	24-06-17	16:02	571.01976	573.4361675	573.6	-88.465	1.04352
6.706755239	22.00379086	38.98204463	-95.96536372	3151	24-06-17	16:05	571.50072	573.3360756	573.6	-96.917	1.33244
6.737642492	22.10512699	38.98249186	-95.96536795	3152	24-06-17	16:08	572.30232	573.683957	573.61	-105.185	1.63336
6.768548127	22.20652344	38.98293908	-95.96536327	3153	24-06-17	16:10	572.78328	573.5760353	573.62	-112.835	1.9351
6.799456594	22.30792917	38.98338631	-95.96535755	3154	24-06-17	16:13	573.38448	573.5747793	573.63	-122.941	2.22927
6.830350522	22.40928721	38.98383353	-95.96535296	3155	24-06-17	16:15	573.7452	573.4215028	573.64	-133.34	2.51158
6.861238236	22.51062485	38.98428076	-95.96534267	3156	24-06-17	16:17	574.26624	573.5288686	573.65	-142.956	2.79115
6.892109791	22.61190949	38.98472798	-95.96534208	3157	24-06-17	16:20	574.66704	573.6289637	573.67	-151.49	3.07869
6.922989699	22.71322153	38.98517521	-95.96534651	3158	24-06-17	16:23	574.98768	573.5733607	573.68	-160.723	3.36903
6.95386965	22.8145337	38.98562243	-95.96534225	3159	24-06-17	16:25	575.38848	573.5906385	573.69	-167.865	3.63873
6.984745356	22.91583195	38.98606966	-95.96535287	3160	24-06-17	16:27	575.66904	573.6039971		-174.71	3.88358
7.002953304	22.97556932	38.98633333	-95.96536464	3161	24-06-17	16:29	575.62896	573.5969546		-177.151	4.09084

B - B' Geophysical Data											
Distance (Miles)	Elevation (Feet)	Latitude (WGS84)	Longitude (WGS84)	Station Number	Date (DD-MM-YY)	Time	Gravity Reading * 0.4008	Complete Bouguer Anomaly (CBA)	Upward Continued CBA	Surface Magnetic Data	NewMag® Residual Magnetic Data
0	1147.47379	38.94313354	-95.9934	2001	03-06-17	14:57	560.79936	567.9253095	567.84	-64.201	-5.2691
0.018558071	1146.325496	38.94311801	-95.99305625	2002	03-06-17	14:53	560.83944	567.8901957	567.84	-64.477	-5.79731
0.049091779	1136.154892	38.94311824	-95.99249082	2003	03-06-17	14:49	561.48072	567.8784215	567.85	-64.93	-6.27548
0.079678497	1122.276939	38.9431168	-95.99192538	2004	03-06-17	14:45	562.5228	568.0212205	567.86	-60.023	-6.71584
0.110193035	1113.877988	38.94311527	-95.99135995	2005	03-06-17	14:41	562.88352	567.8346121	567.87	-47.331	-7.13374
0.140678844	1109.186387	38.94311522	-95.99079452	2006	03-06-17	14:37	563.28432	567.9303624	567.87	-35.277	-7.50757
0.171157837	1107.250692	38.94312182	-95.99022908	2007	03-06-17	14:34	563.20416	567.7232195	567.88	-14.446	-7.8802
0.201638576	1104.068277	38.94312681	-95.98966365	2008	03-06-17	14:31	563.5248	567.8428993	567.89	8.666	-8.22773
0.23213426	1097.965914	38.94312911	-95.98909821	2009	03-06-17	14:29	564.00576	567.9343537	567.9	29.465	-8.56245
0.262629121	1092.224444	38.94313494	-95.98853278	2010	03-06-17	14:25	564.40656	567.9690921	567.9	50.763	-8.89165
0.293169695	1081.594523	38.94313909	-95.98796735	2011	03-06-17	14:22	565.00776	567.8980819	567.91	79.663	-9.17138
0.323665792	1075.49216	38.94314241	-95.98740191	2012	03-06-17	14:18	565.36848	567.8882986	567.92	109.209	-9.41347
0.354141831	1074.147016	38.94313711	-95.98683648	2013	03-06-17	14:15	565.36848	567.7971844	567.93	144.674	-9.64774
0.384617309	1072.473788	38.94313343	-95.98627105	2014	03-06-17	14:11	565.48872	567.7997445	567.94	165.144	-9.83935
0.415094068	1074.015782	38.9431283	-95.98570561	2015	03-06-17	14:08	565.44864	567.8641208	567.95	171.5	-10.0067
0.445987409	1076.345179	38.94320164	-95.98514018	2016	03-06-17	14:05	565.128	567.702152	567.96	168.463	-10.0565
0.478671587	1082.710008	38.94337198	-95.98457474	2017	03-06-17	14:02	564.68712	567.6883468	567.97	157.698	-10.0679
0.511619316	1099.770376	38.94354739	-95.98400931	2018	03-06-17	13:59	564.16608	568.3240703	567.98	139.983	-10.0681
0.543084197	1117.257254	38.94365036	-95.98344388	2019	03-06-17	13:56	562.60296	567.8855227	568	111.418	-10.104
0.574326102	1146.063029	38.94358942	-95.98287844	2020	03-06-17	13:52	560.9196	568.0057389	568.01	82.011	-10.2769
0.61126431	1165.584027	38.94329168	-95.98231301	2021	03-06-17	13:48	559.9176	568.2678509	568.02	58.18	-10.4216
0.643496232	1175.524972	38.94314195	-95.98174758	2022	03-06-17	13:45	559.19616	568.1929568	568.03	30.333	-10.4853
0.673980894	1172.014473	38.94313463	-95.98118214	2023	03-06-17	13:41	558.95568	567.7115136	568.05	-7.777	-10.4328
0.704594022	1158.464604	38.94311417	-95.98061671	2024	03-06-17	13:36	559.87752	567.760319	568.06	-53.301	-10.3409
0.735174919	1145.144394	38.94310703	-95.98005128	2025	03-06-17	13:21	560.87952	567.9422924	568.07	-100.331	-10.1769
0.765822307	1127.919984	38.94310795	-95.97948584	2026	03-06-17	13:17	561.88152	567.8519613	568.09	-126.044	-9.9982
0.796362597	1117.257254	38.94311113	-95.97892041	2027	03-06-17	13:13	562.64304	567.9311287	568.11	-138.395	-9.79073
0.826934956	1104.921295	38.94309995	-95.97835497	2028	03-06-17	13:06	563.20416	567.7295742	568.13	-138.942	-9.52128
0.857538276	1093.53678	38.9430735	-95.97778954	2029	03-06-17	13:03	564.04584	567.8786232	568.15	-138.692	-9.25113
0.888052204	1098.129956	38.94309273	-95.97722411	2030	03-06-17	13:00	564.04584	568.143553	568.17	-126.505	-8.98253
0.918535983	1102.296623	38.94309498	-95.97665867	2031	03-06-17	12:57	563.88552	568.2578211	568.2	-106.978	-8.70136
0.949028262	1106.102398	38.94308304	-95.97609324	2032	03-06-17	12:53	563.64504	568.2795455	568.23	-97.941	-8.39428
0.979508491	1105.774314	38.94307321	-95.97552781	2033	03-06-17	12:49	563.64504	568.2716517	568.25	-90.092	-8.05693
1.010047916	1095.636518	38.94306455	-95.97496237	2034	03-06-17	12:45	564.44664	568.4396162	568.28	-81.805	-7.71748
1.040605691	1083.759877	38.94305916	-95.97439694	2035	03-06-17	12:42	565.04784	568.2913275	568.3	-61.1685	-7.32426
1.071091528	1079.297935	38.94305474	-95.97383151	2036	03-06-17	12:38	565.40856	568.3765258	568.33	-38.506	-6.85584
1.101574389	1076.443604	38.94304679	-95.97326607	2037	03-06-17	12:35	565.5288	568.3250256	568.35	-15.502	-6.38832
1.132055259	1073.753315	38.94303961	-95.97270064	2038	03-06-17	12:32	565.68912	568.3256697	568.38	-4.741	-5.89673
1.162539833	1071.456727	38.94302927	-95.9721352	2039	03-06-17	12:11	565.84944	568.4348319	568.4	0.908	-5.40536
1.193062609	1075.689011	38.94300673	-95.97156977	2040	03-06-17	12:08	565.76928	568.6548579	568.42	1.194	-4.86522
1.223556623	1081.725756	38.94300657	-95.97100434	2041	03-06-17	12:05	565.56888	568.8340532	568.44	-0.597	-4.25729
1.254052403	1087.893736	38.94300462	-95.9704389	2042	03-06-17	12:02	564.76728	568.4324349	568.46	-10.79	-3.64727
1.284542577	1093.274313	38.94300188	-95.96987347	2043	03-06-17	11:59	564.68712	568.7114173	568.48	-17.351	-3.03416
1.315054034	1100.984287	38.94299477	-95.96930804	2044	03-06-17	11:57	564.126	568.6519018	568.49	-17.5405	-2.34692
1.345580951	1109.612896	38.94298342	-95.9687426	2045	03-06-17	11:54	563.88552	568.9805412	568.5	-13.81	-1.64537
1.376103154	1118.700823	38.94297967	-95.96817717	2046	03-06-17	11:51	563.08392	568.7813497	568.51	-13.71	-0.98772
1.406631632	1127.362241	38.94296764	-95.96761173	2047	03-06-17	11:49	562.5228	568.7964841	568.51	-17.625	-0.40692
1.437255482	1142.946231	38.94295705	-95.9670463	2048	03-06-17	11:44	561.36048	568.6571512	568.52	-19.937	0.17784

1.467866789	1158.103712	38.94295	-95.96648087	2049	03-06-17	11:41	560.59896	568.8753596	568.52	-21.157	0.79066
1.498356172	1162.532846	38.94294217	-95.96591543	2050	03-06-17	11:37	560.15808	568.7304169	568.51	-19.53	1.32134
1.560528279	1164.435733	38.94294263	-95.96476182	2051	30-05-17	10:20	559.75728	568.3708292	568.51	-12.684	1.75451
1.592228089	1163.189014	38.94294035	-95.96417364	2052	30-05-17	10:26	559.83744	568.3728713	568.5	-6.293	2.16274
1.623979146	1153.608961	38.94293743	-95.96358546	2053	30-05-17	10:36	558.3144	566.2356672	568.5	2.071	2.51344
1.655869384	1135.203448	38.94293455	-95.96299728	2054	30-05-17	11:21	561.44064	568.2200747	568.51	7.222	2.79229
1.687793905	1115.190324	38.94293617	-95.9624091	2055	30-05-17	11:26	564.68712	570.1785069	568.52	10.884	3.00615
1.719594309	1101.771689	38.94293459	-95.96182092	2056	30-05-17	11:36	563.36448	568.0302499	568.53	13.793	3.15428
1.751366901	1090.551216	38.94294086	-95.96123274	2057	30-05-17	11:43	564.16608	568.142287	568.55	19.299	3.25484
1.783107027	1081.955415	38.94294319	-95.96064457	2058	30-05-17	11:52	564.80736	568.2676505	568.56	23.819	3.31427
1.814809039	1081.627331	38.94295	-95.96005639	2059	30-05-17	11:59	565.00776	568.4689682	568.58	27.405	3.35507
1.846534082	1087.79531	38.94295822	-95.95946821	2060	30-05-17	12:06	564.68712	568.5651724	568.59	27.189	3.37032
1.878251481	1092.749379	38.94295	-95.95888003	2061	30-05-17	12:27	564.60696	568.8839727	568.61	25.286	3.36769
1.909955914	1095.472476	38.9429549	-95.95829185	2062	30-05-17	12:34	564.08592	568.5662164	568.63	20.646	3.3577
1.94165448	1094.98035	38.94295521	-95.95770367	2063	30-05-17	12:40	564.28632	568.759985	568.64	14.471	3.34068
1.973367037	1090.354366	38.94295	-95.95711549	2064	30-05-17	12:46	564.28632	568.4886034	568.66	6.285	3.31567
2.005104094	1082.086649	38.94295	-95.95652731	2065	30-05-17	13:58	564.64704	568.2865293	568.69	-1.666	3.2931
2.036855803	1072.375362	38.94295	-95.95593913	2066	30-05-17	14:03	565.36848	568.3887372	568.71	-11.024	3.27867
2.068674848	1058.103708	38.94294133	-95.95535095	2067	30-05-17	14:08	566.13	568.2551351	568.74	-20.836	3.26955
2.100399929	1052.001346	38.94295	-95.95476277	2068	30-05-17	15:10	566.61096	568.2588164	568.77	-33.635	3.26614
2.132104375	1052.034154	38.942959	-95.95417459	2069	30-05-17	15:14	566.81136	568.44118	568.8	-47.984	3.26697
2.163811046	1054.133892	38.94296781	-95.95358641	2070	30-05-17	15:17	566.81136	568.5832393	568.83	-61.613	3.26551
2.195515769	1056.299246	38.94296076	-95.95299823	2071	30-05-17	15:22	566.81136	568.7449045	568.86	-67.601	3.24692
2.227222081	1059.809745	38.94295709	-95.95241005	2072	30-05-17	15:26	566.81136	568.9877202	568.89	-68.02	3.21483
2.258942398	1065.485598	38.94295	-95.95182187	2073	30-05-17	15:30	566.49072	569.0500813	568.92	-63.122	3.16895
2.290668574	1072.572213	38.94295	-95.9512337	2074	30-05-17	15:34	565.88952	568.921134	568.95	-56.191	3.1085
2.32241821	1081.85699	38.94294412	-95.95064552	2075	30-05-17	15:37	565.80936	569.4565552	568.97	-44.493	3.0306
2.35417768	1092.224444	38.94294176	-95.95005734	2076	30-05-17	15:41	564.64704	568.9831906	569	-28.866	2.93919
2.38594244	1103.018408	38.94294464	-95.94946916	2077	30-05-17	16:09	564.08592	569.2120158	569.02	-14.48	2.85992
2.417660227	1108.891112	38.9429449	-95.94888098	2078	30-05-17	16:12	563.5248	569.0417177	569.04	-0.377	2.79744
2.449358873	1108.30056	38.94294647	-95.9482928	2079	30-05-17	16:14	563.5248	569.0132461	569.06	16.251	2.7615
2.481061639	1105.610272	38.94294411	-95.94770462	2080	30-05-17	16:17	563.5248	568.8510326	569.09	36.945	2.77744
2.512776203	1102.9856	38.94293125	-95.94711644	2081	30-05-17	16:20	563.76528	568.9363211	569.11	62.054	2.8405
2.544485913	1099.114208	38.94292494	-95.94652826	2082	30-05-17	16:23	564.16608	569.1013973	569.13	84.367	2.93487
2.576188229	1097.375363	38.94291932	-95.94594008	2083	30-05-17	17:28	564.08592	568.894909	569.16	92.795	3.11066
2.607893908	1099.376676	38.94291101	-95.9453519	2084	30-05-17	17:32	564.24624	569.1847546	569.18	96.145	3.40316
2.639592508	1098.786124	38.94291258	-95.94476372	2085	30-05-17	17:35	564.40656	569.3311404	569.2	93.583	3.7898
2.671291701	1099.114208	38.94291609	-95.94417554	2086	30-05-17	17:39	564.3264	569.2625187	569.22	89.101	4.30667
2.702995927	1099.835993	38.94292483	-95.94358736	2087	30-05-17	17:43	564.3264	569.3008639	569.23	75.323	4.91049
2.734752754	1109.809747	38.94291916	-95.94299918	2088	30-05-17	17:46	564.04584	569.6333208	569.24	61.053	5.63775
2.766500598	1118.733632	38.94291085	-95.94241101	2089	30-05-17	17:49	563.5248	569.6730679	569.26	51.851	6.50024
2.798238855	1125.721821	38.94289796	-95.94182283	2090	30-05-17	18:17	562.9236	569.4724257	569.27	41.188	7.28788
2.829974295	1133.72707	38.94289424	-95.94123465	2091	30-05-17	18:21	562.28232	569.3331382	569.28	24.325	8.02138
2.86176703	1146.65358	38.94289578	-95.94064647	2092	30-05-17	18:26	561.9216	569.7906937	569.29	3.532	9.07411
2.893475345	1150.820247	38.94289794	-95.94005829	2093	30-05-17	18:30	561.16008	569.2926061	569.3	-17.724	10.0909
2.925230086	1140.813685	38.94289817	-95.93947011	2094	30-05-17	18:37	561.12	568.5932265	569.32	-33.003	11.0806
2.956941965	1135.892425	38.94289904	-95.93888193	2095	30-05-17	18:41	561.48072	568.6390529	569.35	-43.7105	12.0821
2.988755995	1121.587962	38.94290122	-95.93829375	2096	30-05-17	18:48	562.04184	568.2713271		-49.329	13.1305
3.025298978	1112.40161	38.94291504	-95.93761667	2097	30-05-17	18:56	563.80536	569.4379116		-53.621	14.1348

Gravity Base Station Data						
Elevation (Feet)	Latitude (WGS84)	Longitude (WGS84)	Station Number	Date (DD-MM-YY)	Time	Gravity Reading * 0.4008
1164.304499	38.94295	-95.96535	1001	06-06-17	12:40	560.35848
1164.304499	38.94295	-95.96535	1001	06-06-17	14:41	560.67912
1164.304499	38.94295	-95.96535	1001	06-06-17	15:36	560.55888
1164.304499	38.94295	-95.96535	1001	14-06-17	10:22	561.28032
1164.304499	38.94295	-95.96535	1001	14-06-17	12:26	561.60096
1164.304499	38.94295	-95.96535	1001	26-06-17	10:35	563.44464
1164.304499	38.94295	-95.96535	1001	26-06-17	12:51	563.28432
1164.304499	38.94295	-95.96535	1001	26-06-17	13:17	563.44464
1164.304499	38.94295	-95.96535	1001	24-06-17	11:56	563.04384
1164.304499	38.94295	-95.96535	1001	24-06-17	13:56	563.28432
1164.304499	38.94295	-95.96535	1001	24-06-17	15:52	563.44464
1164.304499	38.94295	-95.96535	1001	24-06-17	16:42	563.48472
1164.304499	38.94295	-95.96535	1001	30-05-17	10:13	559.75728
1164.304499	38.94295	-95.96535	1001	30-05-17	11:04	559.83744
1164.304499	38.94295	-95.96535	1001	30-05-17	13:02	559.43664
1164.304499	38.94295	-95.96535	1001	30-05-17	15:00	559.75728
1164.304499	38.94295	-95.96535	1001	30-05-17	16:32	559.43664
1164.304499	38.94295	-95.96535	1001	30-05-17	18:10	559.5168
1164.304499	38.94295	-95.96535	1001	30-05-17	19:12	559.63704
1164.304499	38.94295	-95.96535	1001	03-06-17	11:29	559.79736
1164.304499	38.94295	-95.96535	1001	03-06-17	13:29	560.19816
1164.304499	38.94295	-95.96535	1001	03-06-17	15:06	560.15808

Appendix C - GM-SYS® Model Parameters

Letter	Block Name	Density (g/cc)	Susceptibility (SI)
A	Topography	2.34	0.0005
B	Above Oread Limestone	2.44	0.0005
C	Oread Limestone	2.59	0.0002
D	Heebner Shale	2.4	0.0007
E	Lansing Group	2.55	0.0002
F	Base of the Kansas City Group	2.45	0.0007
G	Altamont Limestone	2.47	0.0002
H	Cherokee Group	2.41	0.0004
I	"Mississippi Lime"	2.58	0.0002
J	Chattanooga Shale	2.59	0.0007
K	"Hunton Group"	2.65	0.0002
L	Maquoketa (Sylvan) Shale	2.57	0.0007
M	Viola (Kimmswick) Limestone	2.66	0.0002
N	Simpson Group	2.5	0.0004
O	Arbuckle Group	2.62	0.0002
P	Basal Sandstone	2.34	0.0004
Q	Granite	2.7	0.034
R	Cataclastic Granite	2.62	0.034

Appendix D - Thin Section Data

Well	Unique Identifier (Depth-Size of Cuttings-Number)	Quartz Grains	Quartz Grains (PDFs)
Andrew Wendland 1	2830-63-1	2	0
	2830-63-2	6	0
	2830-63-3	14	0
	2830-63-4	16	0
	2830-63-5	13	0
	2830-125-1	1	0
	2840-63-1	9	0
	2840-63-2	6	0
	2840-63-3	7	0
	2840-63-4	6	0
	2840-63-5	6	0
	2840-125-1	0	0
	2850-63-1	3	0
	2850-63-2	5	0
	2850-63-3	8	0
	2850-63-4	3	0
	2850-63-5	8	0
	2850-125-1	1	0
	2860-1-1	205	0
	2860-63-1	16	0
	2860-63-2	30	0
	2860-63-3	15	0
	2860-63-4	6	0
	2860-63-5	9	0
	2860-125-1	32	0
	2870-1-1	332	0
	2870-63-1	8	0
	2870-63-2	4	0
	2870-63-3	6	0
	2870-63-4	10	0
	2870-63-5	6	0
	2870-125-1	3	0
	2870-125-2	4	0
	2880-1-1	213	0
	2880-63-1	27	0
	2880-63-2	39	0
	2880-63-3	13	0
	2880-63-4	27	0
	2880-63-5	15	0
	2880-125-1	57	0
	2880-125-2	10	0
	2890-63-1	36	0
	2890-63-2	43	0
	2890-63-3	44	0

	2890-63-4	13	0
	2890-63-5	98	0
	2890-125-1	15	0
	2890-125-2	71	0
	2900-1-1	1387	0
	2900-63-1	31	0
	2900-63-2	58	0
	2900-63-3	74	0
	2900-63-4	43	0
	2900-63-5	26	0
	2900-125-1	0	0
	2900-125-2	12	0
	2910-1-1	123	0
	2910-63-1	152	0
	2910-63-2	255	0
	2910-63-3	66	0
	2910-63-4	265	0
	2910-63-5	257	0
	2910-125-1	351	0
	2910-125-2	46	0
	2920-1-1	153	0
	2920-63-1	6	0
	2920-63-2	15	0
	2920-63-3	16	0
	2920-63-4	14	0
	2920-63-5	6	0
	2920-125-1	8	0
	2920-125-2	13	0
	2930-1-1	55	0
	2930-63-1	18	0
	2930-63-2	12	0
	2930-63-3	14	0
	2930-63-4	10	0
	2930-63-5	3	0
	2930-125-1	0	0
	2930-125-1	6	0
	2940-1-1	385	0
	2940-63-1	11	0
	2940-63-2	2	0
	2940-63-4	8	0
	2940-63-4	6	0
	2940-63-5	11	0
	2940-125-1	4	0
	2940-125-2	13	0

Dorothy Wendland 1	3050-63-1	1030	0
	3050-63-2	223	0
	3050-63-3	252	0
	3050-63-4	235	0
	3050-63-5	216	0
	3050-63-6	245	0
	3050-63-7	180	0
	3050-63-8	387	0
	3050-63-9	217	0
	3050-63-10	315	0
	3050-63-11	477	0
	3050-63-12	531	0
	3050-125-1	1157	0
	3050-125-2	236	0

Total Quartz Grains	Total Quartz Grains (PDFs)
11157	0